

LIGHTNING CURRENTS AND ELECTROMAGNETIC FIELDS ASSOCIATED WITH RETURN STROKES TO ELEVATED STRIKE OBJECTS

THÈSE N° 2741 (2003)

PRÉSENTÉE À LA FACULTÉ SCIENCES ET TECHNIQUES DE L'INGÉNIEUR

SECTION D'ÉLECTRICITÉ

ÉCOLE POLYTECHNIQUE FÉDÉRALE DE LAUSANNE

POUR L'OBTENTION DU GRADE DE DOCTEUR ÈS SCIENCES TECHNIQUES

PAR

José-Luis BERMUDEZ ARBOLEDA

ingénieur électricien, Universidad del Valle, Cali, Colombie
et de nationalité colombienne

acceptée sur proposition du jury:

Dr F. Rachidi-Haeri, directeur de thèse

Dr W. Chisholm, rapporteur

Prof. M. Rubinstein, rapporteur

Prof. A. Skrivervik Favre, rapporteur

Lausanne, EPFL
2003

To Adona

Résumé

L'objectif de ce travail de thèse est la modélisation des arcs en retour associés à des coups de foudre tombant sur des objets élevés tels que les tours de télécommunications. Les travaux théoriques et expérimentaux effectués dans le cadre de cette thèse ont permis de quantifier les effets introduits par la présence d'un objet élevé sur la distribution spatiale et temporelle du courant de foudre, le long du canal et le long de l'objet foudroyé, ainsi que sur le champ électromagnétique rayonné associé à cette distribution du courant.

Les trois premiers chapitres de la thèse contiennent, une courte description de la décharge orageuse atmosphérique, ainsi qu'un bref aperçu des données expérimentales utiles pour la modélisation de leurs effets électromagnétiques, et enfin, un aperçu des modèles existants de la phase d'arc en retour de la foudre tombant directement au sol. Les principales contributions originales de cette thèse sont présentées dans les chapitres 4 à 6. Elles comportent les parties expérimentales et théoriques suivantes.

Afin de valider les modèles théoriques développés dans ce travail, nous avons participé à deux campagnes expérimentales en été 2000 et été 2001 à Toronto, Canada, où nous avons mesuré, en collaboration avec le groupe de recherche sur la foudre de l'Université de Toronto, le courant et le champ électromagnétique associés aux éclairs tombant sur la tour CN (CN Tower). La tour CN est à ce jour la structure autosupportée la plus élevée dans le monde (553 m). Les données expérimentales obtenues lors de ces deux campagnes constituent les premières mesures simultanées de courant de foudre, de champs électrique et magnétique à deux distances du point d'impact, ainsi que des mesures optiques obtenues en utilisant un système d'enregistrement rapide.

Outre les enregistrements effectués à Toronto, d'autres données expérimentales ont été également utilisées pour valider les modèles théoriques. Il s'agit (a) d'enregistrements du courant de foudre obtenus simultanément à deux hauteurs de la tour de Peissenberg en Allemagne, fournis par le Prof. Fridolin Heidler, et (b) de mesures effectuées sur un modèle à échelle réduite conçu, réalisé, et testé dans le cadre de cette thèse. Les données cumulées nous ont ainsi permis de caractériser l'objet élevé foudroyé et de valider les différentes expressions théoriques développées dans cette thèse.

Nous avons généralisé, dans le chapitre 4, les modèles d'arcs en retour dits d'« ingénieur » ('engineering models') pour tenir compte de la présence d'un objet élevé foudroyé. La généralisation est basée sur une représentation en termes de sources réparties de courant le long du canal de foudre, qui a conduit à l'obtention des expressions plus générales et plus compactes de ces modèles. Cette représentation a permis en particulier de traiter de manière cohérente la discontinuité de l'impédance au sommet de la tour, contrairement aux représentations précédentes qui étaient fondées sur une source de courant concentrée à la base du canal. Quant à l'objet foudroyé, il a été modélisé comme une ligne de transmission uniforme et sans pertes, caractérisée par des coefficients de réflexion à ses extrémités. Des expressions distinctes ont été également développées pour le cas des structures électriquement courtes. Ces dernières peuvent être employées pour quantifier les effets des conditions au sol sur la distribution du courant le long de l'objet foudroyé ainsi que le long du canal de foudre.

Les expressions générales établies au chapitre 4 décrivant la distribution spatio-temporelle du courant dans le canal de foudre et dans l'objet foudroyé, ont été utilisées dans le chapitre 5 pour obtenir de nouvelles expressions des champs électromagnétiques lointains. Ces expressions ont été évaluées pour le cas de structures électriquement longues et électriquement courtes. Pour les structures électriquement longues, nous avons pu établir que la présence de l'objet foudroyé renforce l'amplitude du champ électromagnétique, ce par rapport aux arcs en retour tombant directement au sol. Nous avons montré que l'amplification du champ électromagnétique due à la présence d'une structure élevée (par exemple une tour de télécommunication) peut être quantifiée par un facteur multiplicatif qui dépend de la vitesse de l'arc en retour et du coefficient de réflexion au sommet de l'objet foudroyé.

Les enregistrements simultanés du courant et du champ électromagnétique à deux distances associés aux éclairs tombant sur la Tour CN, mentionnés auparavant, ont été utilisés pour valider les expressions théoriques et un bon accord a été trouvé. Ces expressions peuvent trouver une application utile dans l'évaluation de la performance des systèmes de détection et de localisation de foudre (Lightning Location Systems - LLS) lorsque les courants de foudre sont mesurés directement sur les tours instrumentées.

Dans le chapitre 6, nous avons effectué une analyse détaillée dans le domaine fréquentiel de la distribution spatio-temporelle du courant de foudre le long de l'objet foudroyé. Nous avons développé une expression compacte pour évaluer cette distribution qui tient compte de la dépendance fréquentielle des coefficients de réflexion au sommet et à la base de l'objet foudroyé.

D'autre part, nous avons proposé une méthode pour déterminer le coefficient de réflexion à la base de l'objet foudroyé en fonction de la fréquence, ce à partir de courants mesurés simultanément à deux hauteurs différentes le long de l'objet. Nous avons pu montrer que ce coefficient de réflexion à la base de l'objet peut être déterminé sans qu'il soit nécessaire de connaître le coefficient de réflexion au sommet.

Nous avons également démontré qu'il est impossible, dans les limites des hypothèses adoptées et quel que soit le nombre de points de mesure du courant le long de l'objet foudroyé, de déterminer rigoureusement le coefficient de réflexion au sommet de l'objet foudroyé ; sauf lorsque la tour est suffisamment longue pour que le courant injecté au sommet de l'objet ou sa dérivée chutent à zéro avant l'arrivée des réflexions. Nous avons proposé deux méthodes qui permettent d'estimer à partir d'enregistrements expérimentaux, le coefficient de réflexion au sommet de l'objet.

Les méthodes proposées ont été appliquées aux données expérimentales obtenues sur la tour de Peissenberg où le courant de foudre a été mesuré simultanément à deux hauteurs différentes. Nous avons pu mettre en évidence que le coefficient de réflexion à la base de l'objet peut être considéré comme pratiquement constant sur une bande de fréquences s'étendant de 100 kHz jusqu'à 800 kHz. Quant au coefficient de réflexion au sommet de l'objet, les valeurs estimées sont en bon accord avec estimations d'autres auteurs et publiées dans la littérature. Néanmoins, nous avons constaté que les valeurs pour le coefficient de réflexion au sommet de l'objet foudroyé estimées par la méthode d'extrapolation, sont inférieures à celles trouvées en utilisant la méthode basée sur la dérivée du courant. La différence pourrait être due aux possibles erreurs expérimentales et également au fait que la méthode d'extrapolation fournit des valeurs pour le coefficient de réflexion au sommet calculés à partir de la partie 'lente' (basse fréquence) des formes d'onde du courant, alors que la méthode de la dérivée du courant utilise la partie 'rapide' de la forme d'onde. Cette observation suggère que le coefficient de réflexion au sommet dépend de la fréquence.

A la fin du chapitre 6, un algorithme génétique a été appliqué pour extraire automatiquement paramètres primaires du courant de foudre à partir des mesures expérimentales obtenus sur des tours instrumentées. L'algorithme a d'abord été testé sur des formes d'onde théoriques obtenues en adoptant des valeurs connues pour les coefficients de réflexion à la base et au sommet de l'objet foudroyé, ainsi que pour le courant initial. Ensuite, l'algorithme a été appliqué aux courants de foudre mesurés sur la tour de Peissenberg en Allemagne. Les meilleurs individus satisfaisant la fonction de corrélation (fitness function) ont été choisis comme gagnants et comparés aux formes d'onde mesurées. Un bon accord a été trouvé.

Summary

The aim of this thesis is the modeling of lightning return strokes impacting elevated strike objects such as towers. The theoretical and experimental work done led to the evaluation of the effect of the presence of the strike object on the spatial and temporal distribution of the current along the channel and along the strike object, as well as on the radiated electromagnetic fields associated with that current distribution.

The first three chapters of the thesis contain a brief description of the lightning discharge, a review of the relevant experimental data available and an overview of the existing return strokes models for lightning initiated at ground level. The main original contributions of this thesis are presented in Chapters 4 through 6. They consist of experimental and theoretical work as follows.

For the purpose of validating our theoretical models versus measurements, we participated, during the summers of 2000 and 2001, in experimental campaigns in Toronto, Canada, where we measured currents and electromagnetic fields associated with lightning strikes to the CN Tower in collaboration with the lightning research group of the University of Toronto. The CN Tower is today's tallest free-standing structure in the world (553 m). The collected data constitute the first simultaneous measurements of lightning current, electric and magnetic fields at two distances from the lightning channel, as well as optical measurements using a fast-speed camera system.

The set of measurements obtained in Canada was complemented, in the framework of this thesis, with (a) experimental data of lightning return stroke currents measured simultaneously at two locations at the Peissenberg tower in Germany, provided by Prof. Fridolin Heidler, and (b) measurement results obtained using a reduced-scale model also designed, constructed, and tested in the framework of this thesis. The cumulated data allowed us to characterize the elevated strike object and to validate various theoretical expressions developed in this thesis.

We generalized in Chapter 4 the so-called engineering models to include the presence of an elevated strike object. The generalization is based on a distributed-source representation of the return stroke channel, which allowed more general and straightforward formulations of these models, including a self-consistent treatment of the impedance discontinuity at the tower top, as opposed to previous representations implying a lumped current source at the bottom of the channel.

We modeled the strike object as a vertically-extended, lossless uniform transmission line, characterized by reflection coefficients at its extremities. Special expressions were also derived for the case of electrically short structures. These expressions can be used to quantify the effect of grounding conditions on the current distribution along the strike object and along the channel.

In Chapter 5, using the general expressions for the spatial-temporal distribution of the current in the channel and in the elevated strike object, new expressions for the electric and magnetic fields at far distances were derived. These expressions were evaluated for the cases of electrically-tall and electrically-short structures. For electrically-tall structures, it was found that the presence of the strike object enhances the radiated electric and magnetic field peaks in comparison to return strokes initiated at ground level. The enhancement was quantified through a simple multiplicative factor that depends on the return stroke speed and on the top reflection coefficient associated with the strike object.

The mentioned simultaneously measured currents and fields associated with lightning strikes to the CN Tower were used to test the theoretical expressions and a reasonable agreement was found. The derived expressions could find a useful application when lightning currents are measured directly on instrumented towers to calibrate the performance of lightning location systems.

In Chapter 6, we analyzed the current into the elevated strike object in the frequency domain, and we derived a closed form expression to evaluate this current taking into account frequency-dependent reflection coefficients at the top and at the bottom of the elevated strike object.

We derived an expression to calculate the reflection coefficient as a function of frequency at the bottom of the lightning strike object from two currents measured simultaneously at different heights along the strike object. We found that the ground reflection coefficient can be found without prior knowledge of the reflection coefficient at the top of the strike object.

We showed that, unless the tower is tall enough that the current injected at the top of the object or its derivative drop to zero before the arrival of reflections, it is impossible, at least under our assumptions, to derive either the reflection coefficient at the top of the strike object or the “undisturbed” current from any number of simultaneous current measurements. We proposed two methods to estimate the top reflection coefficient.

The proposed methods were applied to the experimental data obtained on Peissenberg Tower where lightning currents were measured simultaneously at two heights. It was found that the reflection coefficient at ground level can be considered as practically constant over a relatively wide range of frequencies from 100 kHz up to 800 kHz.

The estimated top reflection coefficients are in good agreement with values found in the literature. Nevertheless, we found that the estimated values for the top reflection coefficient from the extrapolation method are lower than those found employing the current derivative method. The difference might be due to possible experimental errors and also to the fact that the extrapolation method provides values for the top reflection coefficient calculated from the low-frequency tail of the current waveforms, while the current derivative method uses values associated with the faster parts of the waveform. This observation suggests that the top reflection coefficient is frequency dependent.

Finally, a genetic algorithm was applied to extract automatically primary lightning parameters from experimental records obtained on instrumented towers. The algorithm was first tested using theoretical waveforms obtained by assuming values for the ground and top reflection coefficients, and an assumed ‘undisturbed’ current expressed in terms of two Heidler’s functions. The algorithm was then applied to the actual, measured lightning return stroke currents obtained at the Peissenberg tower in Germany. The individuals that best satisfied the genetic algorithm’s fitness function were selected and compared with the measured waveforms. A good agreement was found.

Remerciements

Le déroulement d'une thèse de doctorat permet, en parallèle avec les recherches scientifiques, de rencontrer jour après jour des personnes, ou plutôt des personnalités très intéressantes, qui nous enseignent, l'intégrité, les valeurs et les bonnes manières de vivre dans une communauté scientifique. J'ai eu le plaisir de rencontrer en mon directeur de thèse, Dr. Farhad Rachidi, une de ces personnes qui en plus d'être un ami, a guidé mon travail de recherche tout en me faisant profiter de ses vastes compétences. Merci Farhad.

Le Professeur Alain Germond, directeur du laboratoire de réseaux électriques (LRE), a eu la gentillesse de m'accorder une lettre de soutien grâce à la quelle j'ai obtenu une bourse du gouvernement Suisse en 1994. Merci Alain pour cette lettre qui a donné une impulsion à ma carrière scientifique et aussi pour m'avoir accueilli dans ton laboratoire. Un grand merci au Professeur Michel Ianoz, grand connaisseur de la CEM et du monde, qui a guidé mes premiers pas dans la recherche.

Un remerciement très spécial est voué au Professeur Marcos Rubinstein, un grand ami et un excellent scientifique. Marcos a occupé dans ce travail de recherche plusieurs rôles, entre autres partenaire scientifique, membre du jury et fin correcteur du manuscrit de ma thèse. Merci Marcos aussi par tes conseils et ton sens de l'humour.

Mon travail de doctorat a été financé partiellement par le Fond National Suisse de la Recherche Scientifique (FNRS) à qui je dois transmettre mes plus amples remerciements. Je veux aussi remercier les responsables des bourses de la confédération qui m'ont permis de venir en Suisse. Tout particulièrement, je remercie Madame Catherine Vinckenbosh et Madame Annette Jaccard, du Service d'orientation et conseil, mobilité et service social (SOC), de l'EPFL pour avoir contribué à notre adaptation en Suisse.

Sans la coopération de nos partenaires scientifiques en Suisse et à l'étranger, les modèles développés dans mon travail n'auraient pas pu être confrontés à des mesures réelles. Merci au 'CN Tower Lightning Research Group', et à sa tête le Prof. Wasyl Janischewskyj pour m'avoir permis de participer deux fois de suite aux campagnes de mesures à Toronto, Canada. Je remercie également le Professeur Fridolin Heidler pour nous avoir fourni de précieux enregistrements de courant de foudre tombant sur la tour Peissenberg en Allemagne. Un grand merci à Dr. W. Chisholm pour ses conseils précieux quant au développement du modèle à échelle réduite d'une tour foudroyée. Je tiens à remercier également MM. Markus Nyffeler et Beat Reusser du Groupement de

l'Armement (NEMP Labor Spiez) pour leur soutien et pour nous avoir gracieusement prêté du matériel de mesure.

Tout au long de mon travail de thèse, j'ai eu la chance et le plaisir de collaborer avec plusieurs collègues, en particulier le Prof. C.A. Nucci et le Dr. M. Paolone (Université de Bologne), Prof. V. Rakov (Université de Floride), Prof. V. Shostak (Université de Kiev), Prof. A.M. Hussein (Université de Toronto), Prof. J.S. Chang (Mc Master University), Dr. Carlos Andrés Peña-Reyes (EPFL), Prof. Horacio Torres (Univerdad Nacional), Prof. Guillermo Aponte (Universidad del Valle), M. Eric Montandon (EMC Consulting) et Dr. Paul Joe (Environment Canada). Je les remercie pour leur soutien et leur apport scientifique.

J'adresse mes sincères remerciements au Dr. Jean-Philippe Thiran pour avoir accepté la présidence du jury, ainsi qu'aux membres du jury, Prof. Anja Skrivervik, Dr. William A. Chisholm et Professeur Marcos Rubinstein pour leurs suggestions et remarques constructives.

Un grand merci à tous mes amis et collègues du LRE : Andrée Moinat, Anne-Claude Maillefer, Elvira Kägi-Kolisnychenko, Rachid Cherkaoui, Pierre Zweiacker, Stéphane Gerbex, Alexandre Oudalov, Emmanuel Marthe, Abraham Rubinstein, Emanuel Petrache et Davide Pavanello; ainsi que à tous les étudiants qui ont participé d'une manière ou d'une autre dans ce projet, Elisa Garavini, Vitthawat Ngampradit, Etienne Perron, Martin Klauser, Fabio Laloli, Joseph Duron, Tobias Nef, Daniel Porto, Grégoire Chabloz, Jérémie Chabloz, Georg Kriebel. Merci aussi à toute l'équipe de l'atelier mécanique qui a contribué à la construction du modèle à échelle réduit.

Habiter loin de chez soi n'est pas toujours facile, la Colombie est à des milliers de kilomètres de la Suisse et la famille nous manque énormément. A mon arrivé en Suisse, une pièce de cinq francs dans une cabine téléphonique disparaissait à la vitesse de l'éclair (ce qui a probablement donné des idées pour mon projet). Aujourd'hui les communications sont moins chères donc plus accessibles. Néanmoins, il manque quelque chose, la chaleur de mes proches. Mais j'ai retrouvé cette chaleur grâce à un solide groupe de colombiens qui est venu élargir ces connaissances à l'EPFL. Merci les amis. Merci aussi aux Sanchez, Martica, Maria Isabel, Pilar Cristina et Eduardo, ma famille en Suisse, qui m'a accueilli à bras ouverts depuis mon arrivée.

J'aimerais finir d'une manière symétrique, comme tout ingénieur aime bien le faire, en remerciant ma famille, j'ai eu la chance d'avoir deux pères et deux mères, j'ai la chance d'en avoir encore deux avec moi, merci Emmita, Jesus Antonio, Diofelia et Efrain, à toujours merci. Merci à Adona, mon épouse, grâce à qui j'ai eu le courage de commencer et pour qui j'ai terminé cette thèse.

Table of Contents

Résumé	i
Summary.....	v
Remerciements	ix
Chapter 1: Introduction.....	1-1
Chapter 2: Lightning Return Stroke Parameters: Experimental Data	
2.1 Description of the phenomenon.....	2-1
2.2 Lightning return stroke parameters useful for electromagnetic modeling: Measurement techniques.....	2-6
2.2.1 Electromagnetic field.....	2-7
2.2.2 Return stroke speed.....	2-7
2.2.3 Channel-base current.....	2-11
2.3 Characterization of return stroke electromagnetic fields with distance.....	2-13
2.3.1 Measurements at distances of 1 km and beyond.....	2-13
2.3.2 Measurements at distances below 1 km	2-17
2.4 Characterization of lightning return stroke velocity	2-18
2.5 Characterization of lightning return stroke currents.....	2-20
2.5.1 Data from short towers.....	2-20
2.5.2 Triggered lightning data	2-24
2.5.3 Data from tall towers	2-26
2.6 Indirect estimation of currents from lightning location systems	2-31
2.7 Discussion on the relevance and accuracy of lightning return stroke current data obtained using instrumented towers.....	2-34
2.8 References Chapter 2	2-35
Chapter 3: Lightning Return Stroke Modeling	
3.1 Electromagnetic field associated with a return stroke.....	3-1
3.2 Return stroke current models.....	3-4
3.2.1 The Bruce-Golde (BG) model	3-6
3.2.2 The Transmission Line (TL) model	3-6
3.2.3 The Modified Transmission Line (MTL) model.....	3-7
3.2.4 The Traveling Current Source (TCS) model	3-8
3.2.5 Generalization of the RS Models	3-8

3.3	Channel base current.....	3-9
3.4	Discussion on the adequacy of engineering return stroke models.....	3-10
3.5	References Chapter 3.....	3-12

Chapter 4: Modeling of lightning return strokes to a vertically-extended elevated strike object

4.1	Introduction.....	4-1
4.2	MTLE model for a return stroke initiated at ground level	4-3
4.3	MTLE model in the presence of a vertically-extended strike object	4-4
4.3.1	Distribution of current along the lightning channel.....	4-6
4.3.2	Distribution of current along the strike object	4-8
4.4	Extension to other models.....	4-10
4.5	Special case: Electrically-short strike structures	4-12
4.5.1	Current along the lightning channel for electrically-short strike objects	4-13
4.5.2	Current along the strike object for electrically-short strike objects	4-14
4.6	Comments and conclusions.....	4-15
4.7	References Chapter 4.....	4-15

Chapter 5: Electromagnetic fields radiated by lightning return strokes to vertically extended elevated structures

5.1	Introduction.....	5-1
5.2	Description of the extended TL model and derivation of the far field – current relationship.....	5-2
5.2.1	Electrically-tall strike object ($t_f < h/c$).....	5-6
5.2.2	Electrically-short strike object ($t_f \gg h/c$).....	5-8
5.3	Measurement system and experimental data	5-9
5.3.1	CN Tower measurement set-up	5-9
5.3.2	CN Tower experimental data	5-11
5.4	Comparison between theoretical expressions and experimental data.....	5-14
5.5	Summary and conclusions	5-16
5.6	References Chapter 5.....	5-17

Chapter 6: Characterization of the elevated strike object and extraction of primary current waveform

6.1	Introduction.....	6-1
6.2	Model of a vertically-extended strike object	6-3

6.3	Determination of the ground reflection coefficient from two simultaneous current measurements	6-6
6.4	Estimation of the top reflection coefficient of the strike object	6-7
6.4.1	Extrapolation technique using measured current waveforms at the top of the tower	6-9
6.4.2	No-overlap current derivative components method	6-11
6.5	Application of the proposed methodology to Peissenberg Tower	6-13
6.5.1	Peissenberg Tower measurement set-up and experimental data	6-13
6.5.2	Application of the methodology in the frequency domain to recover the ground reflection coefficient	6-14
6.5.3	Application of the methodology to recover the top reflection coefficient in the time domain	6-15
6.6	Use of genetic algorithms to extract primary lightning current parameters	6-18
6.6.1	Genetic algorithms	6-18
6.6.2	Application of genetic algorithms (GA) to extract lightning current and reflection coefficients	6-19
6.6.3	Application of the algorithm to a theoretical case	6-20
6.6.4	Application of the GA to experimental data obtained on the Peissenberg Tower	6-22
6.7	Comments and conclusions	6-23
6.8	References Chapter 6	6-24

Chapter 7: Conclusions and Perspectives..... 7-1

Appendices

Appendix 1 - Derivation of equations (5-11) and (5-12)	A-1
A1.1 Approach based on the superposition principle	A-1
A1.2 Direct approach	A-3
Appendix 2 - Derivation of equations (5-25) and (5-26)	A-7
Appendix 3 - Numerical validation of equations (6-6a) and (6-10)	A-9
A3.1 The closed form current equation	A-9
A3.2 The ground reflection coefficient formula	A-11
Appendix 4 - Reduced-scale model to evaluate the response of nonuniform vertically-extended object struck by lightning	A-14
A4.1 Experimental Set-up	A-14
A4.2 Simulations and comparison with experimental data	A-16

Curriculum vitaeCV-1

Chapter 1

Introduction

Lightning electromagnetic effects are nowadays a major issue in electromagnetic compatibility. Lightning can damage a wide range of electrical systems, from electronic chips to overhead electric power and communication systems to boats and aircrafts. The study of interaction of lightning electromagnetic effects with electrical systems and the design of appropriate protection measures are generally based on statistical data of the lightning current measured at its channel base.

Lightning current parameters (peak value, front-steepness, duration) have been obtained, essentially, from direct measurements using instrumented towers or triggered lightning. The significant experimental data obtained using two instrumented towers in Monte San Salvatore (Switzerland) during the 1970's represents the most complete statistical characterization of lightning current parameters. Today, most of the studies dealing with lightning electromagnetic effects are based on the above-mentioned statistical data. More recently, experimental observations on tall telecommunication towers as well as theoretical analyses suggest, however, that the lightning current and current-derivative data obtained by means of instrumented towers might be affected ('contaminated') by the presence of the tower itself.

On the other hand, the indirect estimation of lightning current parameters from measured fields has grown in importance in the past few years due to the pervasive use of lightning location systems (LLS). The basic aim of such systems is to provide density maps of lightning return strokes. However, more recently, LLS have also been used to estimate lightning current parameters. Because of the enormous amount of data they can provide and the possibility of offering local statistical data, it can be expected that LLS will become more and more important in the near future. As a consequence, the problem of the accurate determination of the peak return stroke current from remotely measured electric and/or magnetic fields has gained an increased interest among researchers and engineers.

The above observations constitute the motivation for the present study, whose aim is the evaluation of the effect of an elevated strike object on both, the measured currents and the radiated electromagnetic field.

The present work focuses on the analysis and modeling of lightning strikes to elevated strike objects and, more specifically, on the return stroke process in such strikes. The original developments presented in this thesis are the result of my personal work, under the guidance of my advisor. It is

nonetheless important to mention that part of the work was developed in the framework of an international cooperation.

This thesis is organized in 7 chapters. The reader will notice that some of the material that appears in some of the chapters has already been addressed in other chapters. We have allowed for this limited redundancy in an effort to make each chapter as self-contained as possible, so that those readers interested in one particular part of the thesis do not have to read the whole document sequentially.

After this brief introduction, Chapter 2 gives a general overview of the cloud-to-ground lightning discharge phenomenon, a description of the measurement techniques, and a characterization of the parameters useful for return stroke electromagnetic modeling, namely the lightning return stroke current, the electric and magnetic fields, and, the return stroke speed. The issue of the statistical estimation of lightning return stroke currents from measurements of electromagnetic fields is also introduced in this chapter. The reader will also find in that chapter a discussion on the relevance and accuracy of lightning return stroke current data obtained using instrumented towers.

Chapter 3 contains an overview of the modeling of the cloud-to-ground lightning return stroke. Different classes of models are briefly described, with particular attention given to the so-called engineering models, in which a spatial and temporal distribution of the channel current (or the channel line charge density) is specified. It is only these engineering models that are applied in the remainder of the thesis since they are characterized by a small number of adjustable parameters and, moreover, they allow the return stroke current at any point along the lightning channel to be simply related to a specified channel-base current. Indeed, it is only the channel-base current that can be measured directly and for which experimental data are available. The chapter ends with a discussion on the adequacy of the engineering return stroke models.

A general model of a lightning return stroke impacting a vertically extended strike object is developed in Chapter 4. Based on a distributed-source representation of the lightning channel, expressions for the current distribution along the channel and along the strike object are derived for the engineering models introduced in Chapter 3. Special expressions are also derived for the case of electrically-short structures which can be used to quantify the effect of grounding conditions on the current distribution along the strike object and along the channel.

Chapter 5 is dedicated to the electromagnetic field radiated by a lightning discharge impacting an elevated strike object. New expressions for the radiated electric and magnetic fields are derived, taking into account the presence of the strike object and the special cases of electrically-tall and -short structures are considered. The chapter presents, additionally, the experimental data obtained during the summers of 2000 and 2001 in Toronto, Canada, where we performed simultaneous measurements of lightning current and electromagnetic fields at two distances associated with lightning strikes to the CN Tower. These data are used to validate the theoretical expressions for the electromagnetic field associated with lightning to tall structures.

Chapter 6 is devoted to the characterization of the elevated strike object and methods to extract the primary lightning current waveform are given in it. In this chapter, we also propose methods to estimate, from measured current waveforms, the reflection coefficients associated with the elevated strike objects. The methods are also tested with experimental data obtained using the Peissenberg tower in Germany. Additionally, a technique based on genetic algorithms is proposed to extract the parameters associated with the primary lightning current. The method is also tested versus experimental observations obtained at the Peissenberg Tower.

Finally, the conclusions of this study, as well as proposed future work are presented in Chapter 7.

Chapter 2

Lightning Return Stroke Parameters: Experimental Data

2.1 Description of the phenomenon

Lightning is probably one of the most widely studied natural phenomena, first for its power of destruction and then for its magnificent appearance. Initially the lightning phenomenon was considered as a messenger or a symbol from divinities in different cultures (religion and/or mythologies); in our days this belief has been replaced by a scientific knowledge, and researchers in many countries around the world have contributed to the advancement of our understanding of the lightning discharge. Nevertheless, up to now, the lightning phenomenon is still not completely understood and some of its processes are yet to be fully explained. For example, the origin of the accumulation of charge in the clouds, the effects of the strike point on the associated electromagnetic fields, as well as the consequences of these parameters on natural and human made systems are still the subject of scientific debate and controversy.

This section does not contain a complete description of the physics of the lightning phenomenon. Only aspects relevant to the work in the rest of this thesis will be covered.

Lightning is known to contribute to the electric equilibrium between the earth and the atmosphere (Fig. 2.1). It is also believed to be at the origin of life itself, as stated by Uman:

“Lightning has likely been present for the period of time during which life has evolved on earth, and, in fact, lightning has been suggested as a source for generating the necessary molecules from which life could evolve.” ([Uman, 1987]-page 29).

A lightning discharge is a fantastic visual spectacle, but it is, at the same time, the cause of forest fires, of human and animal casualties, of damage to electric and telecommunication systems, etc.

A thunderstorm (thundercloud or cumulonimbus) is defined in the literature as a cloud with a particular concentration of charges. In Fig. 2.2, the charge distribution inside a thundercloud is shown. Three parts in the cloud can be distinguished: first, a main negative charge region located at

the lower part of the cloud; second, a main positive charge region displaced to the top of the cloud and, finally, a small center of positive charge remains in the lower part of the cloud. It is believed that this third charge concentration has the function of initiator of the lightning discharge.

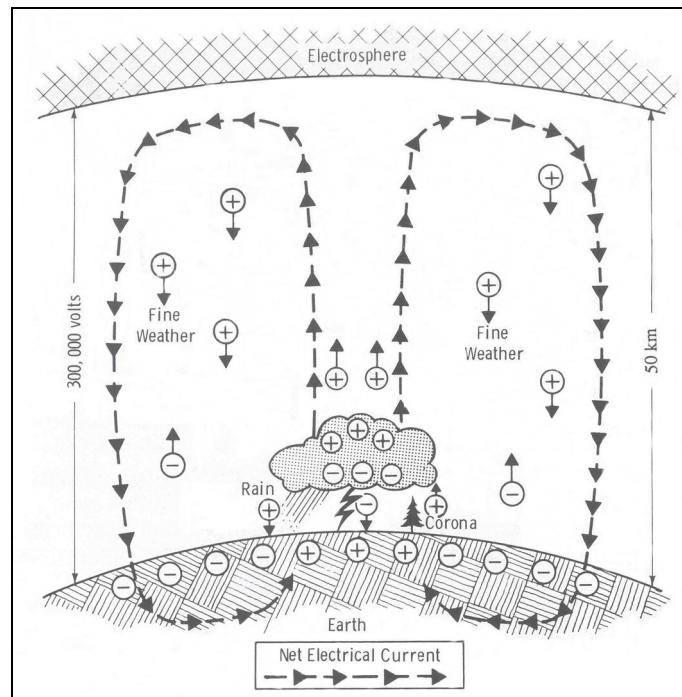


Figure 2.1 - Electrical equilibrium between the earth and the atmosphere through lightning (adapted from [Uman, 1987])

At ground level, the accumulation of charges in the thundercloud produces a concentration of the electrostatic field below the cloud (lower waveform in Fig. 2.2.). The electrostatic field associated with a thundercloud and the displacement of these clouds by the action of the air, have helped researchers to define methods of prediction of lightning discharges. Today, one can find systems which are capable of measuring the electrostatic field in the environment, and differentiate a thundercloud from other, cloud types¹. One can use the static electric field at ground level to infer when enough charge has accumulated in the thundercloud to start a lightning process. These systems provide then alarms to alert outdoor workers of the imminent danger of lightning, thus preventing accidents or damage to equipment. High variability in the lightning parameters makes this phenomenon inherently difficult to predict and these so-called early warning systems are therefore not one hundred percent reliable.

¹ Lightning discharges can also occur in association with active volcanoes, snow storms and even dust storms. Other types of unusual lightning discharges, e.g. ball-lightning, heat-lightning, sheet-lightning, will not be mentioned in this chapter. The interested reader should refer for more information to Gary, C., *La foudre: Des mythologies antiques à la recherche moderne*, MASSON, Paris, France, 1995, Golde, R.H., *Lightning*, 496 pp., Academic Press, London, 1977, Uman, M.A., *The lightning discharge*, 377 pp., Academic Press, Inc., Florida, USA, 1987.

When the electric field level necessary to start the process of a lightning discharge is attained, several scenarios are possible: 1) A lightning discharge can be produced and stay confined inside the same cloud, 2) the discharge can take place between separate clouds, 3) the discharge may occur between the cloud and the air, or 4) the discharge may be produced between the cloud and the ground.

Even though cloud-to-ground lightning discharges are not the most frequent discharges produced during a thunderstorm, they are the most studied as they are responsible for direct and indirect damages to the systems at ground level, and they are more easily observed and photographed. We will focus our attention on that type of lightning discharge, which is produced between thunderclouds (cumulonimbus) and ground.

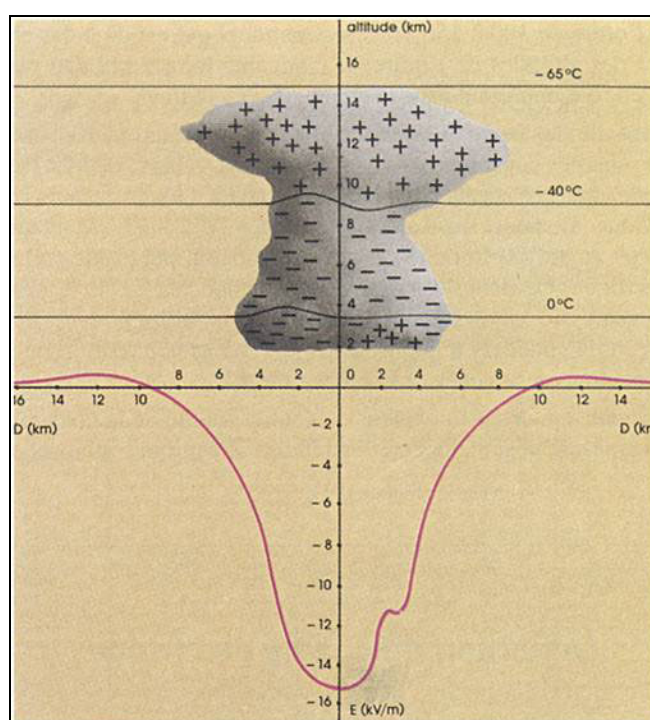


Figure 2.2 - Charge separation within a thunderstorm cloud (adapted from [Gary, 1995])

Berger (1978) cataloged cloud-to-ground natural lightning in four categories as a function of the direction of the motion of the initial leader (upward or downward), and the sign of charge deposited along the channel by that same initial leader (positive or negative). This classification is illustrated in Fig. 2.3. The first category, cloud-to-ground lightning moving negative charge to the ground, is the most common (90% of the world-wide cloud-to-ground lightning). Categories (b) and (d) are initiated by leaders that move upward from the earth (ground-to-cloud lightning). Ground-to-cloud (upward) flashes are relatively rare and generally occur either from mountain tops and tall man-made structures, or they can be triggered from rockets launched toward thunderstorms [Uman, 1987]. Upward flashes may be identified by the upward branching of the flash if a photograph of the flash was taken or by the continuing currents of milliseconds that may be followed immediately

or after short current interruptions by one or several impulse currents (return strokes). Downward flashes, on the other hand, branch downward and do not produce pre-discharge currents lasting more than a few milliseconds [Berger et al., 1975].

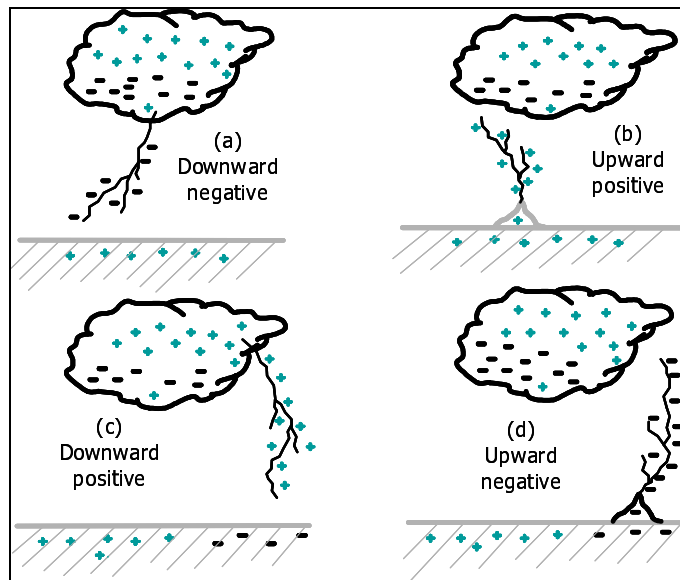


Figure 2.3 - Lightning stroke classification according to Berger (adapted from [Berger et al., 1975])

A complete lightning discharge is known as a flash and its time duration is about half a second. A flash is composed usually of several return strokes. Each stroke lasts a few hundreds of microseconds and, in multiple-stroke flashes, the separation time between strokes ranges from a few milliseconds to a few hundred milliseconds with a mean value in the order of 40 milliseconds. When the separation time between strokes is close to 100 milliseconds, lightning appears to "flicker" in the sky, because the human eye can resolve the individual strokes [ELAT, 2002].

The return stroke process is initiated when the first preliminary discharge at the lower part of the thundercloud appears, then, a series of processes, represented in Fig. 2.4 for a negative cloud-to-ground lightning discharge, can be distinguished [Uman, 1987].

The preliminary discharge starts the process and it is followed by the stepped leader. The stepped leader propagates down in a series of discrete steps. The stepped leader branches in several directions during its progression to ground producing the downward-branched geometrical structure. When the leader approaches the ground, the electric field at pointed objects on the ground exceeds the breakdown value of the air and one or more upward-moving discharges are initiated (upper-discharges on Fig. 2.4.). Finally, one of these upper-discharges contacts the leader (usually some tens of meters above ground). This is called the attachment process. The leader is connected to the ground potential, and it starts to be discharged by a ground potential wave propagating up through the leader path, a process known as the first return stroke. After about 100 μ s, the ground

potential wavefront has discharged the leader and the first return stroke is over. If additional charges are still available in the cloud, one or more leader-return stroke sequences may ensue, this time following the same ionized path previously created by the first return stroke. The subsequent leaders are called dart leaders. Dart leaders and subsequent return strokes are usually not branched. Specific characteristics of the first return stroke and subsequent return strokes will be given in Section 2.3. Often, a current of the order of 100 A continues to flow for a few milliseconds to tens of milliseconds after a return stroke. This current flow is called the continuing current which produces a slow, more or less linear, field change in close electric field records and which is responsible for forest fires.

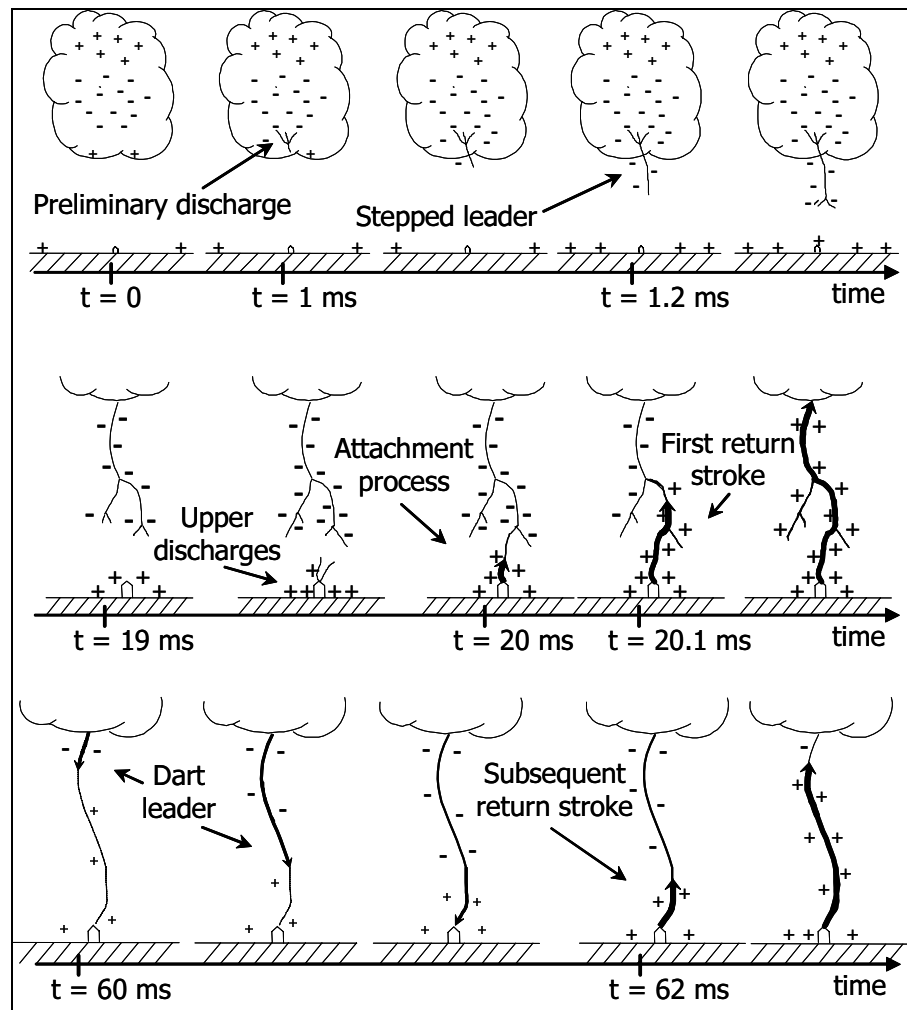


Figure 2.4 - Return stroke process for a downward negative cloud-to-ground lightning (adapted from [Uman, 1987])

A schematic representation in time of a cloud-to-ground lightning discharge with a first and two subsequent return strokes is presented in Fig. 2.5a, and Fig. 2.5.b shows a streak-camera photograph of a 12-return stroke flash.

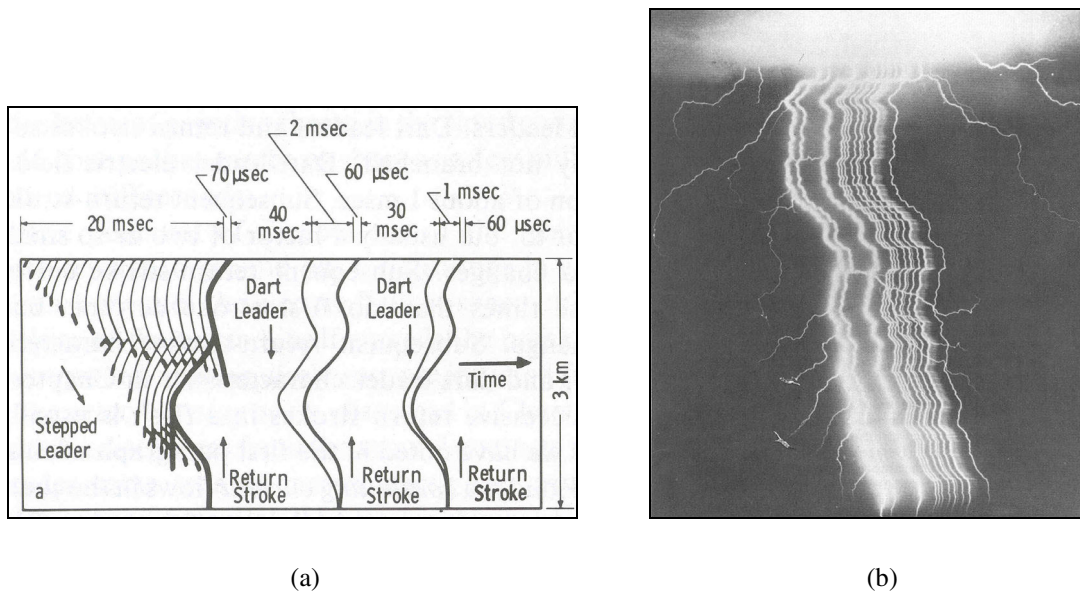


Figure 2.5 - (a) Drawing of the luminous features of a lightning flash below a 3-km cloud base as would be recorded by a streak camera, (b) Streak camera photograph of a 12-stroke lightning flash (Adapted from [Uman, 1987])

2.2 Lightning return stroke parameters useful for electromagnetic modeling: Measurement techniques

The progress made in the instrumentation and the work of researchers permitted the evolution of the knowledge on lightning discharges in several directions. The photography was probably one of the first experimental methods employed to observe the nature of lightning flashes. The invention of the double-lens streak camera in 1926 by Sir Charles Vernon Boys in England allowed the observation of the direction and the speed of the lightning discharges.

The first lightning current measurements were probably made by Pockels (1897, 1898, and 1900) in Germany. He analyzed the residual magnetic field induced in basalt by nearby lightning currents. Basalt is largely employed to measure the lightning currents in electric lines struck by lightning because of its low cost [Gary, 1995; Uman, 1987].

For modern lightning studies, sophisticated instrumentation is employed able to measure lightning discharge parameters such as: electromagnetic fields at different distances, speed of the return stroke at different heights, return stroke current at the base of the channel, branches of the channel, lightning luminosity, optical spectrum of the lightning channel, observation of the temperature and water vapor content of a lightning channel (spectroscopic system), etc. This section will focus only on the first three parameters (return stroke current, electromagnetic fields and speed), which are directly involved in the modeling of electromagnetic effects associated with lightning return

strokes. We will briefly describe experimental techniques used today to measure these parameters. The characterization of the parameters will be presented in sections 2.3 to 2.6.

2.2.1 Electromagnetic field

The electromagnetic fields associated with a lightning return stroke are characterized by a particular waveform signature which depends principally upon the distance to the impact point of the lightning return stroke, which makes them easily identifiable.

Lightning discharges have typical time durations of the order of one second, while the individual physical processes comprising these discharges and described in the previous section can vary on a millisecond, microsecond, or even submicrosecond time scale. It follows that variations of current and charge associated with a lightning flash produce “wideband” electric and magnetic fields with significant frequency content in a frequency range from 0.1 Hz to well over 10 MHz [Uman, 1987].

2.2.1.1 Electric field measurements

Concerning the lightning electric field, two different types of field sensors are used in order to measure, respectively, the electrostatic field (low frequency) and the field change associated with return strokes (high frequency).

The electrostatic **fluxmeter** or **field mill** is composed essentially by two segmented plates, in which the top grounded plate rotates so as to cover and uncover the other fixed field-detecting plate beneath it, as illustrated in Fig. 2.6. The field mill operates by sensing the charge induced on the fixed plate by the ambient electric field. The rotating top plate converts a relatively slow time-varying electric field into an ac voltage signal applied to a sensitive resistor. The voltage amplitude is proportional to the ambient electric field. A field mill can sense a dc or relatively steady field such as the one existing in fine weather or beneath clouds and it can sense lightning field changes with an upper frequency response in the 1- to 19-kHz range [Uman, 1987].

These field mills are used to measure the low frequencies components of lightning discharges as well as to detect the increasing electrostatic field beneath thunderclouds.

The second type of sensor consists of a **flat plate** or **sphere** or **vertical wire (whip)**, on which the electric field can terminate. The charge $Q(t)$ induced on the antenna by the electric field is sensed by an electronic circuit and transmitted to a recording system, as illustrated in Fig. 2.7. In the circuits shown in Fig. 2.7, either a capacitor to ground or an electronic integrator is used to integrate the

current, $Q(t)/dt$ flowing to the antenna plate. A decay time constant is present in the integrator circuit, which determines the upper frequency cutoff of the sensor.

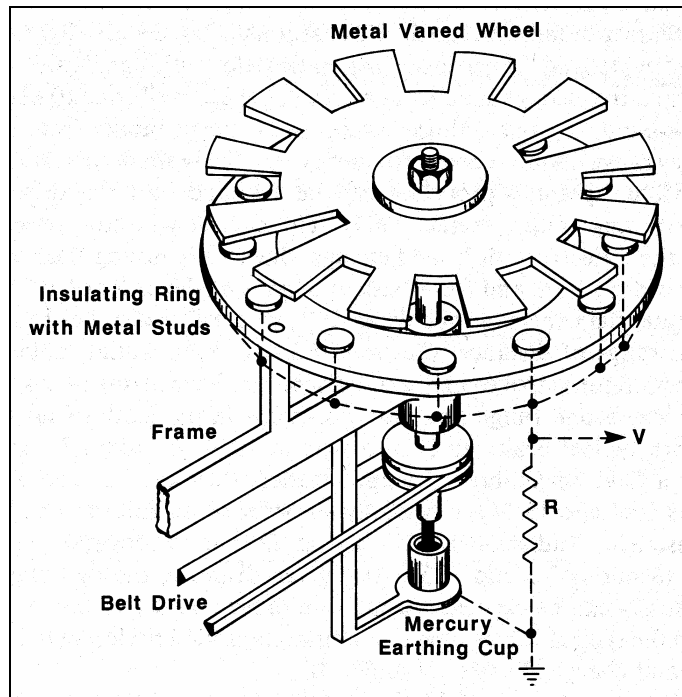


Figure 2.6 - Drawing of a field mill (adapted from [Uman, 1987]).

The electric field measuring systems in Fig. 2.7 are designed to measure the vertical component of the electric field at ground. Combined systems, e.g. spherical antennas, exist to measure simultaneously the three perpendicular components of the electric fields. Other, more complex systems combine modern filtering techniques to measure electric fields in a narrow range of frequencies to study more specific parts of the frequency spectrum of lightning [Uman, 1987].

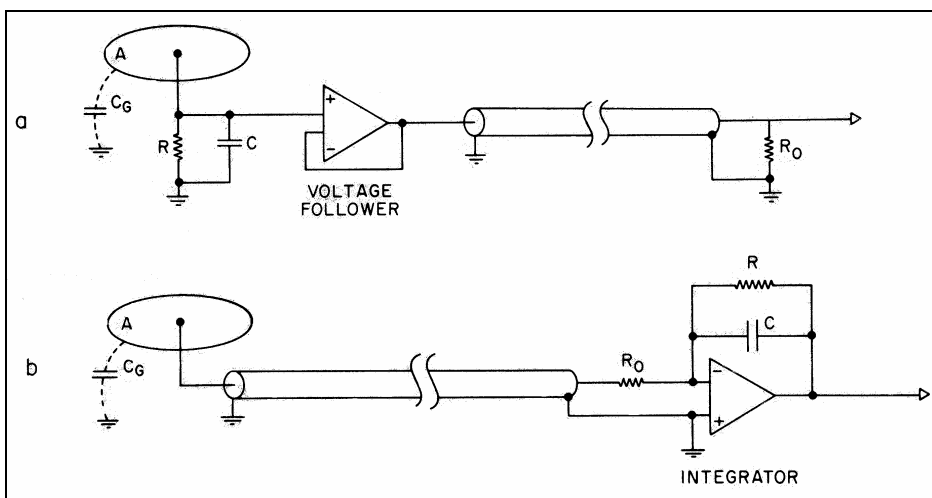


Figure 2.7 - Diagram of two electric field plate antennas (adapted from [Uman, 1987]).

2.2.1.2 Magnetic field measurements

Perhaps the simplest sensor to measure the magnetic field is an **open-circuited loop** of wire. The voltage induced in the loop is proportional to the time derivative of the magnetic flux density perpendicular to the antenna. The measured signal has then to be integrated to obtain the magnetic field. Fig. 2.8 shows a drawing of a magnetic field system and associated electronics. Besides magnetic loop-sensors, several other types of sensors have been used to measure lightning magnetic fields. For relatively low frequencies measurements, ballistic magnetometers have been used. Hall Effect or other solid-state magnetometers could also be used to measure lightning magnetic fields with very fast time response [Uman, 1987].

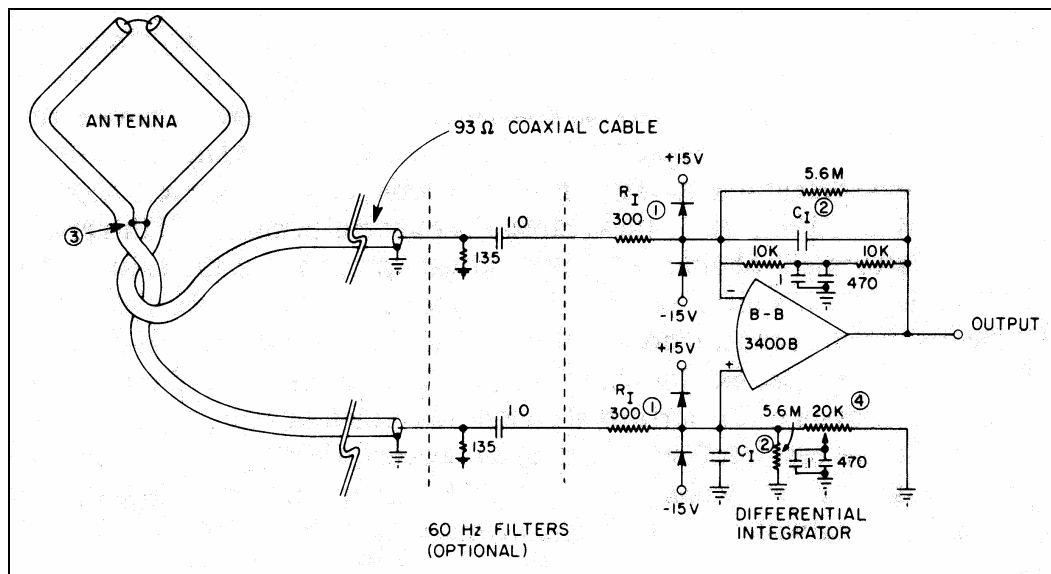


Figure 2.8 - Magnetic field antenna and associated electronics (adapted from [Uman, 1987]).

2.2.2 Return stroke speed

Another important parameter used in lightning return stroke modeling is the return stroke speed. From a theoretical point of view, the return stroke speed consists of the speed observed at the return stroke wavefront when it propagates toward the cloud or to the ground. Practically, however, to measure the return stroke speed in a flash could represent a difficult task. The luminosity of the return stroke wavefront has a shape that varies with height, so that it is not obvious how to identify the same luminous feature at different heights. However, it is believed that the error involved in identifying the time of initial exposure on streak photographs, as a basis for the speed measurements, is small, especially near ground [Uman, 1987].

2.2.2.1 Double-lens streak camera

The double-lens streak camera (called Boys camera after its inventor Sir Charles Vernon Boys, 1926) was probably the first instrument used to estimate the velocity of a lightning return-stroke. It

allows to observe the direction and the speed of the lightning discharge thanks to its continuous relative motion between the lens and the film. Fig. 2.9 shows a diagram of a Boys camera with moving film and stationary optics. Luminosity moving, for example, vertically upward, such as in a return stroke, is streaked in different directions through each of the two lenses, thus making possible a determination of return stroke speed by comparison of the two streak images and knowledge of the speed of motion of the film.

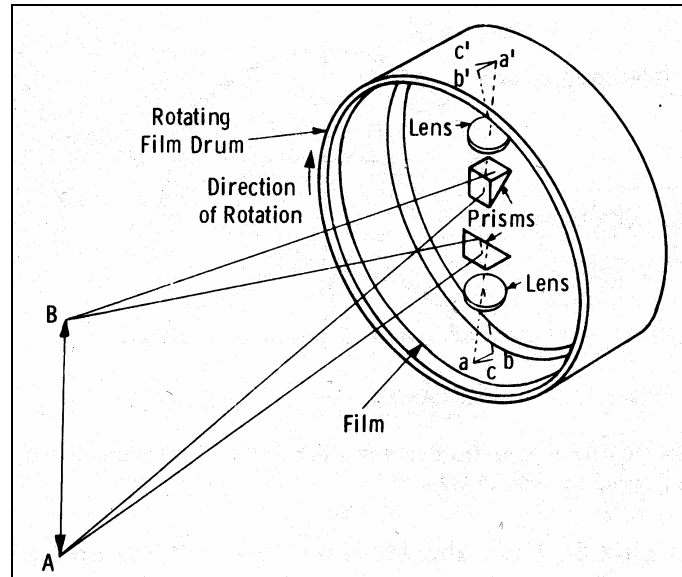


Figure 2.9 - Diagram of a Boys camera (adapted from [Uman, 1987]).

2.2.2.2 Photoelectric return-stroke velocity system

A more modern instrument to measure lightning-channel propagation velocities was developed in the 1980's. It consists of eight **solid state silicon photo-detectors** mounted behind precision horizontal slits in the focal plane of a 50-mm lens on a 35-mm camera body. Each detector has a 0.1 degree vertical field of view that is separated from adjacent detector slits by 2.8 degrees. [Mach and Rust, 1989b].

More recently, Japanese researchers have developed the so-called Automatic Lightning Discharge Progressing Feature Observation System (**ALPS**), consisting of an array of photodiodes associated with a conventional 35-mm single-lens reflex camera to infer the lightning return stroke velocity. For example, a standard 35-mm single-lens reflex camera is adapted with an array of long thin photodiodes placed behind the lens in the film chamber. Each photodiode is connected to a digital recorder which is controlled by a computer. The light emitted from a lightning path is caught by the above photodiodes and is converted to an electrical signal. As the lightning flash image in the chamber moves upward or downward, it triggers the photodiodes which are on its way. Knowing the distance represented by each segment (e.g. 29 m) and the time of propagation between the

segments, the velocity within each segment can be inferred [Hussein et al., 1995; Yokoyama et al., 1990].

2.2.3 Channel-base current

To measure a lightning return stroke current directly, knowledge of the lightning impact point is required. To carry out such measurements, two techniques are used today: (1) artificially initiated lightning using small rockets (triggered lightning, Fig. 2.10) and (2) instrumented towers (Fig. 2.11).

In both techniques, the main idea is to increase the probability of lightning impacts to a predefined point; in the first case using a rocket launched under the thundercloud, and in the second case by using a permanent elevated object (usually telecommunications towers). In both cases, the lightning return-stroke currents are measured at or near the base of the channel (typically, some meters up to some hundreds of meters above the ground).

Briefly, the technique of triggered lightning (rocket-triggered lightning) is based on the firing of a small rocket trailing a grounded wire, when the electric field at ground is sufficiently high, generally 4 to 10 kV/m. Typically, an upward positive leader starts from the tip of the rocket when the rocket is about 200-300 m high, vaporizing the trailing wire and initiating a current of the order of several hundred amperes lasting for a period of the order of several hundred milliseconds [Fisher et al., 1993], after which sequences of dart leader-return strokes similar to natural subsequent stroke occur.

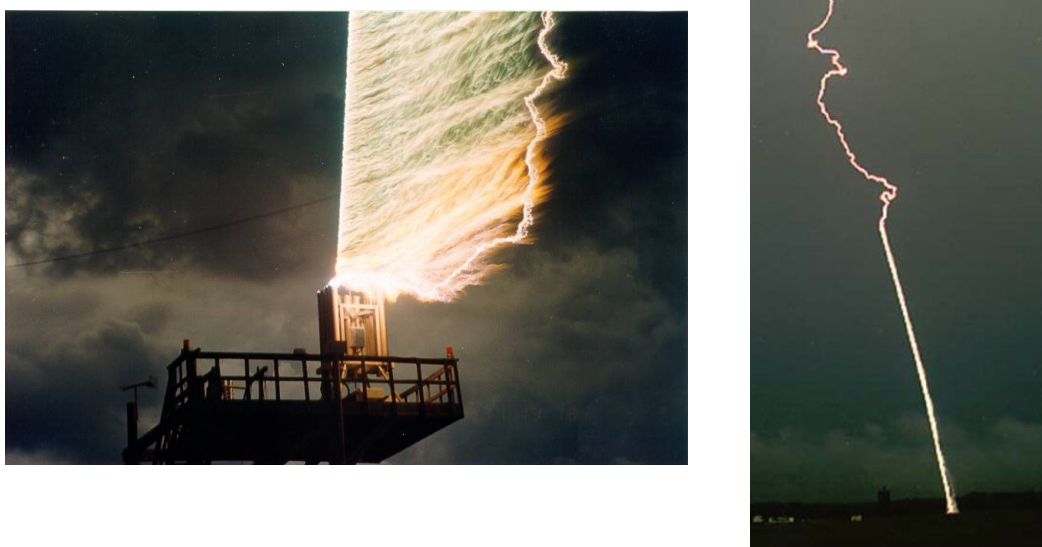


Figure 2.10 - Artificially initiated lightning via small rocket in Florida (courtesy of Lightning Research Group, University of Florida)

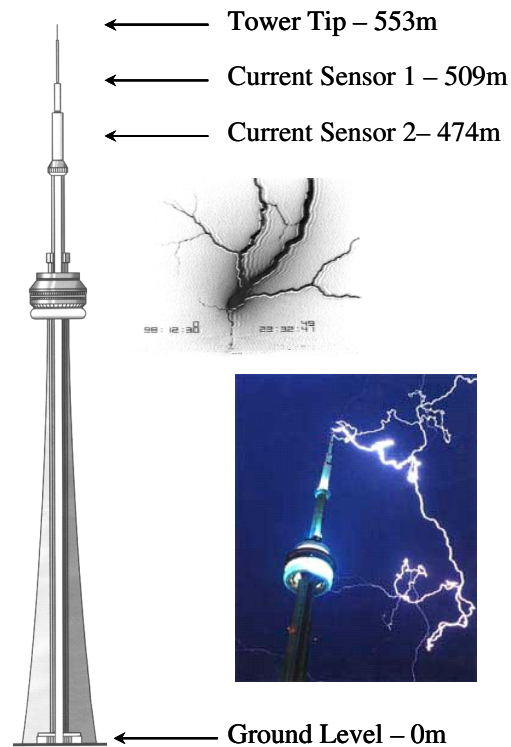


Figure 2.11 - Measurement of lightning return stroke current using instrumented towers, CN Tower in Toronto, Canada (courtesy of CN Tower Lightning Studies Group)

In general, “artificially initiated lightning” is referred to as a discharge that occurs because of the presence of a man-made structure or an artificially produced event. Artificially initiated lightning is characterized by an initial upward-moving leader either positively or negatively charged (Fig. 2.3 b and d). These types of discharges also occur naturally, for example, from mountain tops. Upward-initiated lightning has usually no “first return stroke” of the type always observed in normal downward-initiated lightning. The preliminary phase (characterized by upward-moving leaders) is often followed by combinations of downward-moving dart or dart-stepped leaders and upward-moving subsequent return strokes that appear to be very similar to subsequent strokes in normal cloud-to-ground flashes.

The most commonly occurring artificially initiated lightning is that generated by leaders moving upward from the tops of tall man-made structures such as the Empire State Building in New York, United States, the towers of Monte San Salvatore in Lugano, Switzerland, the television tower in Moscow, Russia, and the CN Tower in Toronto, Canada. The frequency distribution of lightning discharges could then vary with such factors as the height of the structure, altitude of the terrain and soil resistivity [Golde, 1977].

Lightning return stroke currents have been measured, in artificially initiated lightning, by two methods: using resistive shunts or inductive coils.

2.2.3.1 The precision shunt

The precision shunt was the first method to record the waveshape of a lightning current. The current is measured by the potential drop produced across the shunt resistance when the current crosses its terminals. In this method, the system has to be located below the top of the structure without any bypass or in a down conductor, provided this carries the full lightning current. The precision shunt provides in principle all the spectrum of frequency of the lightning current and it is perhaps the best method to measure lightning currents. Nevertheless, it is not always easy to install it in existing towers or structures, and the large variation in the magnitude of the lightning current requires very expensive constructions.

2.2.3.2 Inductive coils or loops

Inductive coils or loops are usually employed to measure the induced voltage, or the integrated voltage u with respect to time, produced by a lightning current. A toroidal coil or a pulse transformer is appropriate for these purposes. A system employing a non-ferrous, long toroidal coil with many turns, arranged on an insulated core, can be installed around the current-carrying object, e.g. in a telecommunication tower. Such coils are known in the literature as “Rogowski-coils” [Rogowski and Steinhaus, 1912]. In these coils, the induced voltage is proportional to the current time-derivative. The pulse transformer includes, in addition to the toroidal coils, a magnetic core for high frequencies. A disadvantage of these devices is the limited bandwidth in frequency. Therefore, they are suitable for measurements of impulse current (return stroke currents) but not for continuing currents [Golde, 1977].

Once the lightning return stroke current is measured, the recorded signal is generally converted to an optical signal and transmitted through optical links to a recording system, where the received signal is digitalized and stored.

2.3 Characterization of return stroke electromagnetic fields with distance

2.3.1 Measurements at distances of 1 km and beyond

Lightning return-stroke vertical electric field and horizontal magnetic flux density changes on a microsecond and submicrosecond time scale at distances superior to 1 km have been reported by many research groups. Figs. 2.12 and 2.13 present the characterization made by [Lin et al., 1979], for the E-field and H-field waveforms as a function of distance, for first and subsequent return strokes. The waveforms presented on figs. 2.12 and 2.13, correspond to fields measured from 1 to 200 km.

It can be seen that, for distances within a few kilometers:

The vertical electric field intensity of return strokes is, after the first few tens of microseconds, dominated by the electrostatic component of the total electric field, the only field component which is not zero after the stroke current has ceased to flow.

The horizontal (azimuthal) magnetic field, at similar times, is dominated by the magnetostatic component of the total magnetic field, the component that produces the magnetic field humps (shown in Fig. 2.12).

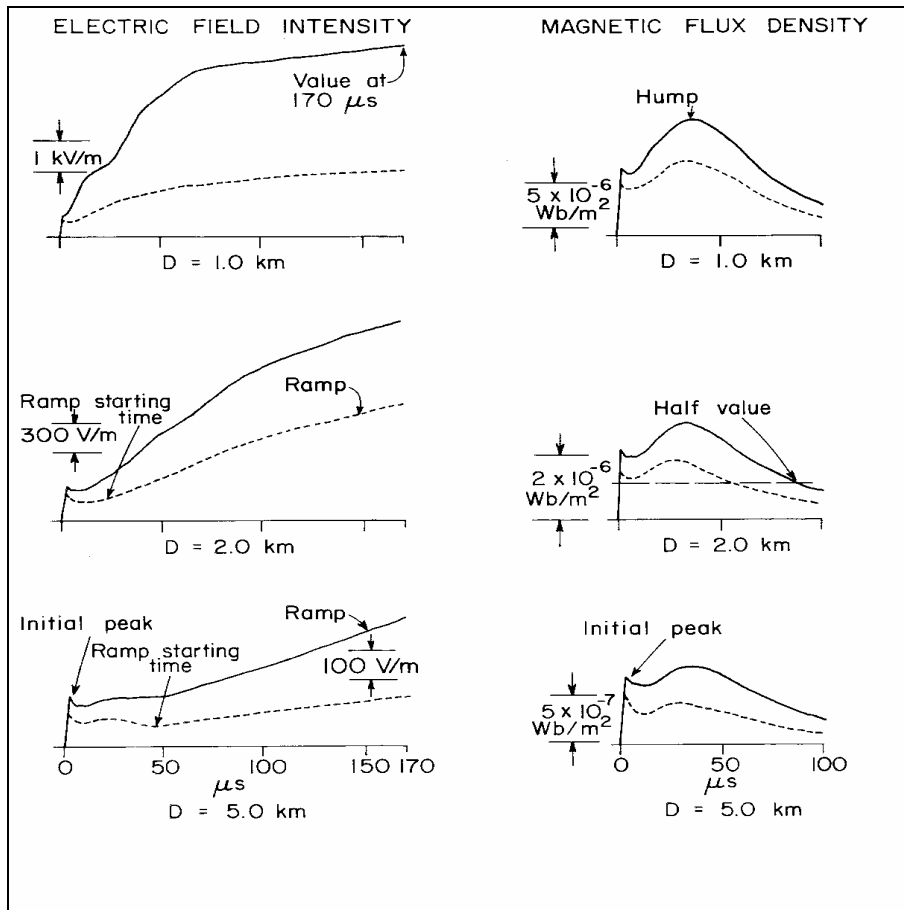


Figure 2.12 - Vertical electric field intensity and horizontal magnetic flux density for first (solid line) and subsequent (dashed line) return strokes at distances of 1, 2, and 5 Km (Adapted from [Lin et al., 1979]).

Distant electric and magnetic fields have essentially the same behavior and are bipolar. Both fields are composed basically of the radiation component of the total fields, characterized by an initial peak followed by a zero crossing at a few tens of microseconds. In practice, the fast rise, which is present at all distances, is an extremely important parameter in the evaluation of the coupling of lightning fields to nearby transmission lines.

The mean value of the electric field initial peak value, normalized to 100 km, is generally found to be in the range of 6-8 V/m for first strokes and 4-6 V/m for subsequent strokes. These values can be used as an indicator for the calibration or selection of threshold levels in experimental field

measurements. Nevertheless, additional external factors, e.g. ground conductivity of the region, can attenuate the fields due to the propagation along a non-perfectly conducting surface. The presence of elevated strike objects can also enhance the electromagnetic fields; we shall come back to this point in Chapter 5.

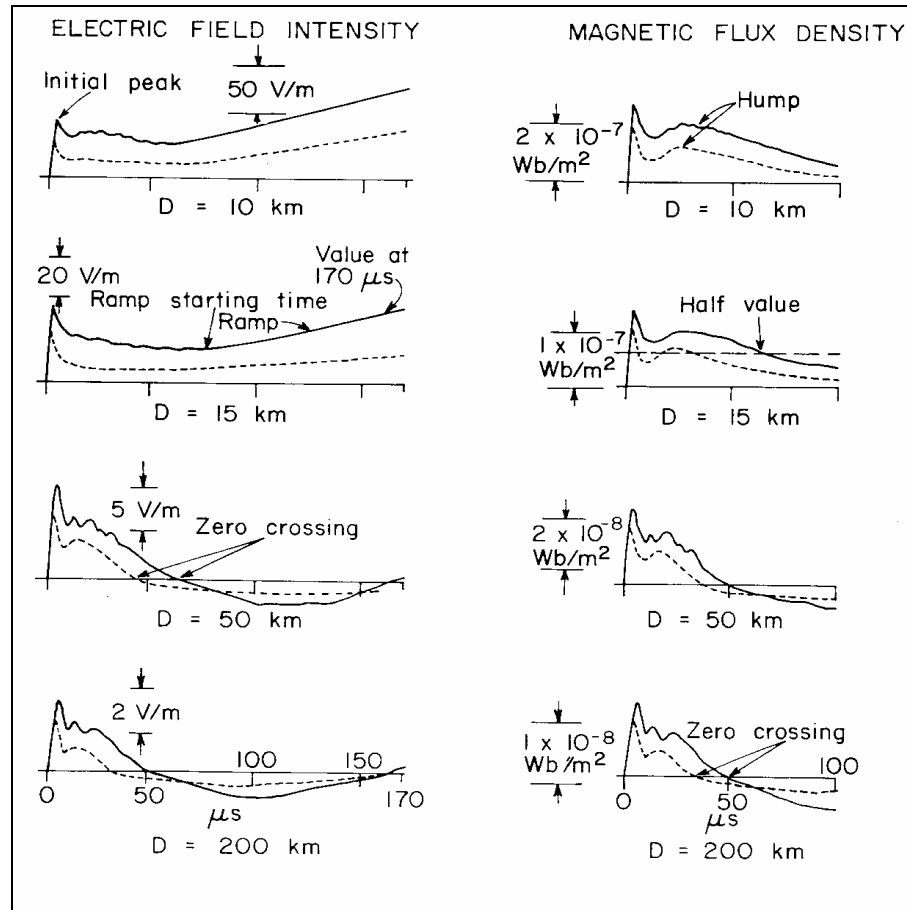


Figure 2.13 - Vertical electric field intensity and horizontal magnetic flux density for first (solid line) and subsequent (dashed line) return strokes at distances of 10, 15, 50, and 200 Km (Adapted from [Lin et al., 1979]).

Other characteristics of the electric and magnetic fields have been studied and measured in various experimental campaigns around the world, see for more details [Thottappillil, 1992]. For example the zero-crossing time for distant measured fields (Fig. 2.13) appears to change appreciably as a function of meteorological conditions, around 50 μs for first strokes measurements made in Florida and Sweden and 90 μs for first strokes measurements made in Sri Lanka. Nevertheless, subsequent strokes presented a similar mean value of around 40 μs in the three regions [Uman, 1987].

Fig. 2.14 shows a detailed waveshape associated with the radiated electric field, normalized to a distance of 100 km. Note that the electric field waveforms exhibit pulses produced during the stepped-leader process prior to the first return stroke field (labeled “L” in the figure). First return stroke fields present, in general, a “slow front” at the beginning, “F” in the figure, followed by a

“fast transition” to peak field, “R”, which exhibits a 10-90% rise time of about 0.1 μ s for field propagation over salt water. A similar behavior (an “F” slow front followed by an “R” fast transition to peak) is found in fields of subsequent strokes but, in this case, the “F” slow front is faster and the “R” fast transitions occupy a larger portion of the total rise to peak than for first strokes.

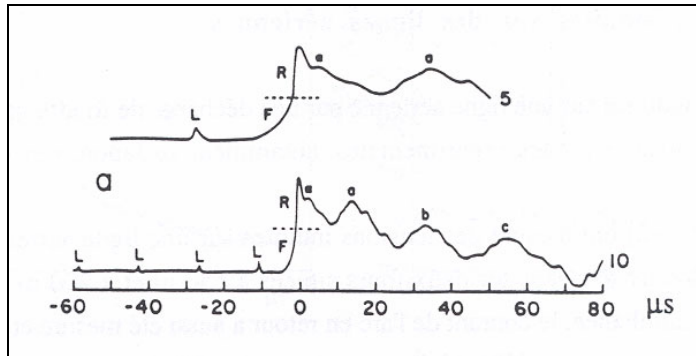


Figure 2.14 - Details of the shape of a first return-stroke radiated fields rise to peak and the fine structure after the initial peak, normalized to 100 km: L represents the small pulses due to leader steps, F is a slow front in the initial part of the waveform, R is the fast transition to peak, α is a small secondary peak or shoulder, and a, b, and c are large subsidiary peaks (Adapted from [Uman, 1987]).

Concerning the frequency spectrum of lightning fields, it was observed that, for relatively close lightning, the spectra below 10^4 Hz are dominated by induction and electrostatic fields, while the distant spectra, primarily radiation fields, exhibit a peak between 10^3 and 10^4 Hz (Fig. 2.15).

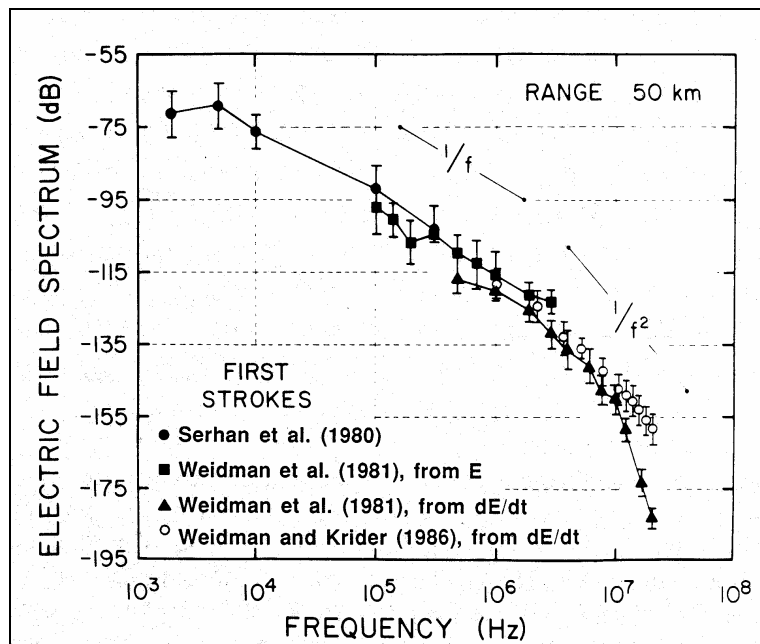


Figure 2.15 - Frequency spectra for first strokes over land and over salt water at a distance of about 50 km (Adapted from [Uman, 1987]).

After the peak for distant field, and for all close lightning, the spectrum varies inversely with frequency and, above 10^6 Hz, the decrease with increasing frequency is faster.

2.3.2 Measurements at distances below 1 km

Field measurements at close distance range (below 1 km) have been made using triggered lightning. The electric field waveform at 30 m and 500 m from triggered lightning in Florida was characterized and presented in [Rubinstein et al., 1995]. In Fig. 2.16, we show a schematic representation of the experimental campaigns at the NASA Kennedy Space Center (KSC). Some samples of data recorded in 1986 (electric field at 500 m) and 1991 (electric field at 30 m), are presented on figs. 2.17 and 2.18, respectively.

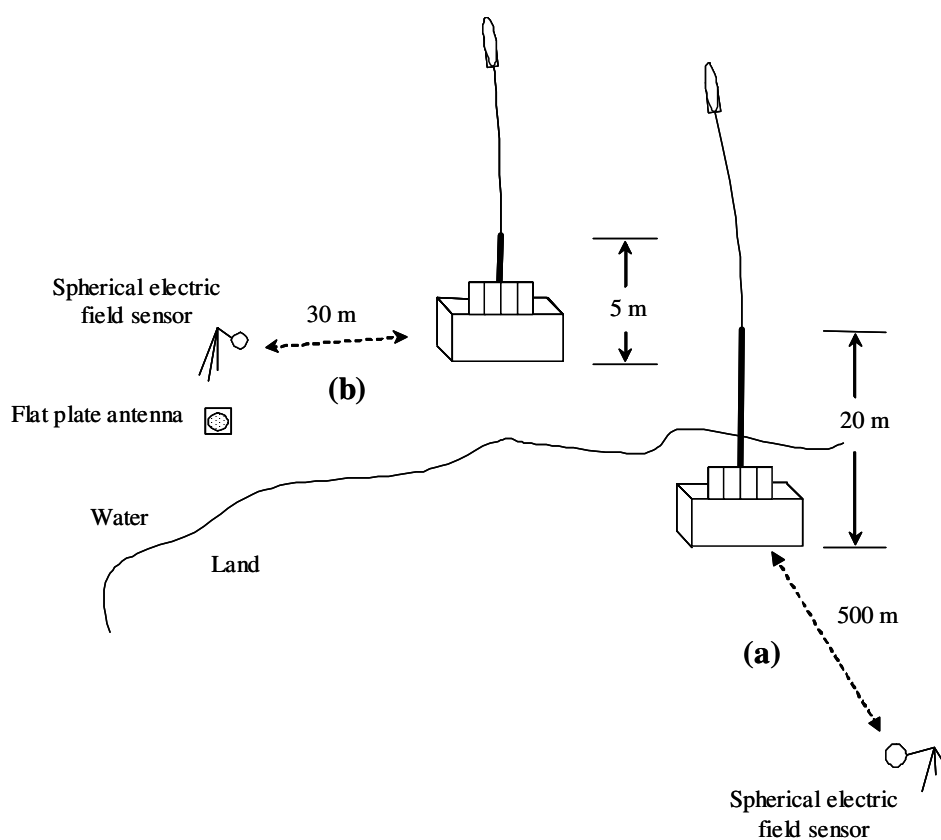


Figure 2.16 - Experimental sites for vertical electric measurements at (a) 500 m in 1986 and (b) 30 m in 1991 (Adapted from [Rubinstein et al., 1995]).

[Rubinstein et al., 1995] analyzed 40 leader-return stroke field waveforms at 500 m and 8 waveforms at 30 m. The waveforms were found to have asymmetrical V shapes, where the bottom of the V is associated with the transition from the leader (the leading edge of the pulse) to the return stroke (the trailing edge of the pulse) [Rakov, 1999; Rubinstein et al., 1995].

Fig. 2.17 presents a time span of approximately $800 \mu\text{s}$ to include part of the behavior of the electric field produced by the leader. This duration is longer than that commonly used to represent the leader return stroke combination, Interestingly, for these close fields, the ionization of the channel

by the leader modifies the vertical electric fields substantially, with a slowly increasing negative ramp. That feature is not discernible for distant fields, in which the progression of the leader remains practically invisible and it is therefore not taken into account in field representations (e.g. figs. 2.12 and 2.13).

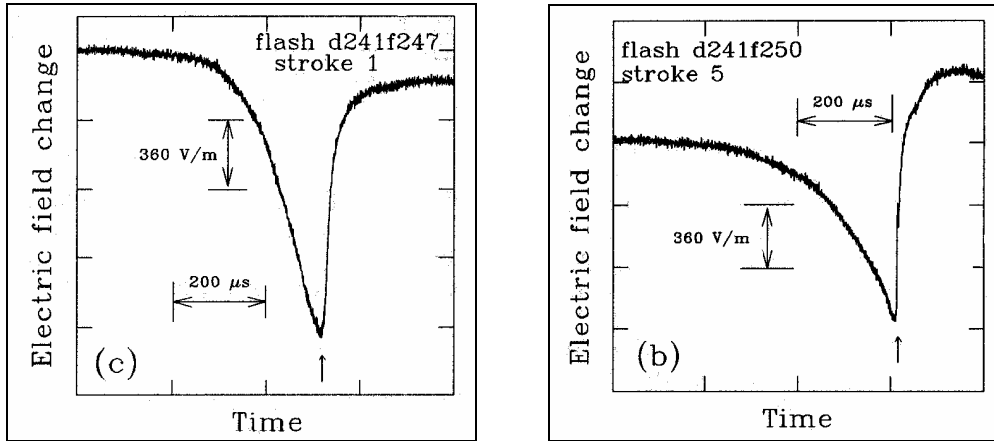


Figure 2.17 - Vertical electric fields for leader-return stroke sequences measured at 500 m in 1986. Arrows mark the assumed start of the return stroke (Adapted from [Rubinstein et al., 1995]).

The start of the neutralization of the charges in the channel by the return stroke is probably associated with the beginning of the fast positive-progression in the vertical electric field (figs. 2.17 and 2.18).

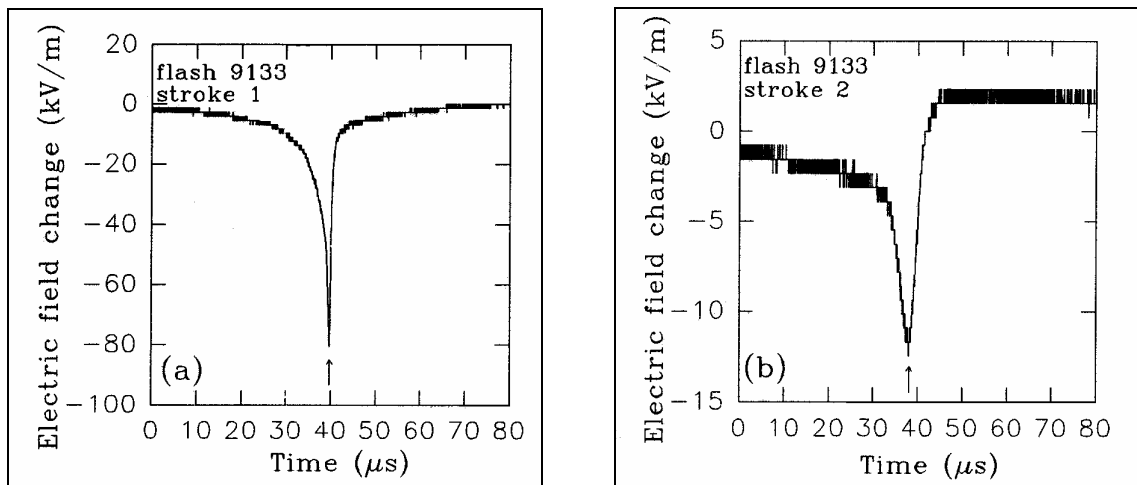


Figure 2.18 - Vertical electric fields for leader-return stroke sequences measured at 30 m in 1991. Arrows mark the assumed start of the return stroke (Adapted from [Rubinstein et al., 1995]).

2.4 Characterization of lightning return stroke velocity

One of the first important efforts to characterize lightning return-stroke velocities was carried out by Idone and coworkers in the 1970's. [Idone and Orville, 1982] measured the return stroke speed

associated with 63 events using two-dimensional high-speed streaking photographic techniques. The most important conclusions of their observations are [Idone and Orville, 1982]:

The return stroke speed was observed to decrease with height in a kilometer scale. The reduction of velocity can be substantial, with velocities in upper channel lengths often decreasing by 25% or more relative to velocities near the ground.

Subsequent return strokes are characterized by higher values for the speed compared to the first strokes. The mean values for 17 first and 43 subsequent return stroke speeds were, respectively, 9.6×10^7 m/s for the first and 1.2×10^8 m/s for subsequent return strokes.

Measurements using a photoelectric measurement system were later reported by [Mach and Rust, 1989a] and were divided in two groups: “short-channel” values with channel segments starting near the ground and less than 500 m in length (average of 330 m) and “long-channel” values that start near the ground and exceed 500 m in length (average of 990 m). Table 2.1 summarizes the values reported by [Mach and Rust, 1989a].

Table 2.1 - Return-stroke velocities reported by [Mach and Rust, 1989a] for “short-channel” and “long-channel” in negative strokes.

Type of channel	Return stroke velocity (m/s)		
	Natural first (average)	Natural Subsequent (average)	Triggered subsequent (average)
Short-channel	1.7×10^8	1.9×10^8	1.4×10^8
Standard deviation	0.7×10^8	0.7×10^8	0.4×10^8
(Number of samples)	(25)	(43)	(39)
Long-channel	1.2×10^8	1.3×10^8	1.2×10^8
Standard deviation	0.6×10^8	0.5×10^8	0.2×10^8
(Number of samples)	(25)	(54)	(40)

Mach and Rust’s measurements agree with those reported by Idone and Orville in the differences of speed between first and subsequent return strokes for natural lightning, but their differences are not as large as reported by Idone and Orville. The decrease of the return-stroke velocity with height is also observed in the Mach and Rust’s measurements.

A maximum value of 1.44×10^8 m/s for a return stroke velocity measured by an ALPS was reported by [Hussein et al., 1995] for a lightning striking to the CN Tower in Canada. Recently, ALPS was installed again to measure lightning return stroke velocities associated with lightning striking the CN Tower in 2002. The measured velocities were found to have an average of 1.2×10^8 m/s with maximum and minimum of 0.654×10^8 m/s and 1.54×10^8 m/s, respectively (provided by Dr. Chang in private communication). The average value is in good correlation with reported values from Mach and Rust for long-segment channel types. The ALPS systems was used also in Florida, as reported by [Wang et al., 1999a; Wang et al., 1999b] to study the attachment process in rocket-

triggered lightning strokes. They report two measurements, both with return-stroke velocity of $1.3 \times 10^8 \pm 20\%$ m/s.

2.5 Characterization of lightning return stroke currents

Experimental data of lightning return stroke currents can be classified into three categories: (1) data obtained using short instrumented towers (less than 100 m) (2) data obtained using triggered lightning, to some extent similar to natural subsequent return strokes, and (3) data obtained using tall instrumented towers (above 100 m).

2.5.1 Data from short towers

The most complete description to date of lightning return stroke currents at the base of the lightning channel was performed by Berger and co-workers in Switzerland using short instrumented towers. The currents were measured using resistive shunts located at the top of two towers, 70- and 90- m tall at the summit of Monte San Salvatore in Lugano. The summit of the Monte San Salvatore is 914 m above sea level and 640 m above the level of Lake Lugano, located at the base of the mountain. The measured currents were recorded using high speed cathode-ray oscillographs (installed in 1958) with four beams to record currents in both towers and two time deflections with a resolution of $0.5 \mu\text{s}$ [Golde, 1977].

About 15% of the measurements reported by Berger and co-workers were due to downward-moving stepped leaders (Fig. 2.3a). Most discharges to the towers were initiated by upward-moving stepped leaders of both polarities (Fig. 2.3b and d).

2.5.1.1 Summary of Berger's data

Figs. 2.19 and 2.20 and Table 2.2, show a compilation of measurements performed by Berger and co-workers, for lightning initiated by downward-moving leaders.

The waveforms in Fig. 2.19 correspond to normalized typical first and subsequent return strokes and are presented in two time scales, for first and subsequent return strokes. "A" corresponds to a large scale going up to $100 \mu\text{s}$ and "B" to a smaller range of $40 \mu\text{s}$ (dashed lines). In Fig. 2.19, it is possible to observe, on average, a faster risetime for the return-stroke current associated with subsequent strokes.

In Fig. 2.20, the peak current distribution is presented for negative first return strokes, negative subsequent return strokes, and positive return strokes. The slanted dashed lines represent a log normal distribution fit to the experimental data for all three cases [Uman, 1987]. The value of the distribution at 50% is around 30 kA for both, first negative and first positive return strokes. A

smaller current value of around 12 kA is observed for the 50 % abscissa for subsequent negative return strokes current-peak. Even if the subsequent return strokes current-peak distribution is somewhat lower than half of the first return-stroke current distribution, the shapes of the distributions are similar, as illustrated in Fig. 2.20 and Table 2.2.

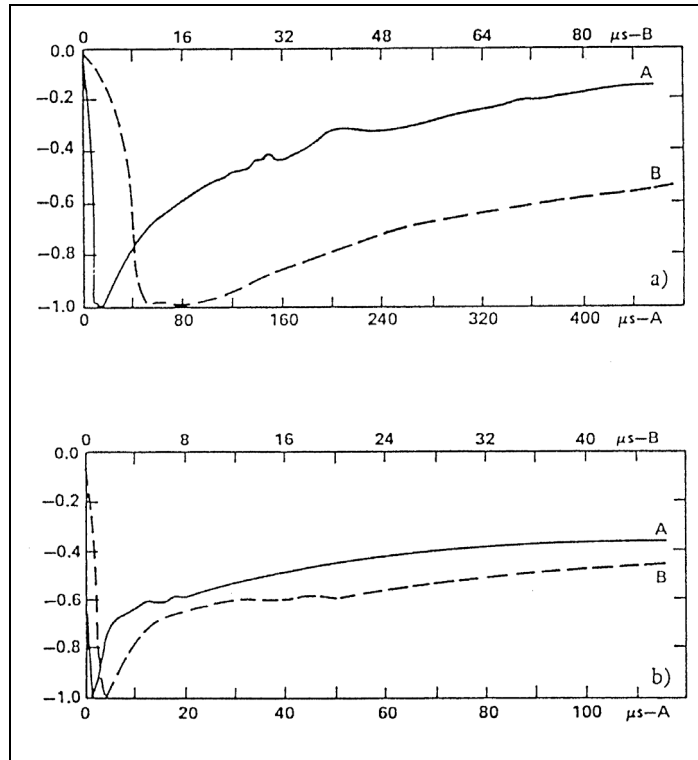


Figure 2.19 - Typical normalized negative return-stroke current waveshapes: (a) First return stroke, (b) Subsequent return stroke (Adapted from [Berger *et al.*, 1975])

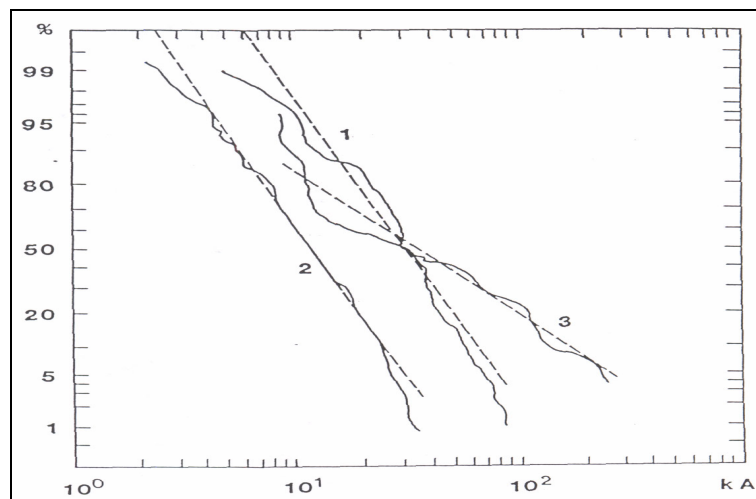


Figure 2.20 - Cumulative statistical distributions of return-stroke current peak (solid-line curves) and their log-normal approximations (slanted dashed lines) for (1) negative first strokes, (2) negative subsequent strokes, and (3) positive first strokes as reported by Berger *et al.* (1975). The vertical scale gives the percentage of peak currents exceeding a given value on the horizontal axis (Adapted from [Berger *et al.*, 1975]).

Table 2.2 - Lightning current parameters for downward flashes. (Adapted from [Berger *et al.*, 1975])

Parameter	Units	Sample size	Percent Exceeding Tabulated Value		
			95%	50%	5%
Peak current (minimum 2 kA)					
Negative first strokes	kA	101	14	30	80
Negative subsequent strokes	kA	135	4.6	12	30
Positive first strokes	kA	26	4.6	35	250
Charge (total charge)					
Negative first strokes	C	93	1.1	5.2	24
Negative subsequent strokes	C	122	0.2	1.4	11
Complete negative flash	C	94	1.3	7.5	40
Impulse charge					
Negative first strokes	C	90	1.1	4.5	20
Negative subsequent strokes	C	117	0.22	0.95	4.0
Positive first strokes	C	25	2.0	16	150
Front duration (2 kA to peak)					
Negative first strokes	μsec	89	1.8	5.5	18
Negative subsequent strokes	μsec	118	0.22	1.1	4.5
Positive first strokes	μsec	19	3.5	22	200
Maximum di/dt					
Negative first strokes	kA/μsec	92	5.5	12	32
Negative subsequent strokes	kA/μsec	122	12	40	120
Positive first strokes	kA/μsec	21	0.20	2.4	32
Stroke duration (2 kA to half-value)					
Negative first strokes	μsec	90	30	75	200
Negative subsequent strokes	μsec	115	6.5	32	140
Positive first strokes	μsec	16	25	230	2000
Integral ($i^2 dt$)					
Negative first strokes	A ² sec	91	6.0×10^3	5.5×10^4	5.5×10^5
Negative subsequent strokes	A ² sec	88	5.5×10^2	6.0×10^3	5.2×10^4
Positive first strokes	A ² sec	26	2.5×10^4	6.5×10^3	1.5×10^7
Time interval					
Between negative strokes	msec	133	7	33	150
Flash duration					
Negative (including single stroke flashes)	msec	94	0.15	13	1100
Negative (excluding single stroke flashes)	msec	39	31	180	900
Positive (only single flashes)	msec	24	14	85	500

The summary presented in Table 2.2, reports, in addition to lightning lowering negative charge to ground, some values for lightning lowering positive charge to ground. As mentioned by [Uman, 1987], there is no clear evidence that these data were not produced by upward-moving negative leaders.

The characterization of Berger's data presented in figures 2.19 and 2.20, and in Table 2.2, allows us to extract the following observations for downward flashes:

First negative return-stroke current amplitudes are larger than subsequent negative return-stroke currents, on average (2.5 times for the 50% column in Table 2.2).

The maximum risetime, di/dt , in subsequent negative return-stroke currents is larger than in first negative return-stroke currents (more than three times for the 50% column in Table 2.2).

The front duration (2 kA to peak) is shorter in subsequent negative return-stroke currents than in first negative return-stroke currents.

The stroke duration of subsequent negative return-stroke currents is shorter than that for the first negative return-strokes (around two times for the 50% column in Table 2.2).

Similar values are observed, in the 50% column of Table 2.2 for the current peak in both positive and negative first return-stroke lightning. Nevertheless, in the 5% column, current peak values in positive lightning are substantially higher than those for negative lightning. Positive strokes are higher than negative strokes, although less frequent. Similarly, positive strokes have larger front durations and larger stroke durations than negative strokes, but they exhibit lower values for the maximum risetime, di/dt , than negatives strokes.

There is, however, a controversy concerning the front duration and the maximum risetime, di/dt in Berger's data. Indeed, the instrumentation used by Berger and co-workers had a limited frequency bandwidth, which may have introduced inaccuracies in their experimental observations.

2.5.1.2 Other data obtained using short towers

Other instrumented short towers have been used around the world to measure lightning return stroke parameters. We will now briefly cite some of them in the next few paragraphs.

Garbagnati, Dellera and co-workers measured currents at the top of 40-m television towers, using resistive shunts and oscillograph recorders. The towers were located on the top of two mountains, each about 900 m above sea level [Golde, 1977; Uman, 1987]. One tower was located in the north of **Italy**, near Mt. San Salvatore (Berger's tower location), and the other tower was located in central Italy. Table 2.3 summarizes the results of the Italian group including data for upward flashes not reported in Table 2.2's Berger's data.

Table 2.3 - Return-stroke current parameters measured by Garbagnati and coworkers in Italy, for discharges lowering negative charge to ground (Adapted from [Uman, 1987]).

Parameter	Downward		Upward	
	First strokes	Subsequent strokes	First strokes	Subsequent strokes
Sample size	42	33	61	142
Peak value (kA)	33	18	7	8
Maximum rate of rise (kA/ μ s)	14	33	5	13
Time to crest (μ sec) – (3 kA to peak)	9	1.1	4	1.3
Time to half value (μ sec)	56	28	35	31
Impulse charge (C) – (to end of impulse of 500 μ sec)	2.8	1.4	0.5	0.6

Eriksson and coworkers measured lightning currents using a 60-m tall tower located above a relatively flat ground in **South Africa** in the 1970's. The tower was insulated from ground and the lightning current was measured at the bottom via a current transformer and a Rogowski coil. More than 50% of the observed flashes were initiated by the usual downward-moving negatively charged stepped leader. No positive flashes were recorded. Very fast current risetimes were observed in these measurements, not observed in other studies. Table 2.4 shows values reported by Anderson and Eriksson in 1980 (adapted from [Fisher et al., 1993]).

Table 2.4 - Return-stroke current parameters measured by Eriksson and coworkers in South Africa, for natural subsequent strokes discharges lowering negative charge to ground (Adapted from [Fisher et al., 1993]).

Parameter	Subsequent natural strokes		
	95%	50%	5%
Sample size	114		
Peak value (kA)	4.9	12	29
10 - 90% average of current steepness (kA/ μ s)	3.3	15	72
10 - 90% time duration (μ sec)	0.1	0.6	2.8

Other data have been obtained using short towers in Japan [Narita et al., 2000], in Austria ALDIS [Diendorfer et al., 2002b; Diendorfer et al., 2000], and in Colombia [Torres, 2000; Torres et al., 1999a; Torres et al., 1999b].

2.5.2 Triggered lightning data

The possibility of initiating lightning artificially by ground-based activity was apparently first investigated in the early 1960's. The first triggered lightning events were produced in 1960 by launching small rockets trailing thin grounded wires from research vessels off the Florida coast. The first triggered lightning over ground was accomplished in 1973, at Saint Privat d'Allier (SPA) in France. In the following decades, a number of triggered-lightning programs have been developed in different countries, e.g. Saint Privat d'Allier in France, Kahokugata in Japan, Langmuir laboratory in New Mexico, Kennedy Space Center in Florida, Okushishiku in Japan, Fort McClellan in Alabama and Camp Blanding in Florida [Rakov, 1999]. This technique provided additional information concerning the return-stroke lightning current at the base of the channel as well as the associated electromagnetic fields. Rocket-triggered lightning are usually upward-moving leader initiated and their characteristics are very similar to natural subsequent strokes.

It is beyond the scope of this section to cover all aspects related with the triggered lightning technique. Only those aspects relevant to this thesis will be addressed. Two techniques of triggered lightning have been reported by researchers, the "classical" triggering and the "altitude" triggering, as shown in Fig. 2.21. Classical triggering is the most effective technique and it differs from the

altitude technique only in the fact that the small rocket is trailing a grounded wire (Fig. 2.21a) while, in altitude technique, the small rocket is trailing an ungrounded wire (Fig. 2.21b).

The advantage of the altitude method is that it can reproduce to some degree the behavior of stepped leaders followed by first return strokes of natural lightning.

Concerning the characterization of return-stroke current waveforms for classical triggered lightning, [Rakov, 1999] summarized observations in Florida and France as shown in Table 2.5.

Table 2.5 - Characterization of return-stroke current peak and peak derivative from classical triggered lightning experiments in KSC-Florida and SPA-France (Adapted from [Rakov, 1999]).

Location	Years	Sample size	Current peak (kA)		Current derivative peak (kA/ μ s)	
			Median	STD	Median	STD
KSC Florida	1985-1991	305/134	12.1	9.0	91.4	97.1
SPA France	1986, 1990-1991	54/47	9.8	5.6	36.8	25.4

As seen in Table 2.5, the median values for the current are 12.1 and 9.8 kA in the USA and France, respectively. These median values differ by approximately 20%. Note the similarity of the value for the median current measured in Florida with the average value reported by Berger et al. (Table 2.2).

The rocket-and-wire technique is now frequently used for artificial initiation of lightning from natural thunderclouds in the context of lightning research. Leader/return stroke sequences in triggered lightning are similar to subsequent strokes in natural downward lightning, although the initial processes in classical triggered lightning are distinctly different from the first leader/return stroke sequence in natural downward lightning. Notwithstanding these differences, triggered lightning is a valuable research tool to investigate natural lightning. Indeed, the results of triggered lightning experiments have provided a number of insights into various lightning processes that would have been virtually impossible to obtain from direct studies of natural lightning due to its random occurrence in space and time.

One must be aware, however, of the differences between some of the properties of artificially initiated lightning when compared to its natural counterpart. Triggered lightning typically occurs in cloud conditions under which the discharge is unlikely to start independently. In addition, there is contamination of the lower portion of the lightning channel by metallic wire residue. Moreover, the channel terminates at a triggered lightning facility having specific geometrical and electrical characteristics [Jordan et al., 1992]. Triggered flashes have been reported to differ from natural

lightning flashes in that they exhibit a larger number of strokes per flash, a higher dart leader velocity, and a shorter interstroke interval duration [Idone and Orville, 1985].

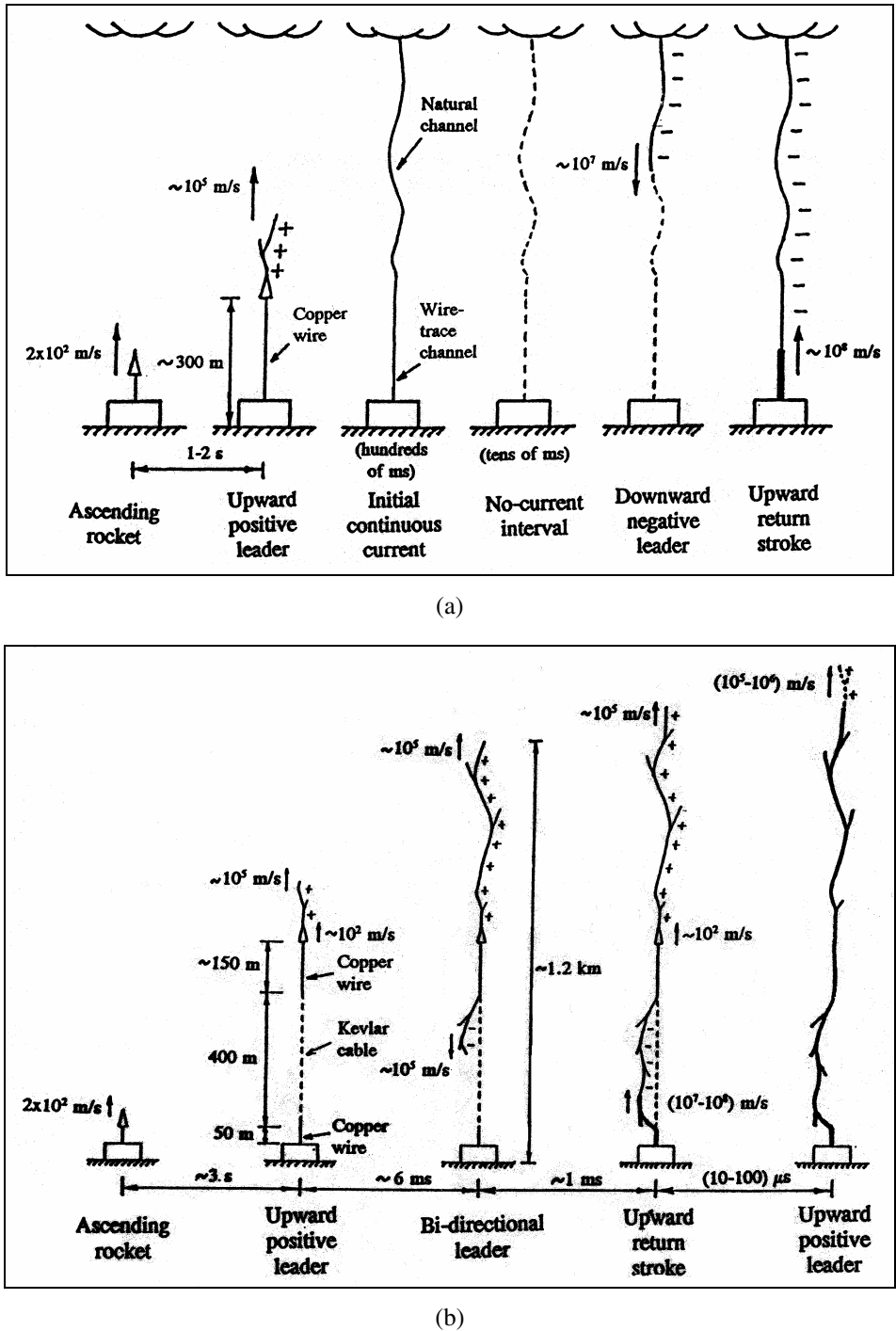


Figure 2.21 - Sequences of events for (a) classical and (b) altitude triggering techniques (Adapted from [Rakov, 1999])

2.5.3 Data from tall towers

Lightning return stroke currents measured on the 540-m high Ostankino tower in Moscow represent the first measurements of currents performed simultaneously in three different locations of the tower. The tower was instrumented with three current sensors at 533, 272 and 47 m above ground level as reported by [Rakov, 2001]. The lightning return-stroke current observations present

different waveshapes at the three observation points (Fig. 2.22). The differences are presumably due to reflections produced at the tower discontinuities during the initial lightning current propagation to ground.

Of the three waveshapes presented in Fig. 2.22, we can see that the largest “absolute peak” amplitude appears at the lower observation point (about 22 kA). It seems that, at the point of discontinuity between the bottom of the tower and the grounding impedance, there is a positive reflection of current that adds to the initial return stroke current. This positive reflection from the bottom is clearly observable at the other two locations some microseconds later. The fact that the peak amplitude of the current measured at 533 m (8 kA) is smaller than the peak amplitude at 272 m (10 kA) indicates that a negative reflection coefficient can be associated with the top of the tower. This coefficient represents the discontinuity between the tower and the “equivalent” impedance of the lightning channel.

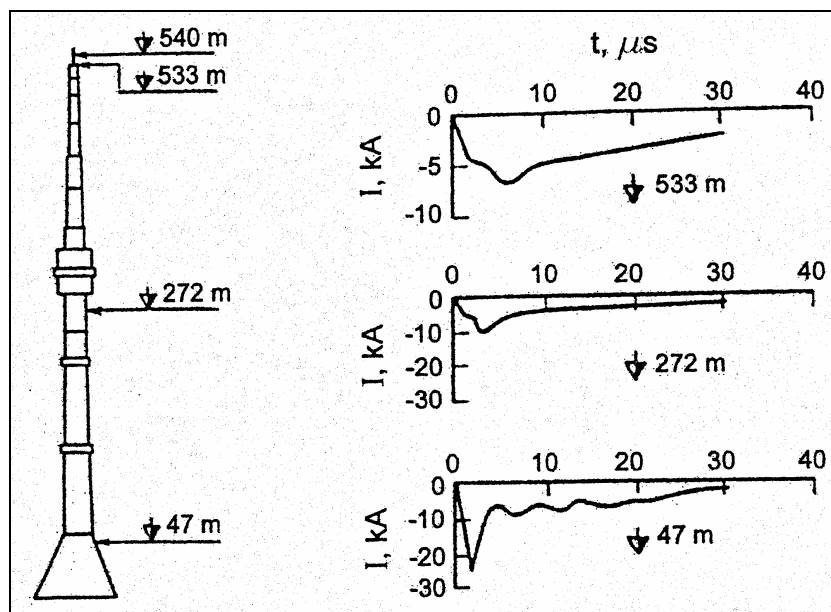


Figure 2.22 - Sample of return stroke current waveshape of upward negative lightning, recorded at three different locations in the Ostankino tower in Moscow (Adapted from [Rakov, 2001]).

Rakov reports a median peak value for currents measured at 47 and 533 m of 18 and 9 kA, respectively. He suggests that the effective grounding impedance of the tower is much smaller than its characteristic impedance and that this is appreciably lower than the equivalent impedance of lightning channel [Rakov, 2001].

Studies on lightning striking the CN Tower (553-m high) in **Toronto-Canada**, the tallest free-standing building in the world, have been performed and reported by the “CN Tower Lightning Studies Group (CNTLSG)” since 1978 (e.g. [Hussein et al., 1995; Janischewskyj et al., 1996a; Janischewskyj et al., 1997; Janischewskyj et al., 1996b]). The lightning return-stroke current

derivatives striking the CN tower are measured by two inductive Rogowski coils located at 509 and 474 m height; together with their associated vertical electric and horizontal magnetic fields at a 2 km distance. A more complete description of the CN Tower systems and of electromagnetic fields measurements at 2 and 16.8 km will be presented in Chapter 5. Fig. 2.11 shows the location of the current sensors in the tower as well as the tower complex geometry.

A sample of lightning return-stroke current observed at the CN Tower in 1999 is presented in Fig. 2.23. Lightning return-stroke currents and current derivatives observed at the CN Tower have been found to exhibit multiple reflections produced at the tower discontinuities. The observed currents and current derivatives are therefore “contaminated” by these reflections.

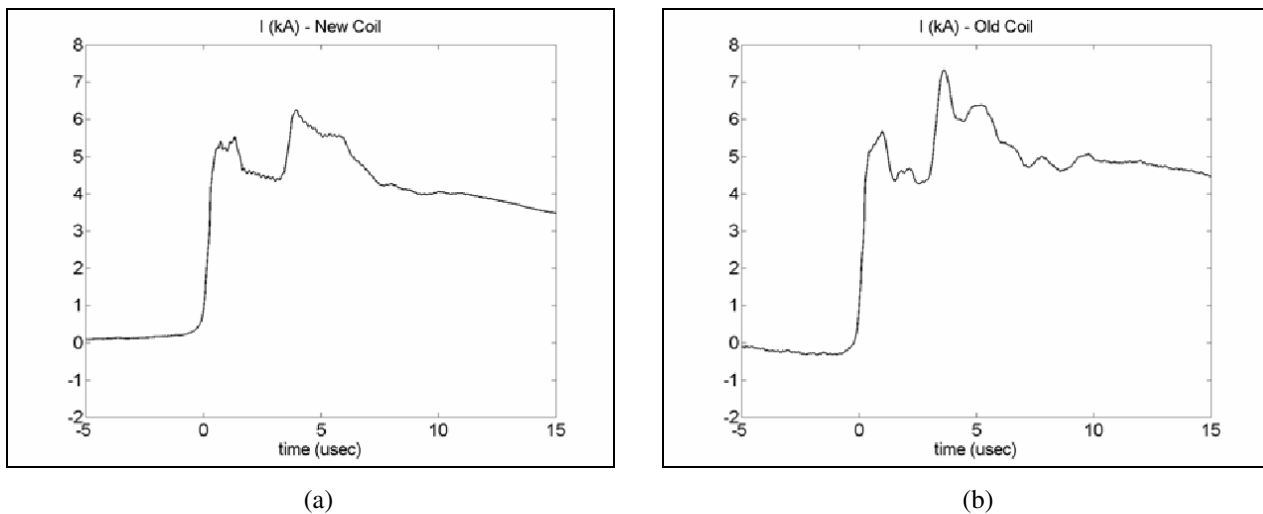


Figure 2.23 - Sample of a lightning return-stroke current observed at (a) 509 and (b) 474 m height at the CN Tower in Toronto (adapted from [Hussein *et al.*, 2002])

The waveshapes of current in Fig. 2.23 exhibit a positive reflection arriving around 3.6 microseconds after the first current maximum. This propagation time corresponds to a round-trip time from the tower top to ground, confirming that this reflection was produced at the lower discontinuity level between the tower-bottom and the grounding impedance. The positive value of the reflection implies a positive ground reflection coefficient. The observed positive reflection is less pronounced for the sensor located closer to the top of the tower. This is similar to the observations at the Ostankino tower, suggesting a negative top reflection coefficient.

However, comparing the waveshapes for the observed currents in figs. 2.22 and 2.23, we can see that the currents observed on the CN Tower exhibit more complex waveshapes than those of the Ostankino Tower. This is probably due to the more complex structure of the CN Tower (see Fig. 2.11), as suggested by Shostak [Shostak, 2001].

Reflections at the CN tower discontinuities are clearly discernible in the current derivative waveshape shown in Fig. 2.24 for a lightning return stroke recorded in 1999.

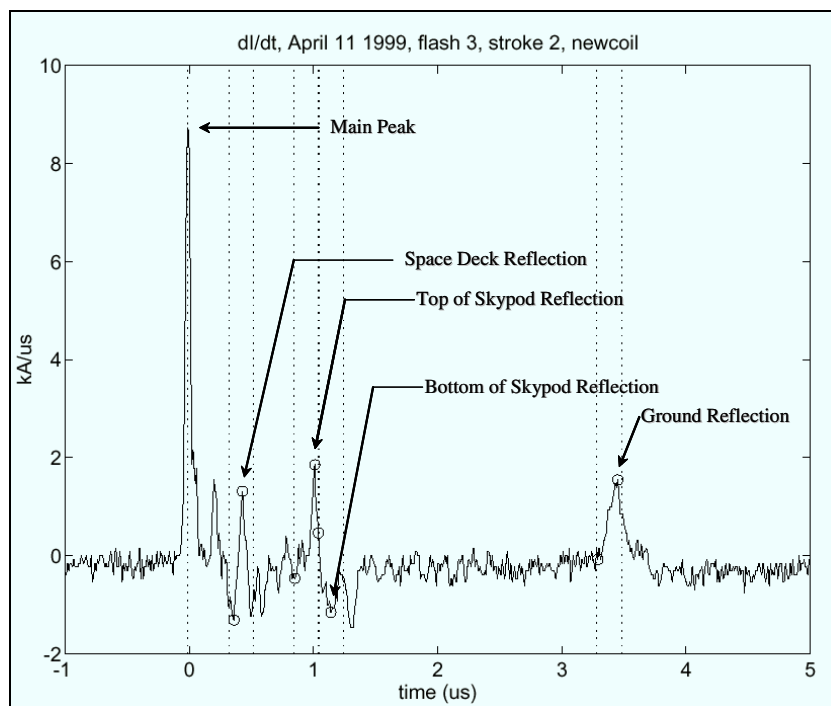


Figure 2.24 - Sample of return stroke current derivative waveshape recorded at 509 m height at the CN Tower in Toronto (courtesy of CN Tower Lightning Studies Group)

A more complete study of reflections produced in the CN Tower data was recently presented by Shostak and coworkers (see [Shostak, 2001; Shostak et al., 2002; Shostak et al., 2000a; Shostak et al., 2000b; Shostak et al., 1999]).

The 168-m high Peissenberg tower located on a ridge 250 m above the surrounding open ground and 950 m above the sea level, nearby Munich in **Germany**, was used since 1978 until 1999 to study lightning currents and their associated electromagnetic fields [Heidler et al., 2001]. The tower had two current measurement systems installed, respectively, at approximately 167 m and 13 m. The systems were able to measure return stroke currents and their derivatives. During the time of exploitation of the tower, only one stroke of a downward negative flash (cloud-to-ground lightning) was recorded by the system. The majority of the strokes recorded at the Peissenberg tower were produced by upward flashes (ground-to-cloud lightning), with negative or positive polarity. Fig. 2.25a shows a photograph of the Peissenberg tower and fig. 2.25b presents waveforms of return-stroke currents measured simultaneously at the bottom and top of the tower in which the “contamination” of the current by multiple reflections are clearly distinguishable.

The current waveshapes in Fig. 2.25b show a higher peak value for the current observed at the tower bottom. A more complete description of the Peissenberg tower system will be given in Chapter 6, as well as a detailed analysis of the reflection coefficients associated with that tower.

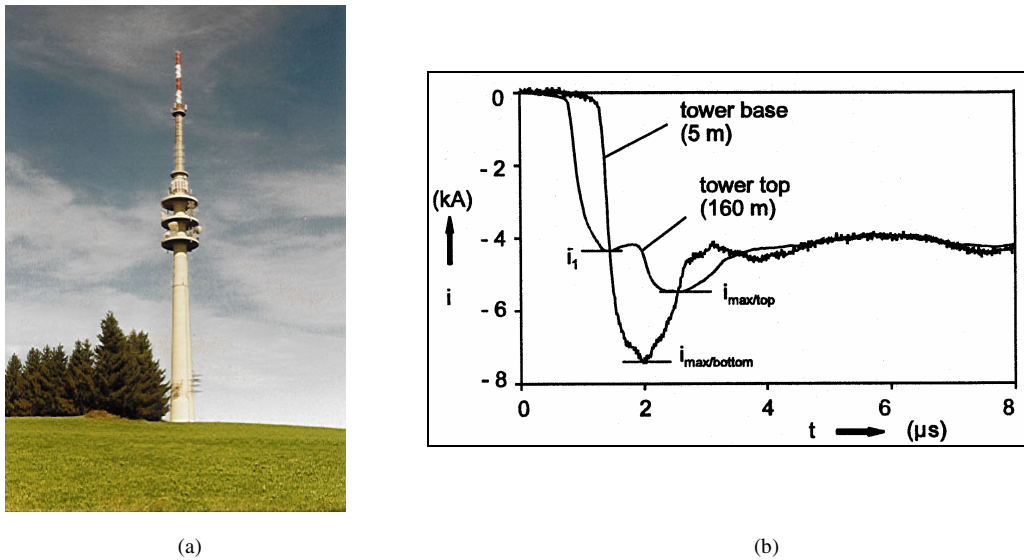


Figure 2.25 - (a) Peissenberg tower and (b) Comparison of a lightning return-stroke current recorded at the Peissenberg tower top and bottom (adapted from [Heidler *et al.*, 2001])

A 250-m tall telecommunication tower was instrumented in St. Chrischona, near Basel in **Switzerland**, with two current loop antennas at 248 and at 175 m, and an additional current probe at the top. The tower was located at the summit of a hill 500 m above sea level. The two current derivative systems as well as a current probe were used for 5 years to record lightning return stroke current waveshapes impacting the tower [Montandon and Beyeler, 1994a; Montandon and Beyeler, 1994b]. Fig. 2.26 shows the location of the measurement systems on the tower.

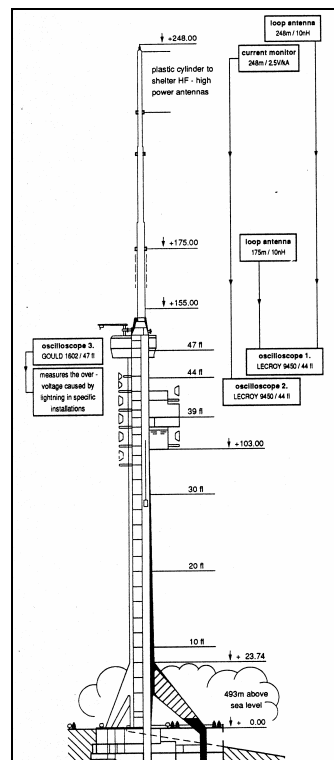


Figure 2.26 - Position of the lightning measurement equipment in the tower St. Chrischona, Switzerland (adapted from [Montandon and Beyeler, 1994b])

The 200-m high Fukui tower in Japan was also used to measure lightning return-stroke currents and their associated electromagnetic fields at the Fukui thermal power plant on the coast of the Sea of Japan. Two coaxial shunt resistors (2 m Ω , 10 m Ω) were installed at the top of the tower [Goshima et al., 2000]. It was found that the measured current was affected by reflected waves at the ground and the top of the tower. Fig. 2.27 presents a schematic representation of the installation of the Fukui tower and electromagnetic field recording system.

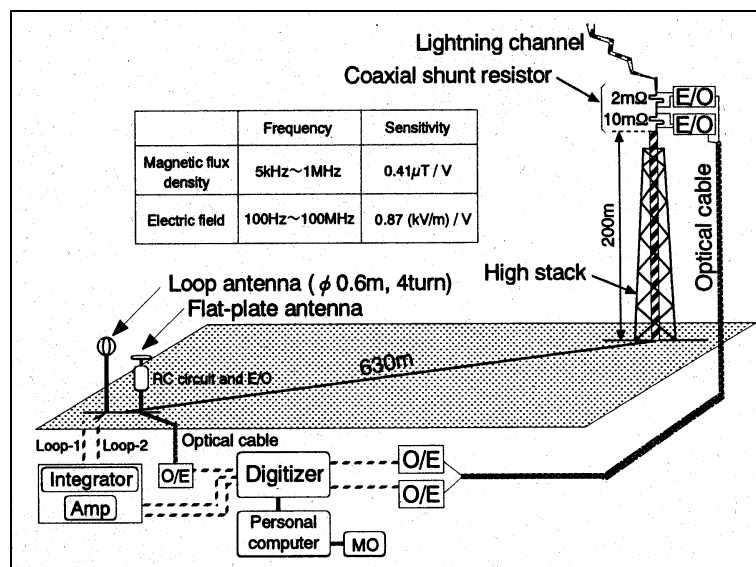


Figure 2.27 - Configuration of lightning stroke current and electromagnetic field observation systems at the Fukui thermal power plant (adapted from [Goshima et al., 2000])

This section can not be closed without mentioning one of the first experimental studies of lightning currents obtained at the top of 380 m high Empire State Building in 1935 reported in [McEachron, 1939]. The current was observed using the crater-lamp oscillograph, magnetic links and, at about 780 m distance, rotating cameras. The majority of the oscillograms recorded indicated negative currents, produced by upward-moving stepped leaders. [McEachron, 1939] was the first to discover the existence of upward-moving leaders. The leader current merged smoothly into a continuous current flow between cloud and building without the occurrence of a return stroke. In about half of these discharges, subsequent return-stroke current peaks initiated by downward-moving dart leaders followed the initial discharge stage. The maximum current recorded was 58 kA, associated to a positive stroke. The upward-moving stepped leader was found to have an average step length of 8.2 m [Golde, 1977; Uman, 1987].

2.6 Indirect estimation of currents from lightning location systems

The problem of the determination of lightning return stroke currents from remote electromagnetic field measurements has gained an increased interest due to the widespread use of lightning location

systems (LLS). Due to the enormous amount of data which can be gathered by means of LLS, such systems represent a promising source of experimental data to be used for the development of local standards related to the protection of power and telecommunication systems against lightning [Rachidi et al., 2002]. A LLS provides large scale information for lightning strikes to ground. In addition to the event time and strike point position, the LLS data can provide estimates for the lightning return-stroke peak current [Diendorfer et al., 2002a].

The most common method, employed by modern LLS, is to infer the currents from measured distant radiation fields (electric or magnetic) produced by lightning return strokes. Although this method has the distinct that it is easily obtained with today's instrumentation and can be applied over large geographical areas, a number of factors limit the accuracy of these estimates, yielding 20-30% error at best for individual discharges [De la Rosa et al., 2000].

Estimates of various lightning current parameters from the measurements of lightning electromagnetic fields are obtained by way of empirical (e.g. [Rakov et al., 1992; Willett et al., 1989]) or theoretical (e.g. [Rachidi and Thottappillil, 1993]) equations relating the electromagnetic field and the lightning current. There is, however, an inherent difficulty in extracting reliable lightning current parameters from LLS data, since unknown parameters – such as the return stroke velocity – along with possible current reflections at the channel base affect the lightning current inferred from remote electromagnetic fields [Guerrieri et al., 1998; Rachidi et al., 2001].

In general, the precise current waveshape is difficult to deduce from the electric or magnetic radiated field waveforms, but the peak current can be estimated within 20% from the measured broadband peak field assuming the simple transmission line model, TL model (this theoretical model correlating lightning return-stroke currents with electric and magnetic fields will be introduced in Chapter 3), provided that the value of the return stroke speed is known. Empirical studies by [Willett et al., 1989] as well as by [Rakov et al., 1992] have demonstrated a strong linear relationship between peak electric field and peak current, suggesting that the one free parameter in the model – return stroke velocity – is fairly constant [De la Rosa et al., 2000]. These studies were developed for subsequent lightning return-strokes in triggered lightning.

Equation (2-1) gives the expression relating the channel-base lightning return-stroke current to the far-radiated electric field and to the return stroke speed, according to the TL model and considering the geometry of Fig. 2.28 [Thottappillil and Uman, 1993].

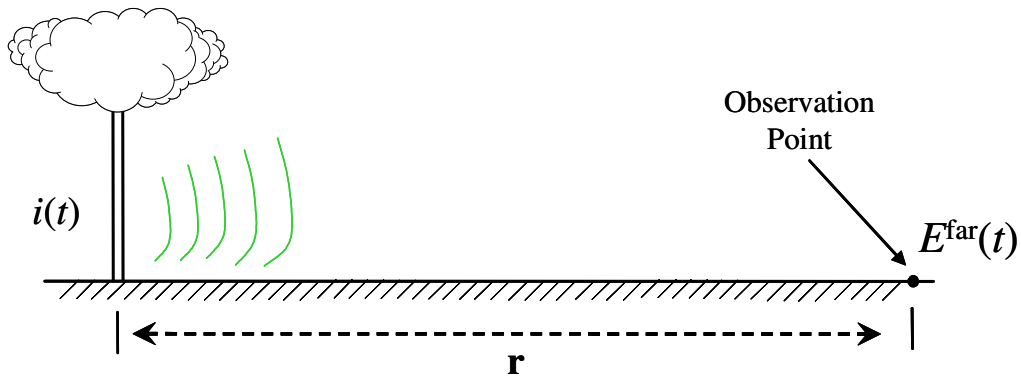


Figure 2.28 - Far electromagnetic field produced by a lightning return-stroke current.

$$i(0, t) = -\frac{2\pi\epsilon_0 c^2 r}{v} E_z^{far}(0, r, t + r/c) \quad (2-1)$$

where r is the distance between the lightning channel and the observation point, v is the associated return-stroke speed, ϵ_0 is the vacuum permittivity, and c is the speed of light.

In other words, to infer the lightning current from the remote electric or magnetic field, one has to assume the value for the return stroke speed. This speed changes, however, from one stroke to another and it could exhibit significant statistical dispersion (e.g. [Idone and Orville, 1982; Mach and Rust, 1989a]). A closer look at the far field-channel base current relations shows that an error in the estimation of return stroke speed would result practically in the same amount of error in the inferred channel-base current.

[Rachidi et al., 2002] have shown that, with the high variability of key parameters such as the return stroke speed, it is impossible to infer the lightning current accurately from the remote field measurement for a given individual event. However, [Rachidi et al., 2002] suggest that statistical estimation (e.g. in terms of mean values and standard deviations) is possible. For the TL model, they have shown that the equation allowing the calculation of the mean value of the return stroke current has the same functional form as the well-known TL far field – current relationship (Equation 2-1).

Neglecting any correlation between current peak and return stroke speed, the equations for the median value and the standard deviation for the radiated electric field in terms of the current peak, is given by [Rachidi et al., 2002]:

$$\eta_E \cong \frac{1}{2\pi\epsilon_0 c^2 r} \eta_v \eta_I \quad (2-2)$$

$$\sigma_E^2 \cong \left(\frac{1}{2\pi\epsilon_0 c^2 r} \eta_I \right)^2 \sigma_v^2 + \left(\frac{1}{2\pi\epsilon_0 c^2 r} \eta_v \right)^2 \sigma_I^2 \quad (2-3)$$

in which η_E , η_I , and η_v are the mean values of the radiated-electric field, the return-stroke current peak and the return stroke speed, respectively.

This result gives to some extent a theoretical justification to the use of LLS to infer statistical parameters of lightning current. In other words, although it seems impossible to infer accurately the return stroke current from remote field measurements for a single event without any knowledge of the return stroke speed, it would be on the other hand possible to describe the return stroke current statistically in terms of mean value and standard deviation from field measurements gathered by LLS, provided that statistical data for the return stroke speed are available.

2.7 Discussion on the relevance and accuracy of lightning return stroke current data obtained using instrumented towers

In this chapter, the electromagnetic fields, velocity and current associated with lightning return strokes have been reviewed, and the most common techniques to measure each of these parameters presented. The characterizations of these three parameters, based on observations reported by research groups around the world, were reported, with a special attention given to measurements of lightning return stroke currents. Indeed, the knowledge of lightning current parameters (peak value, front-steepness, duration) is of primary importance for the appropriate design and coordination of power system protection and insulation.

We have seen in this chapter that lightning current data comes from direct measurements using instrumented towers or triggered lightning. In addition, estimates of lightning current parameters can also be achieved indirectly from measurements of lightning electromagnetic fields.

More recent experimental data of lightning current and current-derivative obtained at the top of tall telecommunications towers have clearly shown the effect of reflections at the top and at the bottom of the tower on the measured current.

As a consequence, the problem of lightning return-stroke current ‘contamination’ from the reflections occurring along the instrumented tower has become a key area of study for lightning researchers around the world during the last years. The final goal would be to extract the primary ‘undisturbed current’ from current measurement records, removing the effect introduced by the tower characteristics.

In addition, the indirect estimation of lightning current parameters from measured fields has grown in importance in the last years due to the extensive use of the lightning location systems (LLS). The

basic aim of such systems is to provide density maps of lightning flashes. However, more recently, LLS have also been used to estimate lightning current parameters using empirical formulae. Because of the enormous amount of data they can provide and the possibility of obtaining local statistical data, it is expected that LLS will become more and more important in the near future [Guerrieri et al., 1998]. Since lightning frequently strikes tall metallic objects such as Franklin rods, radio towers, etc., the presence of such elevated strike objects is to be taken into account when inferring the current from lightning fields.

In the next chapters of this thesis, we will examine the effects of an elevated strike object on both the direct and indirect evaluations of the current parameters. Consequently, we will discuss and analyze the effect of the presence of an elevated strike object on both the directly measured lightning currents and on the associated radiated fields.

2.8 References Chapter 2

- Berger, K., R.B. Anderson, and H. Kroninger, Parameters of Lightning Flashes, *Electra*, 41, 23-37, 1975.
- De la Rosa, F., K. Cummins, L. Deller, G. Diendorfer, A. Galvan, J. Huse, V. Larsen, C.A. Nucci, F. Rachidi, V.A. Rakov, H. Torres, and M.A. Uman, Characterization of lightning for applications in electric power systems, in *Task force 33.01.02 - CIGRE*, pp. 35, 2000.
- Diendorfer, G., W. Hadrian, F. Hofbauer, M. Mair, and W. Schulz, Evaluation of lightning location data employing measurements of direct strikes to a radio tower, pp. 6, Session 2002 CIGRE, Paris, France, 2002a.
- Diendorfer, G., M. Mair, and W. Schulz, Detailed brightness versus lightning current amplitude correlation of flashes to the Gaisberg tower, in *26th ICLP (International Conference on Lightning Protection)*, pp. 8-13, Cracow, Poland, 2002b.
- Diendorfer, G., M. Mair, W. Schulz, and W. Hadrian, Lightning current measurements in Austria-experimental setup and first results, in *25th ICLP (International Conference on Lightning Protection)*, pp. 44-47, Rhodes, Greece, 2000.
- ELAT, Lightning, Atmospheric Electricity Group (ELAT), Brazilian National Institute of Space Research (INPE), "<http://www.lightning.dge.inpe.br/index.html>", 2002.

- Fisher, R.J., G.H. Schnetzer, R. Thottappillil, V.A. Rakov, M.A. Uman, and J.D. Goldberg, Parameters of triggered-lightning flashes in Florida and Alabama, *Journal of Geophysical Research*, 98 (D12), 22887-902, 1993.
- Gary, C., *La foudre: Des mythologies antiques à la recherche moderne*, MASSON, Paris, France, 1995.
- Golde, R.H., *Lightning*, 496 pp., Academic Press, London, 1977.
- Goshima, H., A. Asakawa, T. Shindo, H. Motoyama, A. Wada, and S. Yokoyama, Characteristics of electromagnetic fields due to winter lightning stroke current to a high stack, *Transactions of the Institute of Electrical Engineers of Japan, Part B*, 120 (1), 44-9, 2000.
- Guerrieri, S., C.A. Nucci, F. Rachidi, and M. Rubinstein, On the influence of elevated strike objects on directly measured and indirectly estimated lightning currents, *IEEE Transactions on Power Delivery*, 13 (4), 1543-55, 1998.
- Heidler, F., J. Wiesinger, and W. Zischank, Lightning Currents Measured at a Telecommunication Tower from 1992 to 1998, in *14th International Zurich Symposium on Electromagnetic Compatibility*, pp. 6, Zurich, Switzerland, 2001.
- Hussein, A., W. Janischewskyj, M. Milewski, V. Shostak, J.S. Chang, and W.A. Chisholm, Return-stroke current waveform parameters of lightning to the CN Tower (1992-2001), in *26th ICLP (International Conference on Lightning Protection)*, pp. 161-166, Cracow, Poland, 2002.
- Hussein, A.M., W. Janischewskyj, J.S. Chang, V. Shostak, W.A. Chisholm, P. Dzurevych, and Z.I. Kawasaki, Simultaneous measurement of lightning parameters for strokes to the Toronto Canadian National Tower, *Journal of Geophysical Research*, 100 (D5), 8853-61, 1995.
- Idone, V.P., and R.E. Orville, Lightning return stroke velocities in the Thunderstorm Research International Program (TRIP), *Journal of Geophysical Research*, 87 (C7), 4903-15, 1982.

- Idone, V.P., and R.E. Orville, Correlated peak relative light intensity and peak current in triggered lightning subsequent return strokes, *Journal of Geophysical Research*, 90 (D4), 6159-64, 1985.
- Janischewskyj, W., J.S. Chang, A.M. Hussein, V. Shostak, I. Rusan, and Y. Chen, Parameters of CN Tower lightning during severe and non-severe thunderstorms, in *10th International Conference on Atmospheric Electricity*, Osaka, Japan, 1996a.
- Janischewskyj, W., A.M. Hussein, V. Shostak, I. Rusan, J.X. Li, and J.S. Chang, Statistics of lightning strikes to the Toronto Canadian National Tower (1978-1995), *IEEE Transactions on Power Delivery*, 12 (3), 1210-1221, 1997.
- Janischewskyj, W., V. Shostak, J. Barratt, A.M. Hussein, I. Rusan, and J.S. Chang, Collection and use of lightning return stroke parameters taking into account characteristics of the struck object, in *23rd ICLP (International Conference on Lightning Protection)*, pp. 16-23, Florence, Italy, 1996b.
- Jordan, D.M., V.P. Idone, V.A. Rakov, M.A. Uman, W.H. Beasley, and H. Jurenka, Observed dart leader speed in natural and triggered lightning, *Journal of Geophysical Research*, 97 (D9), 9951-7, 1992.
- Lin, Y.T., M.A. Uman, J.A. Tiller, R.D. Brantley, W.H. Beasley, E.P. Krider, and C.D. Weidman, Characterization of lightning return stroke electric and magnetic fields from simultaneous two-station measurements, *Journal of Geophysical Research*, 84 (C10), 6307-14, 1979.
- Mach, D.M., and W.D. Rust, Photoelectric return stroke velocity and peak current estimates in natural and triggered lightning, *Journal of Geophysical Research*, 94 (D11), 13237-13247, 1989a.
- Mach, D.M., and W.D. Rust, A photoelectric technique for measuring lightning-channel propagation velocities from a mobile laboratory, *Journal of Atmospheric and Oceanic Technology*, 6 (3), 439-45, 1989b.

- McEachron, K.B., Lightning to the Empire State Building, *Journal of Franklin Institute*, 227, 149-217, 1939.
- Montandon, E., and B. Beyeler, Lightning induced voltages on electrical installations on a Swiss PTT instrumented tower in St. Chrischona , Switzerland, in *22nd ICLP (International Conference on Lightning Protection)*, pp. 6, Budapest, Hungary, 1994a.
- Montandon, E., and B. Beyeler, The Lightning Measuring Equipment on the Swiss PTT Telecommunications Tower at St. Chrischona, Switzerland, in *22nd ICLP (International Conference on Lightning Protection)*, pp. 6, Budapest, Hungary, 1994b.
- Narita, T., T. Yamada, A. Mochizuki, E. Zaima, and M. Ishii, Observation of current waveshapes of lightning strokes on transmission towers, *IEEE Transactions on Power Delivery*, 15 (1), 429-35, 2000.
- Rachidi, F., J.L. Bermudez, and M. Rubinstein, Statistical evaluation of lightning current parameters from remote electromagnetic field measurements, in *26th ICLP (International Conference on Lightning Protection)*, Cracow, Poland, 2002.
- Rachidi, F., W. Janischewskyj, A.M. Hussein, C.A. Nucci, S. Guerrieri, B. Kordi, and J.S. Chang, Current and electromagnetic field associated with lightning return strokes to tall towers, *IEEE Transactions on Electromagnetic Compatibility*, 43 (3), 356-366, 2001.
- Rachidi, F., and R. Thottappillil, Determination of lightning currents from far electromagnetic fields, *Journal of Geophysical Research*, 98 (D10), 18315-20, 1993.
- Rakov, V.A., Lightning Discharges Triggered Using Rocket-and-Wire Techniques, in *Recent Research Development on Geophysics*, edited by R. Signpost, pp. 141-171, India, 1999.
- Rakov, V.A., Transient response of a tall object to lightning, *IEEE Transactions on Electromagnetic Compatibility*, 43 (4), 654-61, 2001.

- Rakov, V.A., R. Thottappillil, and M.A. Uman, On the empirical formula of Willett et al. relating lightning return-stroke peak current and peak electric field, *Journal of Geophysical Research*, 97 (D11), 11527-33, 1992.
- Rogowski, W., and W. Steinhaus, Die Messung der magnetischen Spannung (Messung des Linienintegrals der magnetischen Feldstärke), *Archiv für Elektrotechnik*, 1 (4), 141-150, 1912.
- Rubinstein, M., F. Rachidi, M.A. Uman, R. Thottappillil, V.A. Rakov, and C.A. Nucci, Characterization of vertical electric fields 500 m and 30 m from triggered lightning, *Journal of Geophysical Research*, 100 (D5), 8863-8872, 1995.
- Shostak, V., Modeling of return stroke current for lightning events at a complex tall structure, in *2001 International workshop on electromagnetic radiation from lightning to tall structures*, pp. 4, Toronto, Canada, 2001.
- Shostak, V., W. Janischewskyj, A. Hussein, J.S. Chang, F. Rachidi, and J.L. Bermudez, Modeling of the electromagnetic field associated with lightning return strokes to a complex tall tower, in *26th ICLP (International Conference on Lightning Protection)*, pp. 167-172, Cracow, Poland, 2002.
- Shostak, V., W. Janischewskyj, A. Hussein, and B. Kordi, Electromagnetic fields of lightning strikes to a tall tower: a model that accounts for upward-connecting discharges, in *25th ICLP (International Conference on Lightning Protection)*, pp. 60 - 65, Rhodes, Greece, 2000a.
- Shostak, V., W. Janischewskyj, and A.M. Hussein, Expanding the modified transmission line model to account for reflections within the continuously growing lightning return stroke channel, in *IEEE Power Engineering Society Summer Meeting*, Cat. IEEE, Piscataway, USA, 2000b.
- Shostak, V., W. Janischewskyj, A.M. Hussein, and B. Kordi, Characteristics of return stroke current and electromagnetic field waveforms observed in multistroke lightning flashes to a tall

- tower, in *Eleventh International Symposium on High Voltage Engineering*, pp. 4, London, UK, 1999.
- Thottappillil, R., A study of cloud-to-ground lightning processes with emphasis on data analysis and modeling of the return stroke, University of Florida, Florida, 1992.
- Thottappillil, R., and M.A. Uman, Comparison of lightning return-stroke models, *Journal of Geophysical Research*, 98 (D12), 22903-14, 1993.
- Torres, H., Experimental station "Ilyapa" to measure directly lightning parameters in tropical zone, "<http://www.paas.unal.edu.co/investigacion/estacion.htm>", 2000.
- Torres, H., O. Trujillo, F. Amortegui, F. Herrera, G. Pinzon, C. Quintana, D. Gonzalez, D. Rondon, M. Salgado, and D. Avila, Experimental station to measure directly lightning parameters in tropical zone, *Eleventh International Symposium on High Voltage Engineering*, 467 (5), 1999a.
- Torres, H., O. Trujillo, F. Amortegui, G. Pinzon, C. Quintana, D. Gonzalez, D. Rondon, M. Salgado, and D. Avila, Design, construction and calibration of three devices to measure directly lightning parameters, in *Eleventh International Symposium on High Voltage Engineering*, London, UK, 1999b.
- Uman, M.A., *The lightning discharge*, 377 pp., Academic Press, Inc., Florida, USA, 1987.
- Wang, D., V.A. Rakov, M.A. Uman, N. Takagi, T. Watanabe, D.E. Crawford, K.J. Rambo, G.H. Schnetzer, R.J. Fisher, and Z.I. Kawasaki, Attachment process in rocket-triggered lightning strokes, *Journal of Geophysical Research*, 104 (D2), 2143-50, 1999a.
- Wang, D., N. Takagi, T. Watanabe, V.A. Rakov, and M.A. Uman, Observed leader and return-stroke propagation characteristics in the bottom 400 m of a rocket-triggered lightning channel, *Journal of Geophysical Research*, 104 (D12), 14369-76, 1999b.
- Willett, J.C., J.C. Bailley, V.P. Idone, A. Eybert-Berard, and L. Barret, Submicrosecond Intercomparison of Radiation Fields and currents in triggered Lightning Return Strokes

Based on the Transmission-Line Model, *Journal of Geophysical Research*, 94 (D11), 13,275 - 13,286, 1989.

Yokoyama, S., K. Miyake, T. Suzuki, and S. Kanao, Winter lightning on Japan Sea coast-development of measuring system on progressing feature of lightning discharge, *IEEE Transactions on Power Delivery*, 5 (3), 1418-25, 1990.

Chapter 3

Lightning Return Stroke Modeling

“Although lightning is the oldest electrical phenomenon studied, there is still incomplete understanding of all its aspects. This is due to its statistical nature, the hostile environment for measurements and the complexity of the associated ionization mechanisms”

[Christopoulos, 1997]

For the purpose of simulating and interpreting the effects of a lightning flash to earth, it is helpful to have a simple mathematical expression describing the spatial-temporal distribution of lightning current along the channel and its associated electromagnetic fields. However, a complete model of the entire lightning phenomenon is probably impossible to obtain and existing models represent some specific aspects of the physical process involved in the discharge. In this chapter, I will briefly describe some established approaches to model the current and the electromagnetic fields associated with the return stroke phase of a lightning discharge. There is no intention to present an exhaustive literature survey and, in what follows, only those models of interest for engineering applications due to their relative simplicity, with small number of unknowns, will be treated.

The evaluation of electromagnetic effects associated with a lightning return stroke process generally include the following points: (1) Characterization and representation of the return stroke channel-base current; (2) specification of the spatial-temporal distribution of the return-stroke current along the channel (using return-stroke models); (3) calculation of radiated electromagnetic fields; and (4) modeling the coupling of electromagnetic fields to electrical systems. This last part is not covered in this thesis and the reader can find exhaustive analyses in the literature (see e.g. [Nucci, 2001]). The other three parts will be described below in reverse order, starting from the general electromagnetic field equations to the specificity of the models.

The primary aim is to calculate the return stroke electromagnetic field given a certain lightning current or, vice versa, inferring the lightning current from remote electromagnetic field measurements.

3.1 Electromagnetic field associated with a return stroke

Generally, the calculation of electric and magnetic fields associated with a cloud-to-ground lightning return stroke is based on a certain number of commonly-adopted assumptions, namely

- the lightning channel is represented by a straight vertical antenna along which the return stroke front propagates upward at the return stroke speed,
- the ground is assumed to be flat, homogeneous and characterized by its conductivity and its relative permittivity.

Fig. 3.1 shows a schematic representation of the lightning channel’s assumed geometry and indicates also the observation point P where the fields will be calculated. The cylindrical coordinate system is adopted to represent the fields in this geometry.

[Wait, 1996] and [Baños, 1966] treated the complete problem of the electromagnetic radiation of a dipole over a finitely conducting half-space by determining the solution of Maxwell's equations for both media in accordance with the boundary conditions on the air-ground interface. The resulting equations are obtained in the frequency domain and are in terms of slowly converging integrals (Sommerfeld integrals). The problem is greatly simplified if one assumes a perfectly-conducting ground. In that case, the components of the electric and magnetic fields at the location $P(r, \varphi, z)$ produced by a short vertical section of infinitesimal channel dz' at height z' carrying a time-varying current $i(z', t)$ can be computed in the time domain using the following relations, (e.g. [Nucci, 1995; Uman et al., 1975])

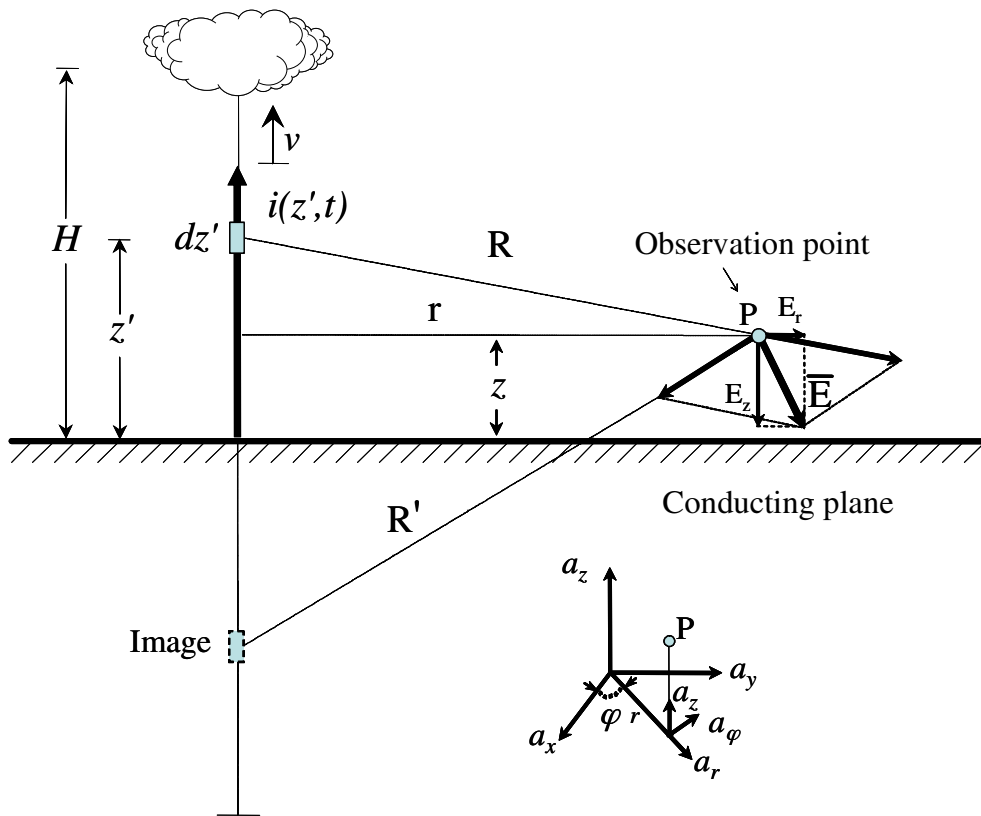


Figure 3.1 - Geometrical parameters used in calculating return stroke fields (adapted from [Uman et al., 1975]).

$$dE_z(r, \varphi, z, t) = \frac{dz'}{4\pi\epsilon_0} \left[\frac{2(z-z')^2 - r^2}{R^5} \int_0^t i(z', \tau - R/c) d\tau + \frac{2(z-z')^2 - r^2}{cR^4} i(z', t - R/c) + \frac{r^2}{c^2 R^3} \frac{\partial i(z', t - R/c)}{\partial t} \right] \quad (3-1)$$

$$dE_r(r, \varphi, z, t) = \frac{dz'}{4\pi\epsilon_0} \left[\frac{3r(z-z')}{R^5} \int_0^t i(z', \tau - R/c) d\tau + \frac{3r(z-z')}{cR^4} i(z', t - R/c) + \frac{r(z-z')}{c^2 R^3} \frac{\partial i(z', t - R/c)}{\partial t} \right] \quad (3-2)$$

$$dB_\varphi(r, \varphi, z, t) = \frac{\mu_0 dz'}{4\pi} \left[\frac{r}{R^3} i(z', t - R/c) + \frac{r}{cR^2} \frac{\partial i(z', t - R/c)}{\partial t} \right] \quad (3-3)$$

where,

- $i(z', t)$ is the current carried by the dz' dipole at time t ;
- ϵ_0 is the permittivity of the vacuum;
- μ_0 is the permeability of the vacuum;
- c is the speed of light;
- R is the distance from the dipole to the observation point, and
- r is the horizontal distance between the channel and the observation point.

In equations (3-1) and (3-2), the terms containing the integral of the current (charge transferred through dz') are called “electrostatic fields” and, because of their $1/r^3$ distance dependence, they are the dominant field component close to the source. The terms containing the derivative of the current are called “radiation fields” and, due to their $1/r$ distance dependence, they are the dominant component far from the source. The terms containing the current are called “induction fields”. In Eq. (3-3), the first term is called “induction or magnetostatic field” and is the dominant field component near the source, and the second term is called “radiation field” and is the dominant field component at far distances from the source.

In these equations the presence of the perfectly conducting ground is taken into account by replacing the ground by an equivalent image as shown in Fig. 3.1.

The total fields produced by the return stroke current at the observation point are obtained by integration of the previous equations along the channel and its image.

For distance ranges beyond several kilometers, the propagation over a ground of finite conductivity results in a noticeable attenuation of high frequency components of the fields (e.g. [Cooray, 1987]). However, for this range of distances, the inducing effect of lightning becomes less important. At

distances from the lightning channel not exceeding about one kilometer, the vertical component of the electric field and the azimuthal magnetic field can be calculated with reasonable approximation assuming the ground as a perfect conductor (e.g. [Rachidi et al., 1996]). However, the horizontal (radial) component of the electric field radiated by lightning is more affected by a finite ground conductivity. Although at some meters above ground its intensity is much smaller than that of the vertical component, within the context of certain field-to-transmission line coupling models (e.g. [Agrawal et al., 1980a; Agrawal et al., 1980b]), the horizontal electric field plays an important role and thus, its calculation requires the use of the rigorous expressions or at least reasonable approximations of those. Of the many approximations proposed in the literature, the Cooray-Rubinstein formula (e.g. [Cooray, 1992; Rubinstein, 1996; Wait, 1997]) represent an efficient tool and it allows the computation of the horizontal electric field above a finitely-conducting ground with reasonable accuracy.

The calculation of the electromagnetic field requires the knowledge of the spatial-temporal distribution of the current along the channel, $i(z',t)$. This distribution is specified using a return stroke current model.

3.2 Return stroke current models

Return stroke modeling is of interest for various reasons, e.g. as a part of a general investigation into the physics of lightning, as a mechanism by which return strokes currents at ground can be determined from remotely measured electric and magnetic fields, and hence by which either currents of individual strokes or statistical distributions of the stroke currents can be obtained, and as a mechanism for calculating realistic fields to be used in “coupling” calculations such as to determine the lightning-induced voltages appearing on electric utility or telecommunication lines when lightning occurs near those lines [Nucci et al., 1990].

Return-stroke current models have been the subject of some reviews in the last years, e.g. [Gomes and Cooray, 2000; Nucci, 1995; Nucci et al., 1990; Rakov, 2002; Rakov and Uman, 1998; Thottappillil et al., 1997; Thottappillil and Uman, 1993]. In [Rakov, 2002], lightning return stroke models are categorized into four classes: (1) the gas dynamic models, (2) the electromagnetic models, (3) the distributed circuit models, and (4) the engineering models. A general description of the four classes of models can be found in [Rakov, 2002; Rakov and Uman, 1998], and is summarized here under:

- a) The first defined class of models, gas dynamic or “physical” models, is primarily concerned with the radial evolution of a short segment of the lightning channel and its associated shock

wave. Principal model's outputs include temperature, pressure, and mass density as a function of the radial coordinate and time (e.g. [Plooster, 1970; Plooster, 1971a; Plooster, 1971b]).

- b) Electromagnetic models, or second class models, are usually based on the so-called lossy thin-wire antenna approximation of the lightning channel. These models involve a numerical solution of Maxwell's equations to find the current distribution along the channel from which remote electric and magnetic field can be computed (e.g. [Moini *et al.*, 2000], [Baba and Ishii, 2001]).
- c) The third class of models is the distributed circuit models, also called RLC transmission line models. They can be viewed as an approximation to the electromagnetic models and they represent the lightning discharge as a transient process on a transmission line characterized by resistance, inductance and capacitance, all per unit length. These models are used to determine the channel current versus time and height and can therefore also be used for the computation of remote electric and magnetic fields. (e.g. [Little, 1978; Price and Pierce, 1972])
- d) The last class is the engineering models in which a spatial and temporal distribution of the channel current (or the channel line charge density) is specified based on such observed lightning return-stroke characteristics as current at the channel base, the speed of the upward-propagating wavefront, and the channel luminosity profile (e.g. [Gomes and Cooray, 2000; Nucci *et al.*, 1990; Rakov and Uman, 1998]). In these models, the physics of the lightning return stroke is deliberately downplayed, and the emphasis is placed on achieving agreement between the model-predicted electromagnetic fields and those observed experimentally at distances from tens of meters to hundreds of kilometers.

In this study, we will consider only the engineering models, essentially for two reasons. First, engineering models are characterized by a small number of adjustable parameters, usually only one or two besides the specified channel-base current. Second, engineering models allow the return stroke current at any point along the lightning channel, $i(z',t)$, to be simply related to a specified channel-base current $i(0,t) = i_o(t)$. Indeed, it is only the channel-base current that can be measured directly and for which experimental data are available.

In what follows, a few engineering return stroke models that are widely used in the literature will be illustrated.

3.2.1 The Bruce-Golde (BG) model [Bruce and Golde, 1941]

This model considers that the current $i(z',t)$ equals the current at ground $i_o(t)$ beneath the wavefront of the upward-moving return stroke; above the wavefront, similar to all the other return stroke models, the current is zero (see Fig. 3.2).

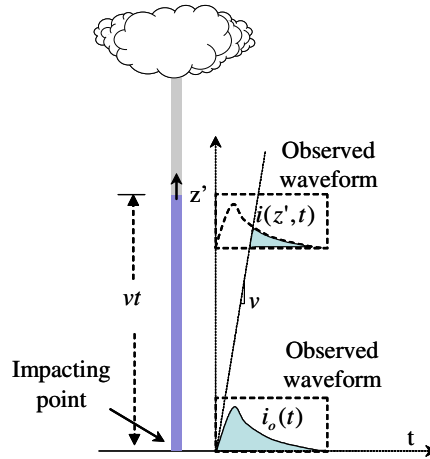


Figure 3.2 - Return stroke current propagating-upward according to the BG Model.

Mathematically,

$$\begin{aligned}
 i(z',t) &= i_o(t) & \forall & z' \leq vt \\
 i(z',t) &= 0 & \forall & z' > vt
 \end{aligned}
 \tag{3-4}$$

where v is the speed of propagation of the return stroke wavefront.

In this model a discontinuity appears at the return-stroke wavefront, which represents an instantaneous removal of charge from the channel at each height $z'=vt$ by the return-stroke wavefront. It is not physically possible for current to have the BG form (although it may be an approximation to the actual current) because, besides the discontinuity mentioned above, if the return stroke current is to be uniform with altitude, every point on the return stroke channel must instantaneously assume the current value at the return stroke wavefront, and such information transfer cannot take place at a finite speed (e.g. [Nucci et al., 1990]).

3.2.2 The Transmission Line (TL) model [Uman and McLain, 1969]

This model assumes that the lightning channel can be represented by a lossless transmission line. Therefore, the current waveform at the ground travels upward undistorted and unattenuated at a constant propagation speed v (see Fig. 3.3). Mathematically, the TL is described by

$$\begin{aligned}
 i(z',t) &= i_o(t - z'/v) & \forall & z' \leq vt \\
 i(z',t) &= 0 & \forall & z' > vt
 \end{aligned}
 \tag{3-5}$$

The TL model allows the transfer of charge from the bottom of the leader channel to the top and does not remove any net charge from the channel [Nucci *et al.*, 1990]. This is one reason why the field calculated from the model does not agree with measurements at longer times [Nucci *et al.*, 1990].

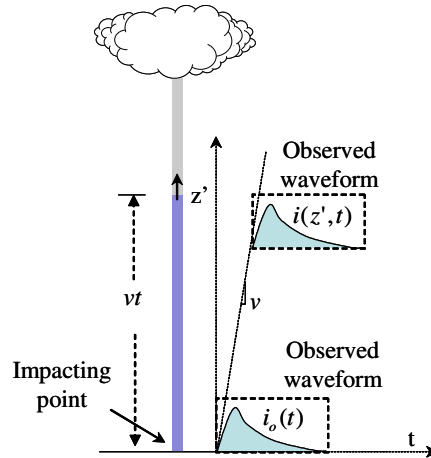


Figure 3.3 - Return stroke current propagating-upward according to the TL Model.

3.2.3 The Modified Transmission Line (MTL) model

Since the TL model does not allow charge to be removed from the leader channel and hence does not produce fields that are realistic at long times, two modifications to the TL model have been proposed by [Nucci *et al.*, 1988] and by [Rakov and Dulzon, 1987]. These two models are described hereunder.

3.2.3.1 MTLE model ([Nucci *et al.*, 1988], [Rachidi and Nucci, 1990])

In the modified transmission line model with exponential decay with height, MTLE, proposed by Nucci *et al.* in 1988, the current intensity is supposed to decay exponentially while propagating up the channel as expressed by,

$$\begin{aligned} i(z', t) &= i_o(t - z'/v) e^{-z'/\lambda} & \forall & z' \leq vt \\ i(z', t) &= 0 & \forall & z' > vt \end{aligned} \quad (3-6)$$

where the factor λ is the decay constant which allows the current to reduce its amplitude with height. This constant has been determined using experimental data to be about 2 km ([Nucci and Rachidi, 1989]). The decay constant was introduced to take into account the effect of charges stored in the corona sheath of the leader which are subsequently neutralized during the return stroke phase.

3.2.3.2 MTL model ([Rakov and Dulzon, 1987])

In the MTL model with linear current decay, MTL, proposed by Rakov and Dulzon in 1987, the current intensity is supposed to decay linearly while propagating up the channel and it is expressed by,

$$\begin{aligned} i(z', t) &= i_o(t - z'/v)(1 - z'/H_{tot}) & \forall z' \leq vt \\ i(z', t) &= 0 & \forall z' > vt \end{aligned} \quad (3-7)$$

where the factor H_{tot} is the total channel height.

3.2.4 The Traveling Current Source (TCS) model ([Heidler, 1985a])

In the TCS model, proposed by Heidler in 1985, a current source travels upward at speed v from ground to the cloud. The current injected by this source at height z' is assumed to propagate down the channel at the speed of light c . Therefore, the current at height z' would be equal to the current at ground at an earlier time z'/c . This is mathematically described by,

$$\begin{aligned} i(z', t) &= i_o(t + z'/c) & \forall z' \leq vt \\ i(z', t) &= 0 & \forall z' > vt \end{aligned} \quad (3-8)$$

3.2.5 Generalization of the RS Models

[Rakov, 1997] and recently [Rakov, 2002] expressed the engineering models (including those described previously) by the following generalized current equation:

$$i(z', t) = u(t - z'/v^*)P(z')i_o(t - z'/v^*) \quad (3-9)$$

where u is the Heaviside function equal to unity for $t \geq z'/v$ and zero otherwise, $P(z')$ is the height-dependent current attenuation factor, and v^* is the current-wave propagation speed. Table 3.1 summarizes $P(z')$ and v^* for the introduced five engineering models, in which, H_{tot} is the total channel height, λ is the current decay constant and c is the speed of light.

Table 3.1 - $P(z')$ and v in Eq. (3-4) for five simple engineering models (Adapted from [Rakov, 1997]).

Model	$P(z')$	v^*
BG	1	∞
TL	1	v
TCS	1	$-c$
MTLL	$1 - z'/H_{tot}$	v
MTLE	$\exp(-z'/\lambda)$	v

The Heaviside function u in the general expression introduces a mathematically more correct expression for the time dependence of the return stroke currents and will further improved estimations for fields.

3.3 Channel base current

An analytical expression usually adopted to represent the channel-base current $i_o(t)$, whose specific waveshape and amplitude can be determined experimentally, is the one proposed by [Heidler, 1985b], and frequently referred to as the “Heidler function”,

$$i_o(t) = \frac{I_o}{\eta} \frac{(t/\tau_1)^n}{1 + (t/\tau_1)^n} e^{(-t/\tau_2)} \quad (3-10)$$

where,

- I_o is the amplitude of the channel-base current
- τ_1 is the front time constant
- τ_2 is the decay time constant
- n exponent having values between 2 to 10
- η is the amplitude correction factor, obtained by Eq. (3-11)

$$\eta = e^{-\left(\frac{\tau_1}{\tau_2}\right) \left(n \frac{\tau_2}{\tau_1}\right)^{1/n}} \quad (3-11)$$

In order to reproduce a specific return stroke waveform, very often a combination of two Heidler functions can be used. Table 3.2 presents the parameters of the Heidler's functions corresponding to typical first and subsequent return strokes, according to the experimental data by Berger et al. [Rachidi et al., 2001].

Table 3.2 - Parameters of the two Heidler's functions used to reproduce the channel-base current waveshape.

	I_{o1} (kA)	τ_{11} (μ s)	τ_{21} (μ s)	n_1	I_{o2} (kA)	τ_{12} (μ s)	τ_{22} (μ s)	n_2
First Stroke	28	1.8	95	2	-	-	-	-
Subsequent Stroke	10.7	0.25	2.5	2	6.5	2	230	2

The Heidler function has a time derivative equal to zero at $t = 0$, consistent with measured return-stroke current wave shapes and, additionally, it allows precise and easy adjustment of the current amplitude, maximum current derivative and electrical charge transferred nearly independently by varying I_o , τ_1 and τ_2 , respectively.

3.4 Discussion on the adequacy of engineering return stroke models

An adequate return-stroke current model should be a model that yields a good approximation to the observed current at the channel-base, to the observed electric and magnetic fields at various distances (with particular reference to the peak fields and peak derivatives) and to the observed return-stroke wavefront speed [Nucci, 1995].

Several authors have studied the ability of the engineering models to predict the electromagnetic field radiated by return strokes; recently [Rakov, 2002] mentions two primary approaches to evaluate that ability:

- The first approach involves using a typical channel-base current waveform and a typical return-stroke propagation speed as model inputs and then comparing the model-predicted electromagnetic fields with typical observed fields.
- The second approach involves using the channel-base current waveform and the propagation speed measured for the same individual event and comparing computed fields with measured fields for that same specific event.

The second approach is able to provide a more definitive answer regarding model validity, but it is feasible only in the case of triggered-lightning return strokes or natural lightning strikes to tall towers where channel-base current can be measured. In the field calculations, the channel is generally assumed to be straight and vertical with its origin at ground ($z' = 0$), conditions which may be better approximations to subsequent strokes, but potentially not for first strokes. The channel length is usually not specified unless it is an inherent feature of the model, as is the case for the MTL model (e.g., [Rakov and Dulzon, 1987]). As a result, the model-predicted fields and associated model validation may not be meaningful after 25-75 μs , the expected time it takes for the return-stroke front to traverse the distance from ground to the cloud charge source.

[Nucci *et al.*, 1990] identified four characteristic features in the fields at 1 to 200 km measured by [Lin *et al.*, 1979] (Chapter 2) and used those features as a benchmark for their validation of the TL, MTLE, BG, and TCS models (also of the MULS model, not considered here). The characteristic features include:

- a sharp initial peak that varies approximately as the inverse distance beyond a kilometer or so in both electric and magnetic fields;
- a slow ramp following the initial peak and lasting in excess of 100 μs for electric fields measured within a few tens of kilometers;

- a hump following the initial peak in magnetic fields within a few tens of kilometers, the maximum of which occurs between 10 and 40 μs ; and finally,
- a zero crossing within tens of microseconds of the initial peak in both electric and magnetic fields at 50 to 200 km.

[*Nucci et al.*, 1990] conclude from their study that all the models evaluated by them using measured fields at distances ranging from 1 to 200 km predict reasonable fields for the first 5-10 μs , and all models, except the TL model, do so for the first 100 μs .

[*Thottappillil et al.*, 1997] noted that measured electric fields at tens to hundreds of meters from triggered lightning (e.g., [*Rakov et al.*, 1998]) exhibit a characteristic flattening within 15 μs or so. The BG, MTLL, TCS, and DU models (the DU [*Diendorfer and Uman*, 1990] model is not considered here), but not the TL and MTLE models, are consistent with this characteristic feature.

[*Thottappillil and Uman*, 1993] compared the TL, TCS, MTLE, DU, and MDU models, using 18 sets of three simultaneously-measured features of triggered-lightning return strokes: channel-base current, return-stroke propagation speed, and electric field at about 5 km from the channel base, the data previously used by [*Willett et al.*, 1989] for their analysis of the TL model. It was found that the TL, MTLE, and DU models each predicted the measured initial electric field peaks within an error whose mean absolute value was about 20 percent, while the TCS model had a mean absolute error about 40 percent.

The overall results of the testing of the validity of the engineering models can be summarized as follows:

- The relation between the initial field peak and the initial current peak is reasonably well predicted by the TL, MTLL, MTLE, and DU models.
- Electric fields at tens of meters from the channel after the first 10-15 μs are reasonably reproduced by the MTLL, BG, TCS and DU model, but not by the TL and MTLE models.
- From the standpoint of the overall field waveforms at 5 km all the models should be considered less than adequate.

It can be concluded that [*Nucci*, 1995] for engineering calculations, most of the considered models are adequate in that they reproduce fields which are reasonable approximations to available experimental data. The modified versions of the TL model (MTLE and MTLL) are probably the most reasonable compromise between mathematical simplicity and accuracy. However, the TL

model is recommended for the estimation of the initial field peak from the current peak or, conversely, the current peak from the field peak, since it is the mathematically simplest model with a predicted peak field/peak current relation that is equally or more accurate than that of the more mathematically complex models.

3.5 References Chapter 3

- Agrawal, A.K., H.J. Price, and S.H. Gurbaxani, Transient response of multiconductor transmission lines excited by a nonuniform electromagnetic field, in *IEEE International Symposium Digest. Antennas and Propagation*, pp. 396 pp, New York, USA, 1980a.
- Agrawal, A.K., H.J. Price, and S.H. Gurbaxani, Transient response of multiconductor transmission lines excited by a nonuniform electromagnetic field, *IEEE Transactions on Electromagnetic Compatibility, EMC22* (2), 119-29, 1980b.
- Baba, Y., and M. Ishii, Numerical electromagnetic field analysis of lightning current in tall structures, *IEEE Transactions on Power Delivery*, 16 (2), 324-8, 2001.
- Baños, A., *Dipole Radiation in the Presence of a Conducting Half-Space*, Oxford, 1966.
- Bruce, C.E.R., and R.H. Golde, The lightning discharge, *Journal of the Institution of Electrical Engineers*, 88 (6), 487-520, 1941.
- Christopoulos, C., Modelling of lightning and its interaction with structures, *Engineering Science and Education Journal*, 149-154, 1997.
- Cooray, V., Effects of propagation on the return stroke radiation fields, *Radio Science*, 22 (5), 757-68, 1987.
- Cooray, V., Horizontal fields generated by return strokes, *Radio Science*, 27 (4), 529-37, 1992.
- Diendorfer, G., and M.A. Uman, An improved return stroke model with specified channel-base current, *Journal of Geophysical Research*, 95 (D9), 13621-44, 1990.
- Gomes, C., and V. Cooray, Concepts of lightning return stroke models, *IEEE Transactions on Electromagnetic Compatibility*, 42 (1), 82-96, 2000.
- Heidler, F., Traveling current source model for LEMP calculation, in *6th Symposium and Technical Exhibition on Electromagnetic Compatibility*, pp. 157-62, Zurich, Switzerland, 1985a.

- Heidler, H., Analytische Blitzstromfunktion zur LEMP- Berechnung, in *18th ICLP (International Conference on Lightning Protection)*, pp. 63-66, Munich, Germany, 1985b.
- Lin, Y.T., M.A. Uman, J.A. Tiller, R.D. Brantley, W.H. Beasley, E.P. Krider, and C.D. Weidman, Characterization of lightning return stroke electric and magnetic fields from simultaneous two-station measurements, *Journal of Geophysical Research*, *84* (C10), 6307-14, 1979.
- Little, P.F., Transmission line representation of a lightning return stroke, *Journal of Physics D*, *11* (13), 1893-910, 1978.
- Moini, R., B. Kordi, G.Z. Rafi, and V.A. Rakov, A new lightning return stroke model based on antenna theory, *Journal of Geophysical Research*, *105* (D24), 29693-702, 2000.
- Nucci, C., Lightning-induced voltages on overhead power lines, in *Electra*, pp. 74-102, 1995.
- Nucci, C., G. Diendorfer, M. Uman, F. Rachidi, M. Ianoz, and C. Mazzetti, Lightning return stroke current models with specified channel-base current: a review and comparison, *Journal of Geophysical Research*, *95* (D12), 20395-408, 1990.
- Nucci, C.A., Tutorial on Lightning-induced effects on transmission lines, in *14th International Zurich Symposium on Electromagnetic Compatibility*, Zurich, Switzerland, 2001.
- Nucci, C.A., C. Mazzetti, F. Rachidi, and M. Ianoz, On lightning return stroke models for LEMP calculations, in *19th international conference on lightning protection*, pp. 463-9, Graz, Austria, 1988.
- Nucci, C.A., and F. Rachidi, Experimental Validation of a Modification to the Transmission Line Model for LEMP Calculations, in *8th International Symposium on Electromagnetic Compatibility*, pp. 6, Zurich, Switzerland, 1989.
- Plooster, M.N., Shock waves from line sources. Numerical solutions and experimental measurements, *Physics of Fluids*, *13* (11), 2665-75, 1970.
- Plooster, M.N., Numerical model of the return stroke of the lightning discharge, *Physics of Fluids*, *14* (10), 2124-33, 1971a.

- Plooster, M.N., Numerical simulation of spark discharges in air, *Physics of Fluids*, 14 (10), 2111-23, 1971b.
- Price, G.H., and E.T. Pierce, The modeling of channel current in the lightning return stroke, *Radio Science*, 12 (3), 381-8, 1972.
- Rachidi, F., W. Janischewskyj, A.M. Hussein, C.A. Nucci, S. Guerrieri, B. Kordi, and J.S. Chang, Current and electromagnetic field associated with lightning return strokes to tall towers, *IEEE Transactions on Electromagnetic Compatibility*, 43 (3), 356-366, 2001.
- Rachidi, F., and C.A. Nucci, On the Master, Uman, Lin, Standler and the Modified Transmission Line lightning return stroke current models, *Journal of Geophysical Research*, 95 (D12), 20389-94, 1990.
- Rachidi, F., C.A. Nucci, M. Ianoz, and C. Mazzetti, Importance of losses in the determination of lightning-induced voltages on overhead lines, *EMC '96 ROMA. International Symposium on Electromagnetic Compatibility. Univ. Rome 'La Sapienza', Rome, Italy, 2, 1996.*
- Rakov, V.A., Lightning electromagnetic fields: Modeling and measurements, in *12th International Zurich symposium and Technical Exhibition on electromagnetic compatibility*, pp. 59-64, Zurich, Switzerland, 1997.
- Rakov, V.A., Lightning Return Stroke Modeling: Recent Developments, in *International Conference on Grounding and Earthing - GROUND 2002*, Rio de Janeiro, Brazil, 2002.
- Rakov, V.A., and A.A. Dulzon, Calculated electromagnetic fields of lightning return strokes, *Tekhnicheskaya Elektrodinamika*, no. 1, 87-9, 1987.
- Rakov, V.A., and M.A. Uman, Review and evaluation of lightning return stroke models including some aspects of their application, *IEEE Transactions on Electromagnetic Compatibility*, 40 (4), 403-26, 1998.
- Rakov, V.A., M.A. Uman, K.J. Rambo, M.I. Fernandez, R.J. Fisher, G.H. Schnetzer, R. Thottappillil, A. Eybert Berard, J.P. Berlandis, P. Lalande, A. Bonamy, P. Laroche, and A. Bondiou Clergeries, New insights into lightning processes gained from triggered-lightning

- experiments in Florida and Alabama, *Journal of Geophysical Research*, 103 (D12), 14117-30, 1998.
- Rubinstein, M., An approximate formula for the calculation of the horizontal electric field from lightning at close, intermediate, and long range, *IEEE Transactions on Electromagnetic Compatibility*, 38 (3), 531-5, 1996.
- Thottappillil, R., V. Rakov, and M. Uman, Distribution of charge along the lightning channel: relation to remote electric and magnetic fields and to return-stroke models, *Journal of Geophysical Research*, 102 (D6), 6987-7006, 1997.
- Thottappillil, R., and M.A. Uman, Comparison of lightning return-stroke models, *Journal of Geophysical Research*, 98 (D12), 22903-14, 1993.
- Uman, M.A., and D.K. McLain, Magnetic field of the lightning return stroke, *Journal of Geophysical Research*, 74 (28), 6899-910, 1969.
- Uman, M.A., D.K. McLain, and E.P. Krider, The electromagnetic radiation from a finite antenna, *American Journal of Physics*, 43 (1), 33-8, 1975.
- Wait, J.R., *Electromagnetic waves in stratified media*, 372 pp., IEEE Press, Oxford, 1996.
- Wait, J.R., Concerning the horizontal electric field of lightning, *IEEE Transactions on Electromagnetic Compatibility*, 39 (2), 186, 1997.
- Willett, J.C., J.C. Bailley, V.P. Idone, A. Eybert-Berard, and L. Barret, Submicrosecond Intercomparison of Radiation Fields and currents in triggered Lightning Return Strokes Based on the Transmission-Line Model, *Journal of Geophysical Research*, 94 (D11), 13,275 - 13,286, 1989.

Chapter 4

Modeling of lightning return strokes to a vertically-extended elevated strike object

4.1 Introduction

The interaction of lightning with tall strike objects has been the object of a number of recent papers (e.g. [Baba and Ishii, 2001; Beierl, 1992; Fuchs, 1998; Guerrieri et al., 1998; Janischewskyj et al., 1996; Montandon and Beyeler, 1994; Rakov, 2001; Shostak et al., 1999b]). The strike object can modify not only the measured lightning return stroke current, as already mentioned in Chapter 2, but it could also influence the associated return-stroke electromagnetic fields (e.g. [Rachidi et al., 2001]).

For this reason, some of the return stroke models introduced in Chapter 3, initially developed for the case of return strokes initiated at ground level, have been extended to take into account the presence of a vertically-extended strike object (e.g. [Diendorfer and Uman, 1990; Goshima et al., 2000; Guerrieri et al., 1996; Guerrieri et al., 2000; Guerrieri et al., 1994; Guerrieri et al., 1998; Janischewskyj et al., 1998; Janischewskyj et al., 1999; Kordi et al., 2000; Motoyama et al., 1996; Rachidi et al., 1992; Rachidi et al., 1998; Rachidi et al., 2001; Rusan et al., 1996; Shostak et al., 2000; Shostak et al., 1999a; Shostak et al., 1999b; Zundl, 1994]).

In some of these models, it is assumed that a current pulse $i_o(t)$ associated with the return-stroke process is injected at the lightning attachment point, both into the strike object and into the lightning channel (e.g. [Goshima et al., 2000; Guerrieri et al., 1996; Guerrieri et al., 1994; Guerrieri et al., 1998; Janischewskyj et al., 1998; Janischewskyj et al., 1999; Motoyama et al., 1996; Rachidi et al., 1998; Rachidi et al., 2001; Rusan et al., 1996; Shostak et al., 1999a]) as shown in Fig. 4.1.

The upward-moving wave propagates along the channel at the return-stroke speed v as specified by the return-stroke model and the downward-moving wave propagates at the speed of light c along the strike object (Fig. 4-1). The strike object is assumed to be a lossless uniform transmission line characterized by its impedance Z_t and with constant non-zero reflection coefficients at its top and its bottom, ρ_t and ρ_g respectively.

As noted by [Guerrieri et al., 2000], the assumption of two identical current waves injected into the lightning channel and into the strike object implies that their characteristic impedances are equal to

each other, which means that, to a certain extent, such models are not self-consistent in that (1) there is no impedance discontinuity at the tower top at the time of lightning attachment to the tower, but (2) there is one when the reflections from ground arrive at the top of the tower.

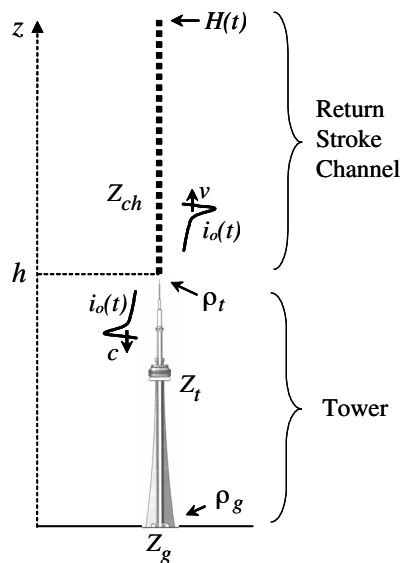


Figure 4.1 - Initial lightning return-stroke current into the strike object and the lightning channel as assumed by [Goshima *et al.*, 2000; Guerrieri *et al.*, 1996; Guerrieri *et al.*, 1994; Guerrieri *et al.*, 1998; Janischewskyj *et al.*, 1998; Janischewskyj *et al.*, 1999; Motoyama *et al.*, 1996; Rachidi *et al.*, 1998; Rachidi *et al.*, 2001; Rusan *et al.*, 1996; Shostak *et al.*, 1999a].

This chapter presents a generalization of the following return stroke models introduced in Chapter 3: the Bruce-Golde model (BG, [Bruce and Golde, 1941]), the transmission line model (TL, [Uman and McLain, 1969]), the traveling current source model (TCS, [Heidler, 1985]), the modified transmission line model with linear current decay with height (MTLL, [Rakov and Dulzon, 1987]), and modified transmission line model with exponential current decay with height (MTLE, [Nucci *et al.*, 1988], [Rachidi and Nucci, 1990]). The changes introduced into these models are made to take into account the presence of a vertically-extended strike object, without employing the assumption that identical current pulses are launched both upward and downward from the object top.

The extension for the TL, MTLL and MTLE models is based on a distributed-source representation of the return-stroke channel [Cooray, 2002; Rachidi and Nucci, 1990], which allows more general and straightforward formulations of these models than the traditional representations implying a lumped current source at the bottom of the channel. The TCS model inherently assumes a distributed-source channel, while the BG model can be viewed as a special case of the TCS model (e.g., [Rakov and Uman, 1998]).

We first consider in detail the MTLE model and then extend the results to the BG, TL, TCS, and

MTLL models. The developments in this chapter are essentially based on [Rachidi *et al.*, 2002].

4.2 MTLE model for a return stroke initiated at ground level

Consider first the case of a return stroke initiated at ground level already introduced in Chapter 3. The spatial and temporal distribution of the current along the vertical channel according to the MTLE model is defined by [Nucci *et al.*, 1988] and [Nucci and Rachidi, 1989] as:

$$i(z,t) = e^{-z/\lambda} i(0,t - z/v) u(t - z/v) \quad (4-1a)$$

where z is the height above ground, λ is the attenuation height constant, $i(0,t)$ is the current at the channel base, and v is the return-stroke speed assumed to be constant. u is the Heaviside unit step function which, for the sake of simplicity, will be omitted in the following equations of Sections 4.2 and 4.3. This model implies a specified current source connected at the bottom of the channel. Note that, although Equation (4-1) given here and Equation (3-6), given in Chapter 3 to describe the same model, have different forms, they are completely equivalent.

As shown by [Rachidi and Nucci, 1990], the MTLE model can also be expressed in terms of current sources distributed along the channel, these sources representing the effect of the charge initially stored in the corona sheath surrounding the leader channel core. Each elemental source is turned “on” when the upward-moving return stroke front reaches its altitude, as illustrated in Fig. 4.2, with the resultant current contribution propagating downward at the speed of light. Fig. 4.2 applies to all the engineering models considered in this paper, although for the BG model c (speed of light) should be replaced with infinity.

The general expression for the current source located at height z' is given by [Rachidi and Nucci, 1990]

$$\begin{aligned} di_s(z',t) &= 0 & t < z'/v \\ di_s(z',t) &= f(t - z'/v) e^{-z'/\lambda} dz' & t \geq z'/v \end{aligned} \quad (4-2)$$

where $f(t)$ is an arbitrary function.

The general expression for the current distribution along the channel can be written as

$$i(z,t) = \int_z^H di_s \left(z', t - \frac{z'-z}{c} \right) = \int_z^H f \left(t - \frac{z'}{v} - \frac{z'-z}{c} \right) e^{-z'/\lambda} dz' \quad (4-3)$$

where c is the speed of light, and H is the return stroke wavefront height as seen by the observer at height z , which is given by $H = H(z,t) = (t + z/c)/(1/v+1/c)$. If the current contributions from the distributed current sources propagated downward at an infinitely large speed, as is the case in the BG model, the expression for H would reduce to $H = vt$.

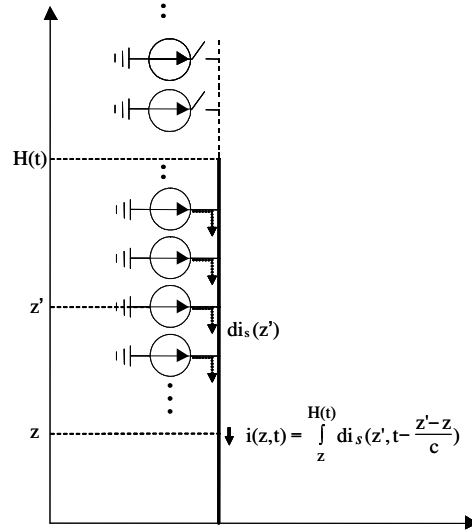


Figure 4.2 - Distributed-source representation of the lightning channel in engineering return-stroke models for the case of no-strike object and no reflections at ground.

In particular, the current at the channel base can be expressed as

$$i(0,t) = \int_0^H f\left(t - \frac{z'}{v} - \frac{z'}{c}\right) e^{-z'/\lambda} dz' \tag{4-4}$$

It is important to note that, in the above formulation, the reflections at ground of the downward propagating contributions from the current sources distributed along the channel have been implicitly disregarded, that is, the equivalent impedance at the strike point has been assumed to be equal to the characteristic impedance of the channel. If this is not the case, the reflections at ground of the downward propagating contributions from the current sources distributed along the channel are to be taken into account and Equation (4-3) assumes a different form. We shall further consider this point at the end of Section 4.3.1.

4.3 MTLE model in the presence of a vertically-extended strike object

The geometry of the problem is shown in Fig. 4.3, which also applies to all other engineering models discussed in this chapter. The strike object (tower) will be considered as a vertically extended lossless uniform transmission line of length h . We will assume that the propagation speed along the strike object is equal to the speed of light, and that the current reflection coefficients at its extremities (the top and the bottom) are constants (the frequency dependence of the reflection

coefficients will be taken into account in Chapter 6). Upward connecting leaders and reflections at the return stroke wavefront will be also disregarded¹.

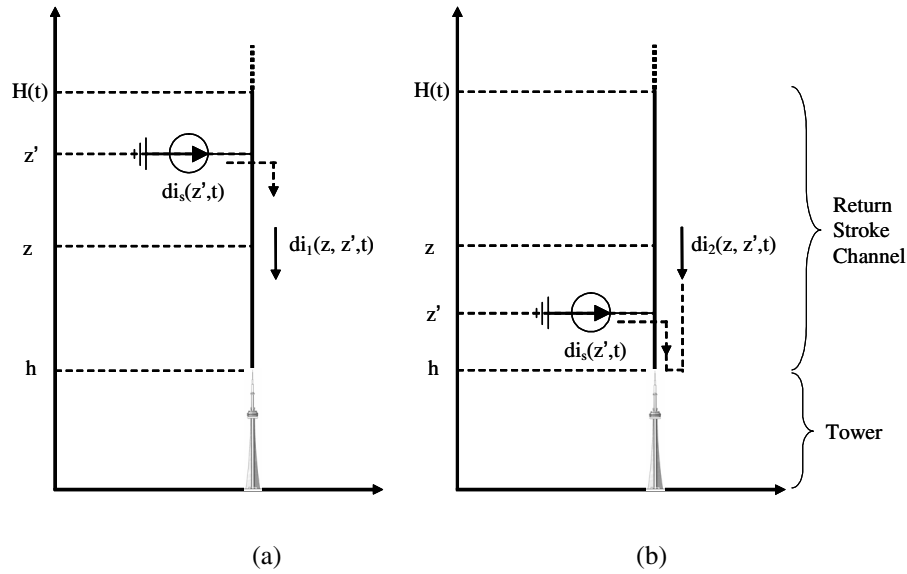


Figure 4.3 - Same as Fig. 4.2, but generalized to include a tall strike object (tower): (a) $z' > z > h$ (only the initial incident wave is shown, di_1 also includes reflections from the top and the bottom of the object); (b) $h < z' < z$ (only reflection from the object top is shown; di_2 also includes reflections from the bottom of the object). The total current $i(z,t)$ is obtained by integrating di_1 and di_2 within appropriate limits and summing the two resultant current contributions.

The reflection coefficient (for the current) at the bottom of the object can be expressed in terms of the characteristic impedance of the strike object Z_t and the equivalent impedance of the grounding system Z_g ²

$$\rho_g = \frac{Z_t - Z_g}{Z_t + Z_g} \quad (4-5)$$

Similarly, we can define two reflection coefficients at the top of the strike object for the upward, ρ_t^+ , and downward, ρ_t^- , propagating current waves,

$$\rho_t^+ = \frac{Z_t - Z_{ch}}{Z_t + Z_{ch}} \quad \rho_t^- = \frac{Z_{ch} - Z_t}{Z_{ch} + Z_t} = -\rho_t^+ \quad (4-6)$$

¹ The physics involved in the process of possible reflections of the upward-propagating current pulses at the return stroke wavefront is rather complicated. These reflections could, in principle, influence the front propagation speed, and they are poorly understood. However, it is possible to include such reflections in the calculations (see, for example, Heidler, F., and C. Hopf, *Lightning Current and Lightning Electromagnetic Impulse Considering Current Reflection at the Earth's Surface*, in *22nd International Conference on Lightning Protection*, pp. 6, Budapest, Hungary, 1994. and Shostak, V., W. Janischewskyj, A.M. Hussein, J.S. Chang, and B. Kordi, *Return-stroke current modeling of lightning striking a tall tower accounting for reflections within the growing channel and for upward-connecting discharges*, in *11th International Conference on Atmospheric Electricity*, pp. 123-6, Guntersville, U.S.A., 1999a.). Shostak et al. have shown that some fine structure of the radiated field could be attributed to these reflections.

² If the grounding system is "electrically long", Z_g can be viewed, at least at early times, as the characteristic impedance of the grounding system.

To simplify the notations, we define

$$\rho_t^+ = \rho_t \quad \rho_t^- = -\rho_t \quad (4-7)$$

4.3.1 Distribution of current along the lightning channel

Consider the current $di_1(z, z', t)$ due to an elemental current source $di_s(z', t)$ located above the observation point at a height $z' > z$ (see Fig. 4.3a). If we assume that both reflection coefficients ρ_t and ρ_g are equal to zero, we can write

$$di_1(z, z', t) = di_s\left(z', t - \frac{z'-z}{c}\right) = e^{-(z'-h)/\lambda} f\left(t - \frac{z'-h}{v} - \frac{z'-z}{c}\right) dz' \quad (4-8)$$

The current in this case is composed only of the original current from the source at z' . Now, for the general case when ρ_t and ρ_g are different from zero, part of the downward propagating current will be transmitted into the tower and part of it will be reflected at the top of the tower. This reflection contributes to the total current seen at height z and it must be added to the right hand side of Equation (4-8). In addition, the part of the current that is transmitted into the tower will generate multiple reflections within the tower. Each time one of these internal reflections arrives at the top of the tower, a part of its current is transmitted into the channel. All of these transmitted components contribute to the total current and must, therefore, be added to the right hand side of Equation (4-8) as well. Taking into account these multiple reflections, we obtain the following expression for the elemental current at height z , for $z' > z$

$$\begin{aligned} di_1(z, z', t) = e^{-(z'-h)/\lambda} dz' \left\{ f\left(t - \frac{z'-h}{v} - \frac{z'-z}{c}\right) - \rho_t f\left(t - \frac{z'-h}{v} - \frac{z'-z}{c} - \frac{2(z-h)}{c}\right) \right. \\ \left. + (1 - \rho_t) \rho_g (1 + \rho_t) f\left(t - \frac{z'-h}{v} - \frac{z'-z}{c} - \frac{2z}{c}\right) \right. \\ \left. + (1 - \rho_t) \rho_g^2 \rho_t (1 + \rho_t) f\left(t - \frac{z'-h}{v} - \frac{z'-z}{c} - \frac{2z}{c} - \frac{2h}{c}\right) \right. \\ \left. + (1 - \rho_t) \rho_g^3 \rho_t^2 (1 + \rho_t) f\left(t - \frac{z'-h}{v} - \frac{z'-z}{c} - \frac{2z}{c} - \frac{4h}{c}\right) + \dots \right\} \quad (4-9) \end{aligned}$$

Regrouping the terms, we get, for $z' > z$

$$\begin{aligned} di_1(z, z', t) = e^{-(z'-h)/\lambda} dz' \left\{ f\left(t - \frac{z'-h}{v} - \frac{z'-z}{c}\right) - \rho_t f\left(t - \frac{z'-h}{v} - \frac{z'-z}{c} - \frac{2(z-h)}{c}\right) \right. \\ \left. + (1 - \rho_t) (1 + \rho_t) \sum_{n=1}^{\infty} \rho_g^n \rho_t^{n-1} f\left(t - \frac{z'-h}{v} - \frac{z'-z}{c} - \frac{2z}{c} - \frac{2(n-1)h}{c}\right) \right\} \quad (4-10a) \end{aligned}$$

where the index n represents the successive multiple reflections occurring at the two ends of the

strike object.

Consider now the case of a current $di_2(z, z', t)$ due to an elemental current source $di_s(z', t)$ located below the observation point at a height $z' < z$ (see Fig. 4.3b). This time, the initial downward propagating current is not seen at the observation point. The current $di_2(z, z', t)$ seen at the observation point and due to an elemental current source $di_s(z', t)$ located at height $h < z' < z$ is thus given by

$$di_2(z, z', t) = e^{-(z'-h)/\lambda} dz' \left\{ -\rho_t f\left(t - \frac{z'-h}{v} - \frac{z'-z}{c} - \frac{2(z-h)}{c}\right) + (1-\rho_t)(1+\rho_t) \sum_{n=1}^{\infty} \rho_g^n \rho_t^{n-1} f\left(t - \frac{z'-h}{v} - \frac{z'-z}{c} - \frac{2z}{c} - \frac{2(n-1)h}{c}\right) \right\} \quad (4-10b)$$

The total current at height z can be obtained by integrating equations (4-10a) and (4-10b) within appropriate limits and summing the two resultant current contributions

$$i(z, t) = \int_z^H di_1(z, z', t) + \int_h^z di_2(z, z', t) \quad (4-11a)$$

Substituting equations (4-10a) and (4-10b) into Equation (4-11a) and regrouping similar terms in the integral, we obtain

$$i(z, t) = \int_z^H f\left(t - \frac{z'-h}{v} - \frac{z'-z}{c}\right) e^{-(z'-h)/\lambda} dz' - \int_h^H \left[\rho_t f\left(t - \frac{z'-h}{v} - \frac{z'-z}{c} - \frac{2(z-h)}{c}\right) \right] e^{-(z'-h)/\lambda} dz' + \int_h^H \left[(1-\rho_t)(1+\rho_t) \sum_{n=1}^{\infty} \rho_g^n \rho_t^{n-1} f\left(t - \frac{z'-h}{v} - \frac{z'-z}{c} - \frac{2z}{c} - \frac{2(n-1)h}{c}\right) \right] e^{-(z'-h)/\lambda} dz' \quad (4.11b)$$

We now wish to particularize Equation (4.11b) for the case of the MTLE model including the effect of an elevated strike object. We begin by considering the MTLE model for the case of the return stroke initiated at ground. We know, from equations (4-1) and (4-3), that $i(z, t)$ equals .

$$i(z, t) = i\left(0, t - \frac{z}{v}\right) e^{-z/\lambda} = \int_z^H f\left(t - \frac{z'}{v} - \frac{z'-z}{c}\right) e^{-z'/\lambda} dz' \quad (4-12)$$

In order to rewrite Equation (4-12) for the geometry of Fig. 4.3 (return stroke initiated at the top of a tall strike object), we will modify the time and height reference so that the current at $z=h$ begins at $t=0$. We further define the ‘undisturbed’ current $i_o(h, t)$ as the current that would be measured at the top of the object (lightning attachment point) if both reflection coefficients ρ_t and ρ_g were equal to zero. Note that, under these ideal conditions, the ‘undisturbed’ current waveform would also be measured at any point along the strike object, even at ground level when $h = 0$.

Applying the above definitions, following the same procedure as in Section 4.2, we can write Equation (4-12) as

$$i(z,t) = i_o \left(h, t - \frac{z-h}{v} \right) e^{-(z-h)/\lambda} = \int_z^H f \left(t - \frac{z'-h}{v} - \frac{z'-z}{c} \right) e^{-(z'-h)/\lambda} dz' \quad (4-13a)$$

Equation (4-13a) for the case of $z = h$, becomes,

$$i_o(h,t) = \int_h^H f \left(t - \frac{z'-h}{v} - \frac{z'-h}{c} \right) e^{-(z'-h)/\lambda} dz' \quad (4-13b)$$

Substituting equations (4-13a) and (4-13b) into (4-11b), and after straightforward mathematical manipulations, we obtain the final expression for the current distribution along the channel for $h < z < H$

$$i(z,t) = e^{-(z-h)/\lambda} i_o \left(h, t - \frac{z-h}{v} \right) - \rho_t i_o \left(h, t - \frac{z-h}{c} \right) + (1 - \rho_t) (1 + \rho_t) \sum_{n=0}^{\infty} \rho_g^{n+1} \rho_t^n i_o \left(h, t - \frac{z+h}{c} - \frac{2nh}{c} \right) \quad (4-14)$$

Note that retaining only one term ($n = 0$) in the sum and setting $\rho_t = 0$ and $h = 0$ in Equation (4-14) we can obtain a generalized form of Equation (4-1a) mentioned at the beginning of Section 4.2, in which the reflections at ground of the downward propagating contributions from the current sources distributed along the channel are taken into account,

$$i(z,t) = e^{-z/\lambda} i_o \left(0, t - \frac{z}{v} \right) + \rho_g^* i_o \left(0, t - \frac{z}{c} \right) \quad (4-1b)$$

where

$$\rho_g^* = \frac{Z_{ch} - Z_g}{Z_{ch} + Z_g}, \text{ and } i_o(0,t) = \int_0^H f \left(t - \frac{z'}{v} - \frac{z'}{c} \right) e^{-z'/\lambda} dz', \text{ this result will be explained in more detail in}$$

Section 4.5.1.

4.3.2 Distribution of current along the strike object

In the previous section, we took into account the reflections at the top and within the strike object to derive an expression for the current in the lightning channel, above the top of the strike object. In this section, we turn our attention to the currents along the strike object, where, $0 < z < h$. Applying the same procedure as in Section 4.3.1, we obtain the following expression for the current at height z due to an elemental source located at z' :

$$\begin{aligned}
di(z, z', t) = e^{-(z'-h)/\lambda} dz' & \left\{ (1 - \rho_t) f\left(t - \frac{z'-h}{v} - \frac{z'-z}{c}\right) + \rho_g (1 - \rho_t) f\left(t - \frac{z'-h}{v} - \frac{z'-z}{c} - \frac{2z}{c}\right) \right. \\
& + \rho_g \rho_t (1 - \rho_t) f\left(t - \frac{z'-h}{v} - \frac{z'-z}{c} - \frac{2h}{c}\right) + \rho_g^2 \rho_t (1 - \rho_t) f\left(t - \frac{z'-h}{v} - \frac{z'-z}{c} - \frac{2z}{c} - \frac{2h}{c}\right) \\
& \left. + \rho_g^2 \rho_t^2 (1 - \rho_t) f\left(t - \frac{z'-h}{v} - \frac{z'-z}{c} - \frac{4h}{c}\right) + \rho_g^3 \rho_t^2 (1 - \rho_t) f\left(t - \frac{z'-h}{v} - \frac{z'-z}{c} - \frac{2z}{c} - \frac{4h}{c}\right) + \dots \right\}
\end{aligned} \quad (4-15)$$

Regrouping terms, we get

$$\begin{aligned}
di(z, z', t) = (1 - \rho_t) e^{-(z'-h)/\lambda} dz' & \sum_{n=0}^{\infty} \left[\rho_g^n \rho_t^n f\left(t - \frac{z'-h}{v} - \frac{z'-z}{c} - \frac{2nh}{c}\right) \right. \\
& \left. + \rho_g^{n+1} \rho_t^n f\left(t - \frac{z'-h}{v} - \frac{z'-z}{c} - \frac{2z}{c} - \frac{2nh}{c}\right) \right]
\end{aligned} \quad (4-16)$$

The total current at an arbitrary height z along the strike object ($0 < z < h$), is given by the integral of the differential contributions given by Equation (4-16)

$$i(z, t) = \int_h^H di(z, z', t) \quad (4-17)$$

Equation (4-13b), which relates the undisturbed current from the MTLE model to the current sources distributed along the channel, is reproduced here for convenience,

$$i_o(h, t) = \int_h^H f\left(t - \frac{z'-h}{v} - \frac{z'-h}{c}\right) e^{-(z'-h)/\lambda} dz' \quad (4-18)$$

Substituting Equation (4-16) into Equation (4-17) and identifying in the resulting equation the terms containing the right-hand side of Equation (4-18), we obtain after straightforward mathematical manipulations, the current distribution along the strike object, $0 < z < h$ as follows

$$i(z, t) = (1 - \rho_t) \sum_{n=0}^{\infty} \left[\rho_g^n \rho_t^n i_o\left(h, t - \frac{h-z}{c} - \frac{2nh}{c}\right) + \rho_g^{n+1} \rho_t^n i_o\left(h, t - \frac{h+z}{c} - \frac{2nh}{c}\right) \right] \quad (4-19)$$

Note that here

$$(1 - \rho_t) = 1 - \frac{Z_t - Z_{ch}}{Z_t + Z_{ch}} = \frac{2Z_{ch}}{Z_t + Z_{ch}} \quad (4-20)$$

which is the transmission coefficient at the junction point between the lightning channel and the strike object for downward-moving current waves.

Note further that when only the first pair of terms ($n = 0$) of the sum is retained, and assuming $z = 0$, $\rho_g = 1$, and $\rho_t = 0$, Equation (4-19) results in $i(0, t) = 2i_o(h, t - h/c)$, and for $h = 0$, $i(0, t) = 2i_o(0, t)$. The

latter result can be also obtained from Equation (4-1b) by setting $\rho_g = 1$ and $z = 0$.

Equation (4-19) can be represented by the equivalent circuit shown in Fig. 4.4. Note that this circuit is similar to the one proposed by ([Rakov, 2001], Fig. 4a), although he used the short-circuit current, I , to define his current source (Norton equivalent circuit), while our current source in Fig. 4.4 is given by $2i_o$, where i_o corresponds to matched conditions ($Z_{ch} = Z_t = Z_g$). As expected, the short-circuit current is twice the matched-conditions current, $I = 2i_o$.

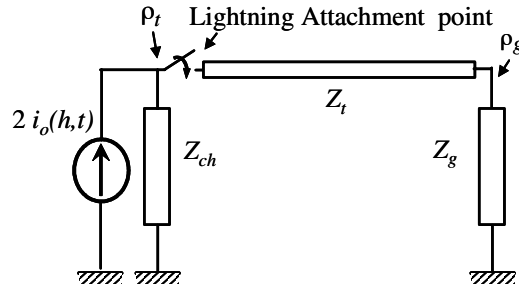


Figure 4.4 - Equivalent circuit for the tower struck by lightning (Equation (4-19)). i_o is the ‘undisturbed current’, Z_{ch} and Z_t are the characteristic impedances of the lightning channel and of the tall strike object respectively, and Z_g is the equivalent grounding impedance.

4.4 Extension to other models

Many of the so-called engineering models can be expressed using the following general expression [Rakov and Uman, 1998] (see Section 3.2.5 in Chapter 3):

$$i(z,t) = P(z) i(0,t - z/v^*) u(t - z/v) \tag{4-21}$$

where $P(z')$ is the current attenuation function, $u(t)$ is the Heaviside unit step function, v is the return stroke front speed, and v^* is the current-wave speed. The unit-step function needs to be shown explicitly in (4-21) in order to describe a possible current discontinuity (inherent in the BG and TCS models) at the return-stroke front. Table 3.1 (Chapter 3), reproduced here in Table 4.1 summarizes the expressions for $P(z')$ and v^* for some of the most commonly used return-stroke models already defined in Chapter 3. In Table 4.1, v is the return-stroke front speed, c is the speed of light, H_{tot} is the total channel height, and λ is the attenuation height.

Recently, [Cooray, 2002] has shown that the current distribution $i(z,t)$ for any engineering model, not only for the MTLE model as previously shown by [Rachidi and Nucci, 1990], can be viewed as due to current sources distributed along the channel. The general expression for the distributed sources is given by

$$di_s(z', t) = \left[-\frac{\partial i(z', t)}{\partial z'} + \frac{1}{c} \frac{\partial i(z', t)}{\partial t} \right] dz' \quad (4-22)$$

where c is the speed of light.

Table 4.1 - $P(z)$ and v^* for different return-stroke models.

Model	$P(z')$	v^*
BG	1	∞
TL	1	v
TCS	1	$-c$
MTLL	$1 - z'/H_{\text{tot}}$	v
MTLE	$\exp(-z'/\lambda)$	v

Inserting (4-21) into (4-22), one gets the expression for distributed current sources as a function of channel-base current:

$$\begin{aligned} di_s(z', t) = & \left[-\frac{dP(z')}{dz'} i(0, t - z'/v^*) u(t - z'/v) \right. \\ & + P(z') \left(\frac{1}{c} + \frac{1}{v^*} \right) \frac{\partial i(0, t - z'/v^*)}{\partial t} u(t - z'/v) \\ & \left. + P(z') \left(\frac{1}{c} + \frac{1}{v} \right) i(0, t - z'/v^*) \delta(t - z'/v) \right] dz' \end{aligned} \quad (4-23)$$

where δ is the Dirac distribution. The last term of (4-23) is non-zero only when there is a current discontinuity at the return stroke front.

Table 4.2 summarizes the resulting functions $di_s(z', t)/dz'$ for the five engineering return stroke models presented in Table 4.1. For the TL, MTLL, and MTLE models, it is assumed that there is no discontinuity at the return-stroke front, and for the BG model c in (4-23) is replaced with infinity.

Now, following a mathematical development similar to that in Section 4.3, we obtain the general expression for the current distribution along the lightning channel,

$$\begin{aligned} i(z, t) = & P(z-h) i_o \left(h, t - \frac{z-h}{v^*} \right) u \left(t - \frac{z-h}{v^*} \right) - \rho_t i_o \left(h, t - \frac{z-h}{c} \right) u \left(t - \frac{z-h}{c} \right) \\ & + (1 - \rho_t) (1 + \rho_t) \sum_{n=0}^{\infty} \rho_g^{n+1} \rho_t^n i_o \left(h, t - \frac{h+z}{c} - \frac{2nh}{c} \right) u \left[t - \frac{h+z}{c} - \frac{2nh}{c} \right] \end{aligned} \quad h < z < H \quad (4-24)$$

and for the current distribution along the strike object,

$$i(z, t) = \left(1 - \rho_t\right) \sum_{n=0}^{\infty} \left[\rho_t^n \rho_g^n i_o \left(h, t - \frac{h-z}{c} - \frac{2nh}{c} \right) u \left(t - \frac{h-z}{c} - \frac{2nh}{c} \right) + \rho_t^n \rho_g^{n+1} i_o \left(h, t - \frac{h+z}{c} - \frac{2nh}{c} \right) u \left(t - \frac{h+z}{c} - \frac{2nh}{c} \right) \right] \quad 0 \leq z \leq h \quad (4-25)$$

Table 4.2 - Expressions for $di_s(z', t)/dz'$ as a function of channel-base current for different return stroke models.

Model	$di_s(z', t)/dz'$
BG	$\frac{1}{v} i(0, t) \delta(t - z'/v)$
TL	$\left(\frac{1}{c} + \frac{1}{v} \right) \frac{\partial i(0, t - z'/v)}{\partial t} u(t - z'/v)$
TCS	$\left(\frac{1}{c} + \frac{1}{v} \right) i(0, t + z'/c) \delta(t - z'/v)$
MTLL	$\left[\left(\frac{1}{c} + \frac{1}{v} \right) \left(1 - \frac{z'}{H_{tot}} \right) \frac{\partial i(0, t - z'/v)}{\partial t} + \frac{i(0, t - z'/v)}{H_{tot}} \right] u(t - z'/v)$
MTLE	$\left[\left(\frac{1}{c} + \frac{1}{v} \right) \exp(-z'/\lambda) \frac{\partial i(0, t - z'/v)}{\partial t} + \frac{i(0, t - z'/v)}{\lambda} \exp(-z'/\lambda) \right] u(t - z'/v)$

Equations (4-24) and (4-25) apply to all engineering models that are described by equation (4-21), although for the BG model c should be replaced with infinity.

Note that Equation (4-25) is identical to Equation (4-19); that is, the current distribution along the strike object is independent of the return-stroke model. This is in agreement with the fact that we have assumed the same undisturbed current for all models. For the MTLE model, $P(z-h) = e^{-(z-h)/\lambda}$, $v^* = v$, and Equation (4-24) becomes identical to Equation (4-14).

4.5 Special case: Electrically-short strike structures

It is interesting to consider the special case when the strike object is electrically short. This would be the case for instance when lightning is initiated artificially using the rocket-triggered lightning technique (see Section 2.5.2.), or when upward-connecting leaders are present (assuming that they can be represented by a vertical transmission line).

Let's first define t_f as the zero-to-peak time associated with the lightning return stroke undisturbed current $i_o(t)$ (see Fig. 4.5).

An electrically-short structure can be characterized by a propagation time (h/c) much shorter than the zero-to-peak rise time, t_f . In those cases, propagation along the tower can be neglected and closed-form expressions can be derived for the spatial-temporal distribution of the current along the

strike object and along the channel.

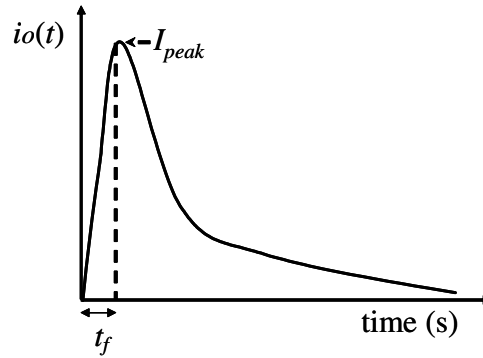


Figure 4.5 - Representation of a return stroke current waveform and definition of zero-to-peak current risetime t_f .

4.5.1 Current along the lightning channel for an electrically-short strike object

In this section, we will rewrite Equation (4-24) for the case of an electrically-short strike object. The Heaviside unit step function, u , will be omitted in the following equations for the sake of simplicity. Neglecting all phenomena of propagation along the tower (note that propagation effects in the channel still need to be taken into account) Equation (4-24) becomes

$$i(z, t) = P(z-h) i_o\left(h, t - \frac{z-h}{v^*}\right) - \rho_t i_o\left(h, t - \frac{z-h}{c}\right) + (1-\rho_t)(1+\rho_t) \sum_{n=0}^{\infty} \rho_g^{n+1} \rho_t^n i_o\left(h, t - \frac{z-h}{c}\right) \quad (4-26)$$

The sum of the terms of a geometrical series is given by

$$\frac{1}{1 \pm r} = 1 \mp r + r^2 \mp r^3 + r^4 - \dots \quad \forall |r| < 1 \quad (4-27)$$

Taking the factor $\rho_g i_o\left(h, t - \frac{z-h}{c}\right)$ out of the sum in Equation (4-26), the third term can be seen to contain as the series

$$\sum_{n=0}^{\infty} [\rho_g^n \rho_t^n] = 1 + \rho_g \rho_t + \rho_g^2 \rho_t^2 + \rho_g^3 \rho_t^3 + \dots \quad (4-28)$$

Therefore, using (4-27), (4-28) reduces to

$$\sum_{n=0}^{\infty} [\rho_g^n \rho_t^n] = \frac{1}{1 - \rho_g \rho_t} \quad (4-29)$$

It is important to note that the effective grounding impedance of the tower is generally much smaller than its characteristic impedance of the tower and this latter impedance is, in turn, appreciably lower than the equivalent impedance of the lightning channel (e.g. [Rakov, 2001]). As a

consequence, the current reflection coefficient at the ground is positive and the top reflection coefficient is negative.

Introducing (4-29) into (4-26) and after straightforward manipulations, we can write

$$i(z,t) = P(z-h) i_o \left(h, t - \frac{z-h}{v^*} \right) + \rho_{ch-g} i_o \left(h, t - \frac{z-h}{c} \right) \quad (4-30)$$

for $h < z < H$

where, $\rho_{ch-g} = \frac{Z_{ch} - Z_g}{Z_{ch} + Z_g}$ represents the reflection coefficient (for current) between the channel and the ground.

It is interesting to note that for the extreme case when $h = 0$, Equation (4-30) becomes,

$$i(z,t) = P(z) i_o \left(0, t - \frac{z}{v^*} \right) + \rho_{ch-g} i_o \left(0, t - \frac{z}{c} \right) \quad (4-31)$$

Equation (4-31), compared with Equation (4-21), includes a new term involving the reflection coefficient between the channel and the ground. Equation (4-31) reduces to Equation (4-1a), which applies to a lightning return stroke initiated at ground level, when the reflection coefficient ρ_{ch-g} equals 0. Note that, for $v^* = v$ and $P(z) = e^{-z/\lambda}$, Equation (4-31) is identical to Equation (4-1b), where $\rho^* = \rho_{ch-g}$.

4.5.2 Current along the strike object for electrically-short strike objects

The same treatment presented in the previous section can be applied for currents observed along the strike object. First, neglecting propagation, Equation (4-25) becomes,

$$i(z,t) = (1 - \rho_t) \sum_{n=0}^{\infty} \left[\rho_g^n \rho_t^n i_o(h,t) + \rho_g^{n+1} \rho_t^n i_o(h,t) \right] \quad \forall \quad 0 < z < h \quad (4-32)$$

Using the formula for the sum of the terms of a geometrical series already given in (4-27), and after straightforward manipulations, we obtain

$$i(z,t) = \frac{2Z_{ch}}{Z_{ch} + Z_g} i_o(h,t) = (1 + \rho_{ch-g}) i_o(h,t) \quad \forall \quad 0 < z < h \quad (4-33)$$

The current along the strike object for an electrically-short tower at any height z , can be obtained from Equation (4-33). This expression could have also been found using the equivalent circuit

presented in Fig. 4.4, by neglecting the transients along the tower represented by the transmission line.

4.6 Comments and conclusions

Based on a distributed-source representation of the lightning channel, five engineering lightning return stroke models (BG, TL, TCS, MTLL, and MTLE models) were extended to include a tall strike object.

As opposed to the traditional representation using a lumped current source at the bottom of the channel, the distributed-source representation of the lightning channel allows more general and straightforward formulations of the TL, MTLL and MTLE models, including a self-consistent treatment of the impedance discontinuity at the tower top.

The strike object was represented by a vertically-extended lossless uniform transmission line, and current reflection coefficients at its extremities were assumed to be constant. The distribution of current along the lightning channel for each model was expressed in terms of the “undisturbed” current $i_o(t)$, the object height h , and the current reflection coefficients at the top and bottom of the object, ρ_t and ρ_g respectively.

The ‘undisturbed current’, defined to be the current under matched conditions, $Z_{ch} = Z_t = Z_g$, is one-half the short-circuit current of the equivalent lightning source (in the absence of the strike object, $Z_g = 0$). The distribution of current along the strike object is clearly independent of the return-stroke model used, provided that the same undisturbed current is specified for each model.

Special expressions were derived for the case of electrically-short structures which can be used to quantify the effect of grounding conditions on the current distribution along the strike object and along the channel.

4.7 References Chapter 4

- Baba, Y., and M. Ishii, Numerical electromagnetic field analysis of lightning current in tall structures, *IEEE Transactions on Power Delivery*, 16 (2), 324-8, 2001.
- Beierl, O., Front Shape Parameters of Negative Subsequent Strokes Measured at the Peissenberg Tower, in *21st ICLP (International Conference on Lightning Protection)*, pp. 19-24, Berlin, Germany, 1992.
- Bruce, C.E.R., and R.H. Golde, The lightning discharge, *Journal of the Institution of Electrical*

- Engineers*, 88 (6), 487-520, 1941.
- Cooray, G.V., On the concepts used in return stroke models applied in engineering practice, *IEEE Trans. on Electromagnetic Compatibility in Press*, 2002.
- Diendorfer, G., and M.A. Uman, An improved return stroke model with specified channel-base current, *Journal of Geophysical Research*, 95 (D9), 13621-44, 1990.
- Fuchs, F., On the transient behaviour of the telecommunication tower at the mountain Hoher Peissenberg, in *24th ICLP (International Conference on Lightning Protection)*, pp. 36-41, Birmingham, U.K., 1998.
- Goshima, H., A. Asakawa, T. Shindo, H. Motoyama, A. Wada, and S. Yokoyama, Characteristics of electromagnetic fields due to winter lightning stroke current to a high stack, *Transactions of the Institute of Electrical Engineers of Japan, Part B*, 120 (1), 44-9, 2000.
- Guerrieri, S., F. Heidler, C.A. Nucci, F. Rachidi, and M. Rubinstein, Extension of two return stroke models to consider the influence of elevated strike objects on the lightning return stroke current and the radiated electromagnetic field: comparison with experimental results, in *EMC '96 (International Symposium on Electromagnetic Compatibility)*, pp. 701-6, Rome, Italy, 1996.
- Guerrieri, S., E.P. Krider, and C.A. Nucci, Effects of Traveling-Waves of Current on the Initial Response of a Tall Franklin Rod, in *ICLP2000*, pp. 94-99, Rhode, Greece, 2000.
- Guerrieri, S., C.A. Nucci, F. Rachidi, and M. Rubinstein, On the influence of elevated strike objects on the lightning return stroke current and the distant electric field, in *International Symposium on Electromagnetic Compatibility*, pp. 38-43, Rome, Italy, 1994.
- Guerrieri, S., C.A. Nucci, F. Rachidi, and M. Rubinstein, On the influence of elevated strike objects on directly measured and indirectly estimated lightning currents, *IEEE Transactions on Power Delivery*, 13 (4), 1543-55, 1998.
- Heidler, F., Traveling current source model for LEMP calculation, in *6th Symposium and Technical Exhibition on Electromagnetic Compatibility*, pp. 157-62, Zurich, Switzerland, 1985.
- Heidler, F., and C. Hopf, Lightning Current and Lightning Electromagnetic Impulse Considering Current Reflection at the Earth's Surface, in *22nd International Conference on Lightning Protection*, pp. 6, Budapest, Hungary, 1994.
- Janischewskyj, W., V. Shostak, J. Barratt, A.M. Hussein, I. Rusan, and J.S. Chang, Collection and use of lightning return stroke parameters taking into account characteristics of the struck object, in *23rd ICLP (International Conference on Lightning Protection)*, pp. 16-23, Florence, Italy, 1996.
- Janischewskyj, W., V. Shostak, and A.M. Hussein, Comparison of lightning electromagnetic field characteristics of first and subsequent return strokes to a tall tower 1. Magnetic field, in *24th*

- ICLP (international conference on lightning Protection)*, pp. 245-251, Birmingham, U.K., 1998.
- Janischewskyj, W., V. Shostak, and A.M. Hussein, Lightning electric field characteristics of first and subsequent return strokes to a tall tower, in *IEE 11th International Symposium on High Voltage Engineering*, pp. 270-4, London, U.K., 1999.
- Kordi, B., R. Moini, W. Janischewskyj, A.M. Hussein, and V. Shostak, Application of the Antenna Theory Model for Determination of the CN Tower Lightning Return Stroke Current, in *25th ICLP (international conference on lightning Protection)*, pp. 109-112, Rhodes, Greece, 2000.
- Montandon, E., and B. Beyeler, The Lightning Measuring Equipment on the Swiss PTT Telecommunications Tower at St. Chrischona, Switzerland, in *22nd ICLP (International Conference on Lightning Protection)*, pp. 6, Budapest, Hungary, 1994.
- Motoyama, H., W. Janischewskyj, A.M. Hussein, R. Rusan, W.A. Chisholm, and J.S. Chang, Electromagnetic field radiation model for lightning strokes to tall structures, *IEEE Transactions on Power Delivery*, 11 (3), 1624-32, 1996.
- Nucci, C.A., C. Mazzetti, F. Rachidi, and M. Ianoz, On lightning return stroke models for LEMP calculations, in *19th international conference on lightning protection*, pp. 463-9, Graz, Austria, 1988.
- Nucci, C.A., and F. Rachidi, Experimental Validation of a Modification to the Transmission Line Model for LEMP Calculations, in *8th International Symposium on Electromagnetic Compatibility*, pp. 6, Zurich, Switzerland, 1989.
- Rachidi, F., M. Ianoz, C.A. Nucci, and C. Mazetti, Modified transmission line model for LEMP calculations. Effect of the return stroke velocity decreasing and elevated strike objects on close fields, in *9th International Conference on Atmospheric Electricity*, pp. 664-667, St. Petersburg, Russia, 1992.
- Rachidi, F., W. Janischewskyj, A.M. Hussein, C.A. Nucci, S. Guerrieri, and J.S. Chang, Electromagnetic fields radiated by lightning return strokes to high towers, in *24th ICLP (International Conference on Lightning Protection)*, Birmingham, UK, 1998.
- Rachidi, F., W. Janischewskyj, A.M. Hussein, C.A. Nucci, S. Guerrieri, B. Kordi, and J.S. Chang, Current and electromagnetic field associated with lightning return strokes to tall towers, *IEEE Transactions on Electromagnetic Compatibility*, 43 (3), 356-366, 2001.
- Rachidi, F., and C.A. Nucci, On the Master, Uman, Lin, Standler and the Modified Transmission Line lightning return stroke current models, *Journal of Geophysical Research*, 95 (D12), 20389-94, 1990.
- Rachidi, F., V.A. Rakov, C.A. Nucci, and J.L. Bermudez, The Effect of Vertically-Extended Strike

- Object on the Distribution of Current Along the Lightning Channel, *Journal of Geophysical Research*, to be published, 2002.
- Rakov, V.A., Transient response of a tall object to lightning, *IEEE Transactions on Electromagnetic Compatibility*, 43 (4), 654-61, 2001.
- Rakov, V.A., and A.A. Dulzon, Calculated electromagnetic fields of lightning return strokes, *Tekhnicheskaya Elektrodinamika*, no. 1, 87-9, 1987.
- Rakov, V.A., and M.A. Uman, Review and evaluation of lightning return stroke models including some aspects of their application, *IEEE Transactions on Electromagnetic Compatibility*, 40 (4), 403-26, 1998.
- Rusan, I., W. Janischewskyj, A.M. Hussein, and J.S. Chang, Comparison of measured and computed electromagnetic fields radiated from lightning strikes to the Toronto CN tower, in *23rd ICLP (International Conference on Lightning Protection)*, pp. 297-303, Florence, Italy, 1996.
- Shostak, V., W. Janischewskyj, A. Hussein, and B. Kordi, Electromagnetic fields of lightning strikes to a tall tower: a model that accounts for upward-connecting discharges, in *25th ICLP (International Conference on Lightning Protection)*, pp. 60 - 65, Rhodes, Greece, 2000.
- Shostak, V., W. Janischewskyj, A.M. Hussein, J.S. Chang, and B. Kordi, Return-stroke current modeling of lightning striking a tall tower accounting for reflections within the growing channel and for upward-connecting discharges, in *11th International Conference on Atmospheric Electricity*, pp. 123-6, Guntersville, U.S.A., 1999a.
- Shostak, V., W. Janischewskyj, A.M. Hussein, and B. Kordi, Characteristics of return stroke current and electromagnetic field waveforms observed in multistroke lightning flashes to a tall tower, in *Eleventh International Symposium on High Voltage Engineering*, pp. 4, London, UK, 1999b.
- Uman, M.A., and D.K. McLain, Magnetic field of the lightning return stroke, *Journal of Geophysical Research*, 74 (28), 6899-910, 1969.
- Zundl, Lightning current and LEMP calculations compared to measurements gained at the Peissenberg tower, in *22nd ICLP (International Conference on Lightning Protection)*, Budapest, Hungary, 1994.

Chapter 5

Electromagnetic fields radiated by lightning return strokes to vertically extended elevated structures

5.1 Introduction

The problem of the determination of the peak return stroke current from remotely measured electric and/or magnetic fields considerably facilitates the collection of data on the lightning return stroke current without having to instrument towers or trigger the lightning artificially, and without the inherent relative inefficiency associated with those methods. This is especially true now because of the widespread use of lightning location systems. Indeed, such systems are also used today to provide estimates of lightning current parameters (e.g. [Cummins *et al.*, 1998; Herodotou *et al.*, 1993]).

The theoretical estimation of return stroke currents from remote electromagnetic fields depends on the adopted return stroke model. Expressions relating radiated fields and return stroke channel base currents have been derived for various ‘engineering’ return stroke models (e.g. [Rachidi and Thottappillil, 1993]). For rocket-triggered cloud-to-ground lightning events, [Willett *et al.*, 1989] compared the predictions obtained using one of these engineering models, namely the transmission line (TL) model, and experimental data sets consisting of simultaneously measured current, electric field and return stroke speed, finding a reasonable agreement. According to the TL model, the radiated (far) electric and magnetic fields, for a vertical lightning channel and an observation point at ground level, are simply proportional to the channel base current (Section 2.6, Fig. 2.28):

$$E_z^{far}(r, t + r/c) = -\frac{v}{2\pi\epsilon_0 c^2 r} i(0, t) \quad (5-1)$$

$$H_\phi^{far}(r, t + r/c) = \frac{v}{2\pi cr} i(0, t) \quad (5-2)$$

in which $i(0, t)$ is the channel-base current, v is the return stroke speed, and r is the distance from the channel base to the observation point. Expressions (5-1) and (5-2) are derived assuming that the return stroke is initiated at ground, which makes their use reasonable, to a certain extent, also for triggered lightning, as in [Willett *et al.*, 1989].

On the other hand, as we have seen in Chapter 2, experimental observations on tall telecommunication towers, such as the 553-m tall CN Tower in Toronto and the 168-m tall Peissenberg tower in Germany, have shown that the presence of the tower tends, in general, to increase substantially the electric and magnetic field peaks and their derivatives (see e.g. [Baba and Ishii, 2000; Janischewskyj et al., 1993; Motoyama et al., 1996; Rachidi et al., 1998; Rachidi et al., 2001]). This observation implies that the presence of the elevated object cannot be disregarded in the mathematical link between radiated field and channel base current. As a result, the use of equations (5-1) and (5-2) appears to be inappropriate for lightning strikes to tall objects.

In this chapter, we derive new expressions relating far radiated field and return stroke current, taking into account the presence of an elevated strike object. The derived expressions are based on the developments presented by [Bermudez et al., 2001], taking into account the self-consistent treatment of the impedance discontinuity at the tower top, as explained in Chapter 4, proposed in [Rachidi et al., 2002].

The developed expressions will be validated using experimental data associated with lightning strikes to the CN Tower. The experimental data were obtained during two experimental campaigns that took place in Toronto in 2000 and 2001. In particular, during the Summer 2001, we performed in collaboration with the University of Toronto, the first simultaneous measurements of return stroke current from lightning striking the CN Tower and the corresponding electric and magnetic fields measured at two distances (2 km and 16.8 km), as well as images using a video recording systems (VHS) and a high-speed camera system.

5.2 Description of the extended TL model and derivation of the far field – current relationship

Several engineering return stroke models have been extended to account for the presence of a tall strike object (see Chapter 4, also [Diendorfer, 1991; Guerrieri et al., 1996; Janischewskyj et al., 1996; Janischewskyj et al., 1998; Rachidi et al., 1992; Rusan et al., 1996; Shostak et al., 2000; Willett et al., 1988]). In the present analysis, we will use one particular model, the extended TL return stroke model. Remember that, in this model, the strike object (tower) is represented as an ideal (lossless) transmission line of length h . We assume the propagation speed along the strike object equal to the speed of light c , and the current reflection coefficients ρ_t and ρ_g at its extremities (the top and the bottom, respectively) as constants (Fig. 5.1). We will also disregard any upward connecting leader and any reflections at the return stroke wavefront, even though it has been shown

by [Shostak et al., 2000] that some features of the radiated field could be attributed to these reflections.

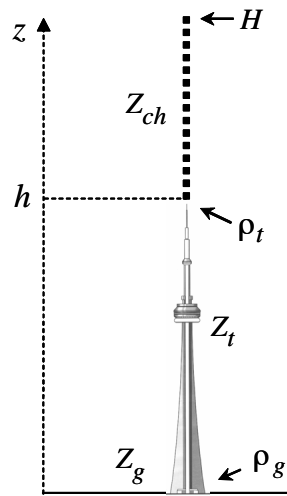


Figure 5.1 - Strike object and channel geometry.

The bottom reflection coefficient, as defined in Chapter 4 (Equation 4-5) for the current in the tower, can be expressed in terms of the characteristic impedance of the tower Z_t and the grounding system impedance Z_g ,

$$\rho_g = \frac{Z_t - Z_g}{Z_t + Z_g} \quad (5-3)$$

As already mentioned in Chapter 4, the top reflection coefficient for the current in the tower can be expressed in terms of the characteristic impedance of the tower Z_t and the equivalent impedance of the lightning return stroke channel Z_{ch} ,

$$\rho_t = \frac{Z_t - Z_{ch}}{Z_t + Z_{ch}} \quad (5-4)$$

This top reflection coefficient can be defined in a similar way for currents observed in the channel and, in that case, the sign on Equation (5-4) must be changed (see also Equation (4-6)).

To extend equations (5-1) and (5-2) to the geometry of Fig. 5.1 (return stroke initiated at the top of a tower), we will use the concept of the ‘undisturbed’ current $i_o(h,t)$ introduced in Section 4.3.1, defined as the current that would be measured at the tower top (lightning attachment point) if both reflection coefficients ρ_t and ρ_g were equal to zero. The expressions describing the spatial and temporal distribution of the current along the tower and along the channel, respectively, developed in Chapter 4 – Section 4.4, read (for the TL model)

$$i(z, t) = \left(1 - \rho_t\right) \sum_{n=0}^{\infty} \left[\rho_t^n \rho_g^n i_o \left(h, t - \frac{h-z}{c} - \frac{2nh}{c} \right) u \left(t - \frac{h-z}{c} - \frac{2nh}{c} \right) + \rho_t^n \rho_g^{n+1} i_o \left(h, t - \frac{h+z}{c} - \frac{2nh}{c} \right) u \left(t - \frac{h+z}{c} - \frac{2nh}{c} \right) \right] \quad 0 \leq z \leq h \quad (5-5)$$

$$i(z, t) = i_o \left(h, t - \frac{z-h}{v} \right) u \left(t - \frac{z-h}{v} \right) - \rho_t i_o \left(h, t - \frac{z-h}{c} \right) u \left(t - \frac{z-h}{c} \right) + (1 - \rho_t)(1 + \rho_t) \sum_{n=0}^{\infty} \rho_g^{n+1} \rho_t^n i_o \left(h, t - \frac{h+z}{c} - \frac{2nh}{c} \right) u \left(t - \frac{h+z}{c} - \frac{2nh}{c} \right) \quad h < z < H_{tot} \quad (5-6)$$

where z is the height along the strike object for Equation (5-5) and along the channel for Equation (5-6), c is the speed of light, v is the return stroke speed, H_{tot} is the total height of both the lightning channel and the elevated strike object, and, $u(t)$ is the Heaviside unit step function. Note that, if the current is calculated up to a given maximum value of time t , the summations in equations (5-5) and (5-6) have a finite number of terms since the current $i_o(t)$ is equal to zero for negative times or, equivalently, since there is a value of n after which the argument of the Heaviside step function becomes and stays negative.

The general expressions for the vertical component of the electric field and the azimuthal component of the magnetic field from a vertical antenna above a perfectly conducting ground, given by [Uman et al., 1975] for an observation point at ground level, were introduced in Chapter 2 and are reproduced here for convenience,

$$E_z(r, t) = \frac{1}{2\pi\epsilon_o} \left[\int_0^H \frac{2z^2 - r^2}{R^5} \int_{R/c}^t i(z, \tau - R/c) d\tau dz + \int_0^H \frac{2z^2 - r^2}{cR^4} i(z, t - R/c) dz - \int_0^H \frac{r^2}{c^2 R^3} \frac{\partial i(z, t - R/c)}{\partial t} dz \right] \quad (5-7)$$

$$H_\phi(r, t) = \frac{1}{2\pi} \left[\int_0^H \frac{r}{R^3} i(z, t - R/c) dz + \int_0^H \frac{r}{cR^2} \frac{\partial i(z, t - R/c)}{\partial t} dz \right] \quad (5-8)$$

where H is the height of the return stroke wavefront as seen by the observer, r is the horizontal distance between the channel and the observation point, and R is the distance between a single dipole located at a height z above ground and the observation point ($R = \sqrt{r^2 + z^2}$) (see Fig. 5.2a).

For distant observation points where $r \gg H$, we can neglect the first two terms (static and induction components) of the electric field, as well as the first term (induction component) of the magnetic field, and consider $R \cong r$. Therefore, the far radiated electric and magnetic fields for an observation point located at ground level reduce to,

$$E_z^{far}(r, t) \cong -\frac{1}{2\pi\epsilon_0 c^2 r} \int_0^H \frac{\partial i(z, t - r/c)}{\partial t} dz \quad (5-9)$$

$$H_\phi^{far}(r, t) \cong \frac{1}{2\pi c r} \int_0^H \frac{\partial i(z, t - r/c)}{\partial t} dz \quad (5-10)$$

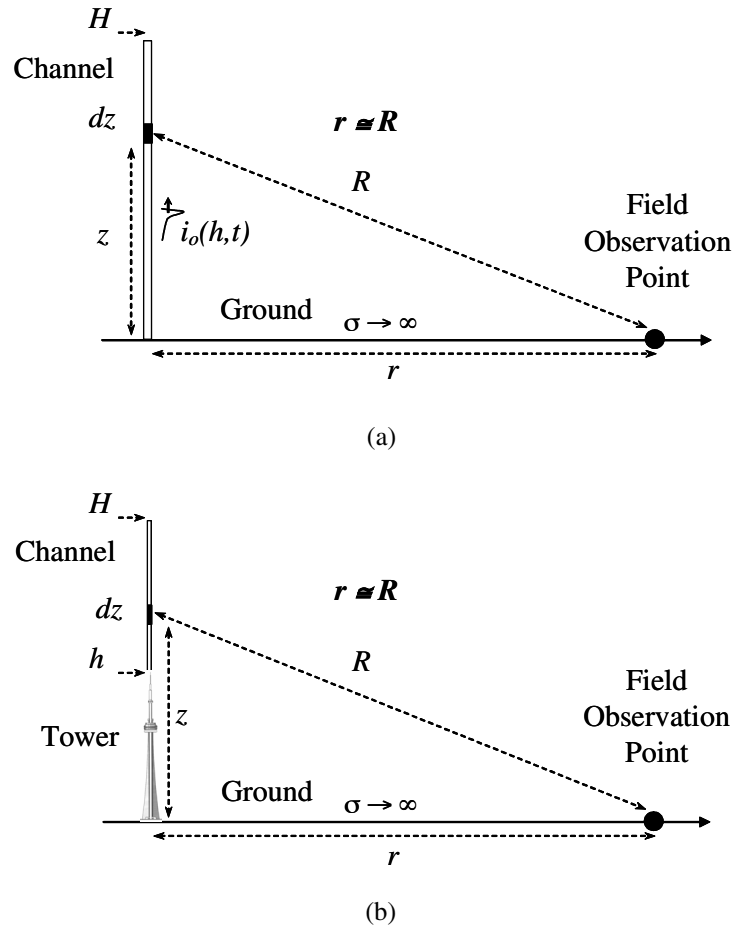


Figure 5.2 - Geometry for the calculation of electric and magnetic fields generated by a lightning return stroke current: (a) return stroke initiated at ground level; (b) return stroke initiated at the tower top.

Introducing the expressions for the spatial and temporal distribution of the current (5-5)-(5-6) into (5-9)-(5-10), and after appropriate mathematical manipulations (see Appendix 1), we obtain,

$$E_z^{far}(r, t + r/c) = -\frac{v}{2\pi\epsilon_0 c^2 r} \left[1 + \frac{c}{v} (1 - 2\rho_t) \right] i_o(h, t) - \frac{(1 - \rho_t)}{2\pi\epsilon_0 c r} \sum_{n=0}^{\infty} \left\{ \begin{array}{l} (\rho_g - 1) \rho_g^n \rho_t^n i_o \left(h, t - \frac{(2n+1)h}{c} \right) \\ + 2\rho_g^{n+1} \rho_t^{n+1} i_o \left(h, t - \frac{2(n+1)h}{c} \right) \end{array} \right\} \quad (5-11)$$

$$H_{\phi}^{far}(r, t + r/c) = \frac{v}{2\pi cr} \left[1 + \frac{c}{v}(1 - 2\rho_t) \right] i_o(h, t) + \frac{(1 - \rho_t)}{2\pi r} \sum_{n=0}^{\infty} \left\{ \begin{aligned} &(\rho_g - 1)\rho_g^n \rho_t^n i_o \left(h, t - \frac{(2n+1)h}{c} \right) \\ &+ 2\rho_g^{n+1} \rho_t^{n+1} i_o \left(h, t - \frac{2(n+1)h}{c} \right) \end{aligned} \right\} \tag{5-12}$$

Equations (5-11) and (5-12) are general expressions to calculate the radiated electric and magnetic fields generated by a lightning return stroke to a tall tower assumed as a homogeneous vertical transmission line.

Fig. 5.3 is a reproduction of Fig. 4.5 introduced in Chapter 4, in which t_f is defined as the zero-to-peak time value of the lightning return stroke current. We will consider two cases:

- (1) electrically-tall structures, for which the propagation time, from top to bottom within the tower (h/c), is greater than the time t_f ; in this case, the current transmitted into the tower reaches its peak before the reflection from the ground arrives (none of the reflections overlap with it); and,
- (2) electrically-short structures, for which the propagation time (h/c), is much shorter than the lightning return stroke current wavefront t_f ; in this case, we can neglect propagation delays along the tower.

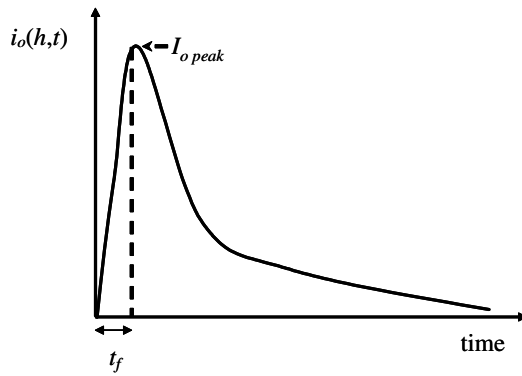


Figure 5.3 - Definition of zero-to-peak risetime t_f of the current $i_o(h,t)$.

5.2.1 Electrically-tall strike object ($t_f < h/c$)

Let us consider first the case when the propagation time (h/c), is greater than the current zero-to-peak risetime t_f . This can be expressed by the following inequality,

$$t_f < \frac{h}{c} \tag{5-13}$$

Noting that all terms on the right hand side of equations (5-11) and (5-12) except for the first are zero for times satisfying the inequality in Equation (5-13), we can write

$$E_z^{far}(r, t_f + r/c) = -\frac{v}{2\pi\epsilon_0 c^2 r} \left[1 + \frac{c}{v}(1 - 2\rho_t) \right] i_o(h, t_f) \quad (5-14)$$

$$H_\phi^{far}(r, t_f + r/c) = \frac{v}{2\pi cr} \left[1 + \frac{c}{v}(1 - 2\rho_t) \right] i_o(h, t_f) \quad (5-15)$$

Since the current on the right hand side of equations (5-14) and (5-15) is the peak of the undisturbed current (see Fig. 5.3), and the electric and magnetic fields on the left hand side are the first peak in the measured fields, we can write

$$E_{z\ peak} = -\frac{v}{2\pi\epsilon_0 c^2 r} \left[1 + \frac{c}{v}(1 - 2\rho_t) \right] I_{o\ peak} \quad (5-16)$$

$$H_{\phi\ peak} = \frac{v}{2\pi cr} \left[1 + \frac{c}{v}(1 - 2\rho_t) \right] I_{o\ peak} \quad (5-17)$$

where $I_{o\ peak}$ is the peak of the undisturbed current $i_o(h, t)$.

It is important to note that the undisturbed current $i_o(h, t)$ is different from the actual current pulse injected from the channel to the tower top. It would be therefore more appropriate to express the electromagnetic field peaks as a function of the current transmitted to the tower for which experimental data are available. To do that, one needs to express the undisturbed current peak $I_{o\ peak}$ as a function of the peak of the current transmitted into the tower, I_{peak} . Under the current conditions of electrically-tall towers ($t_f < h/c$), these two quantities are simply related by

$$I_{peak} = (1 - \rho_t) I_{o\ peak} \quad (5-18)$$

Introducing (5-18) in (5-16) and (5-17) yields

$$E_{z\ peak} = -\frac{v}{2\pi\epsilon_0 c^2 r} k I_{peak} \quad (5-19)$$

$$H_{\phi\ peak} = \frac{v}{2\pi cr} k I_{peak} \quad (5-20)$$

where k is given by

$$k = \frac{1 + (1 - 2\rho_t)c/v}{1 - \rho_t} \quad (5-21)$$

Comparing equations (5-19) and (5-20) with equations (5-1) and (5-2), we can see that the enhancement effect of the tower can be quantified through the factor k .

Because of the restriction $t_f < h/c$, equations (5-19) and (5-20) are independent of the structure's height h and of the ground reflection coefficient ρ_g .

It is also important to note that, as the effective grounding impedance of the tower is generally much smaller than its characteristic impedance and the latter impedance is appreciably lower than the equivalent impedance of the lightning channel (e.g. [Rakov, 2001]), the current reflection coefficient at the ground is positive and the top reflection coefficient is negative. Therefore the factor k in equations (5-19) and (5-20) is greater than 1 implying that the presence of the strike object enhances the electric and magnetic field peaks in comparison to return strokes initiated at ground level.

5.2.2 Electrically-short strike object ($t_f \gg h/c$)

In the case of an electrically-short strike object, the following inequality is satisfied,

$$t_f \gg \frac{h}{c} \quad (5-22)$$

Cases satisfying this condition can represent, for instance, short structures used in artificially-initiated lightning using rockets.

From Section 4.5 in Chapter 4, the current distribution along the tower and the lightning channel is expressed through equations (4-30) and (4-33), which we have adapted here for the TL model used in this chapter,

$$i(z, t) = i_o\left(h, t - \frac{z-h}{v}\right) + \rho_{ch-g} i_o\left(h, t - \frac{z-h}{c}\right) \quad h < z < H_{tot} \quad (5-23)$$

$$i(z, t) = (1 + \rho_{ch-g}) i_o(h, t) \quad 0 \leq z < h \quad (5-24)$$

where $\rho_{ch-g} = (Z_{ch} - Z_g) / (Z_{ch} + Z_g)$ represents the reflection coefficient (for current) at the channel base.

Inserting (5-23) and (5-24) into the far field expressions (5-9) and (5-10), and after mathematical manipulations (see Appendix 2), we obtain

$$E_z^{far} \left(r, t + \frac{r}{c} \right) \cong - \frac{v}{2\pi\epsilon_0 c^2 r} \left(1 + \frac{c}{v} \rho_{ch-g} \right) i_o(h, t) - \frac{(1 + \rho_{ch-g})h}{2\pi\epsilon_0 c^2 r} \frac{\partial i_o(h, t)}{\partial t} \quad (5-25)$$

$$H_\varphi^{far} \left(r, t + \frac{r}{c} \right) \cong \frac{v}{2\pi cr} \left(1 + \frac{c}{v} \rho_{ch-g} \right) i_o(h, t) + \frac{(1 + \rho_{ch-g})h}{2\pi cr} \frac{\partial i_o(h, t)}{\partial t} \quad (5-26)$$

The far electric and magnetic fields associated with lightning strikes to electrically-short structures include two terms: the first one is proportional to the undisturbed current and it represents the contribution of the channel, and the second depends on the current derivative and it represents the contribution of the strike object. Note that setting $h = 0$ in (5-25) and (5-26), we can obtain a generalized form of equations (5-1) and (5-2) for return strokes initiated at ground level, in which the reflections at ground are taken into account; setting additionally $\rho_{ch-g} = 0$, equations (5-25) and (5-26) reduce, as expected, to (5-1) and (5-2).

In Section 5.4, we will compare the results obtained using the derived expression for electrically-tall towers with simultaneous measurements of return stroke current and electric and magnetic fields associated with lightning strikes to the CN Tower in Toronto, recorded during the summers of 2000 and 2001.

5.3 Measurement system and experimental data

5.3.1 CN Tower measurement set-up

Lightning return stroke currents striking the CN Tower are measured by two permanent lightning current derivative systems using two Rogowski coils. Values recorded by the system installed at a height of 474 m above ground level (AGL) will be employed in this section to compare with the expressions developed for field at far distances.

The Rogowski coil installed at 474 m has a nominal risetime of 8.7 ns, a measured sensitivity of 0.359 mV/(kA/μs), and a nominal accuracy of ±6%. It is connected via a 102-m, 50 Ω triaxial cable to the recording system located at 403-m AGL (see Fig. 5.4a). The recording system consists of a 10-ns, 10-bit, two-channel digitizer and a computer controller. The connections between the coil, transmission cable and receiver are all matched to 50 Ω to eliminate reflections. The digitizer features a segmented memory (128 Kbytes per channel), which is used to record waveshapes for up to 8 strokes per lightning flash [Bermudez *et al.*, 2002; Hussein *et al.*, 1995].

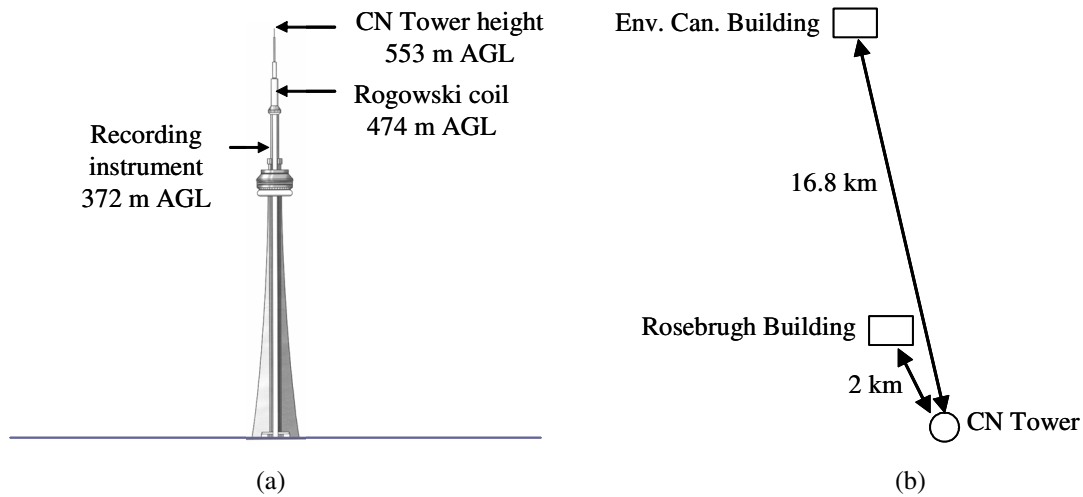


Figure 5.4 - Location of CN Tower lightning return stroke current measuring system (a), and top view showing the locations of field measuring systems (b).

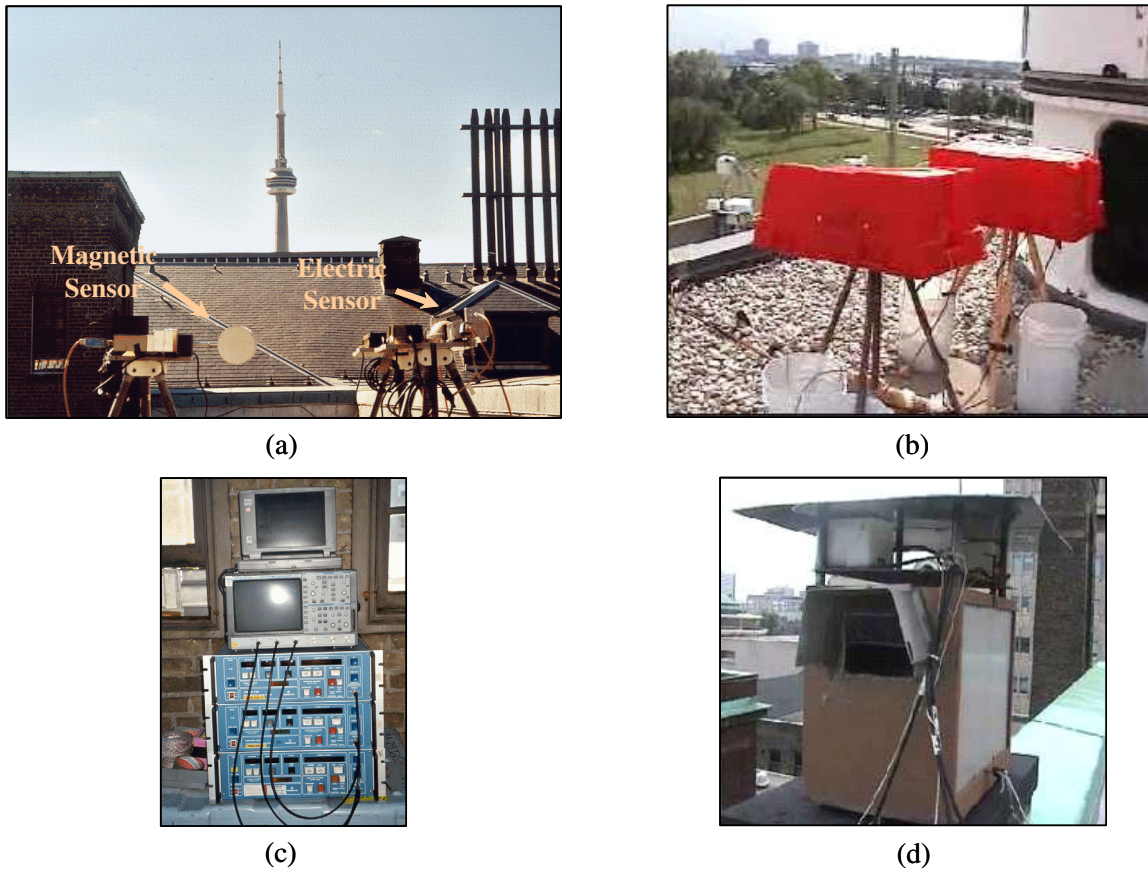


Figure 5.5 - Pictures of electric and magnetic field sensors (a) on the roof of Rosebrugh building, 2 km north of the CN Tower; (b) on the roof of the Environment Canada Building (covered by rain-protecting boxes), 16.8 km north of the CN Tower, as well as pictures of the receiver and digitizer in the building’s penthouse (c), and Video recording system of the University of Toronto (d).

Electric and magnetic fields at two different distances were also measured simultaneously with lightning currents (see Fig. 5.4b). During the summers of 2000 and 2001, the vertical component of the electric field (E_z) and the azimuthal component of the magnetic field (H_ϕ) were measured 2 km

North (Rosebrugh building of the University of Toronto) of the CN Tower (Fig. 5.4b). The sensors were located on the roof of the building (see Fig. 5.5a) near the permanent system of the University of Toronto (Fig. 5.5d) and the receiver and digitizer were installed in the penthouse of the building (Fig. 5.5c). The trigger level was adjusted to record fields striking the CN Tower and in its vicinity. The measurement system was composed of one spherical E-field sensor (TSN 245-E31, Thomson CSF) and one H-field loop antenna sensor (TSN 245-H32, Thomson CSF). The measured signals from the two sensors were relayed via fiber optic cables up to a receiver and an 8-bit digitizing oscilloscope operating at 100 Msamples/sec. The digitizer features a segmented memory (1 Mbyte per 4 channels), which is used to record waveshapes for up to 10 strokes per lightning flash. The operating frequency band of the system, up to but not including the digitizer, is 1 kHz to 130 MHz.

A second, similar measuring system, employed during the summer 2001, was installed to measure the vertical component of the electric field (E_z) and the azimuthal component of the magnetic field (H_ϕ) at 16.8 km north of the CN Tower. The sensors were located on the roof of the Environment Canada building (figs. 5.4b and 5.5b) [Bermudez *et al.*, 2002].

In addition to the field measuring systems, a video recording system and a high-speed camera were also operational.

5.3.2 CN Tower experimental data

During the summer 2000, current derivatives and fields at 2 km were measured simultaneously. For the purpose of analysis, recorded data corresponding to three flashes that struck the CN Tower on July 14th, August 1st, and August 23rd will be used. Table 5.1 summarizes the associated parameters for the three flashes: current peak values and their 10-90% risetimes and the associated electric and magnetic field peaks measured at 2 km.

In the Summer of 2001, current derivatives and fields at two distances (2 km and 16.8 km) were measured simultaneously. On Wednesday, July 4th, 2001 a flash with 5 return strokes hit the tower and was recorded simultaneously by the current derivative system and by the electric and magnetic field systems at two distances, 2 km and 16.8 km. Table 5.2 summarizes the peak values and the 10-90% risetimes of the 5 return stroke currents and their associated electric and magnetic field peak.

Fig. 5.6 presents an example of simultaneous recordings of return stroke current derivative, return stroke current (numerically integrated), electric and magnetic fields at 2 km and those at 16.8 km. It

can be seen that, at 2 km, the electric field is characterized by its initial peak followed by the increasing ramp, and that the magnetic field is characterized by an initial peak followed by a hump. These features are in agreement with characteristics of fields at this distance range for direct strikes to ground as reported by [Lin et al., 1979], although fields associated with strikes to tall structures have a more pronounced initial peak [Rachidi et al., 1998]. At 16.8 km, the electric and magnetic fields are characterized by similar waveshapes, typical of distant fields.

Table 5.1 - Parameters associated with strokes recorded during the summer 2000

Flash	Return stroke No.*	I_{peak} [kA]	10-90% Risetime [μs]	D = 2 km	
				$H\varphi_{\text{peak}}$ [A/m]	Ez_{peak} [kV/m]
14-07-2000 13:47:20	1	6.14	1.11	0.77	0.31
01-08-2000 13:06:10	2	5.51	0.72	1.07	0.46
	3	7.2	1.04	0.72	0.47
	5	11.87	2.99	1.84	0.77
	6	7.49	0.31	1.84	0.72
	7	4.54	0.20	1.07	0.44
	8	7.72	0.44	1.90	0.79
23-08-2000 03:33:05	1	5.50	0.77	1.22	0.44
	2	2.37	0.73	0.46	0.18
	3	1.73	0.38	0.45	0.18
	4	4.87	0.23	1.11	0.46
	5	5.05	0.22	1.15	0.47
	6	3.07	0.21	0.73	0.30
	7	8.27	0.41	1.78	0.71
	8	6.43	0.23	1.54	0.66

* This number corresponds to the recorded sequence by the systems

Table 5.2 - Parameters associated with the event recorded on July 4th, 2001

Flash	Return stroke No.*	I_{peak} [kA]	10-90% Risetime [μs]	D = 2 km		D = 16.8 km	
				$H\varphi_{\text{peak}}$ [A/m]	Ez_{peak} [kV/m]	$H\varphi_{\text{peak}}$ [mA/m]	Ez_{peak} [V/m]
04-07-2001 13:25:54	1	20.8	8.41	3.22	0.91	257.52	119.57
	2	14.2	2.18	3.31	0.98	338.53	154.37
	3	15.4	8.38	2.59	0.81	242.80	104.31
	4	4.4	0.26	1.39	0.40	106.71	48.68
	5	5.1	0.65	1.72	0.47	136.12	69.51

* This number corresponds to the recorded sequence by the systems

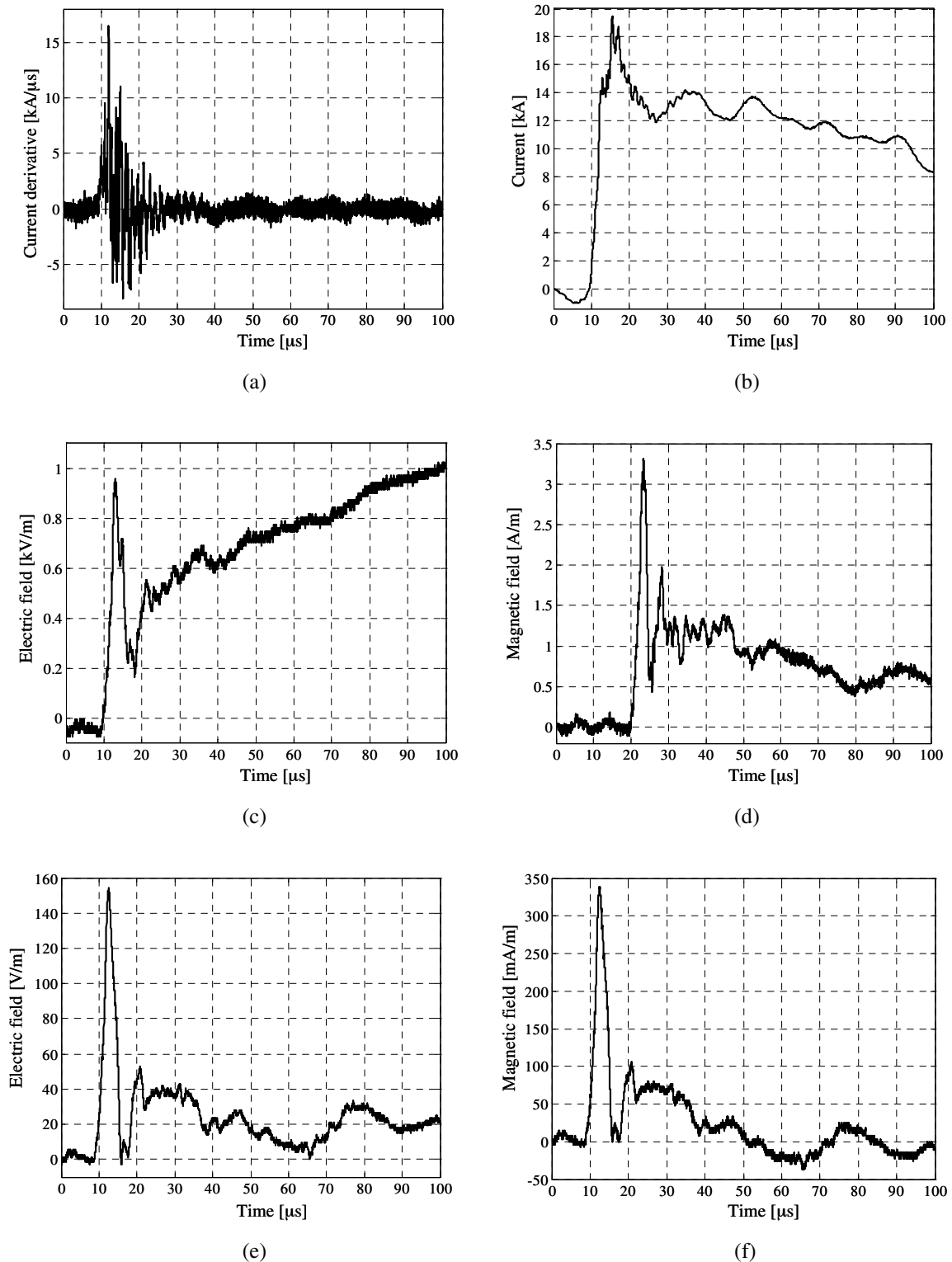


Figure 5.6 - Simultaneous recordings of: return stroke current derivative (a), return stroke current (numerically integrated) (b), electric and magnetic fields at 2 km (c) and (d), and those at 16.8 km (e) and (f), Stroke 2, Flash recorded on July 4th, 2001.

5.4 Comparison between theoretical expressions and experimental data

We will compare in this section values for the peak electric and magnetic fields obtained using equations (5-19) and (5-20), which include the enhancement of the elevated strike object, with the experimental data described in the previous section.

For the comparison, we will assume a return stroke speed of $v = 1.2 \times 10^8$ m/s as reported by [Wang *et al.*, 1995] and a top reflection coefficient $\rho_t = -0.156$ inferred from experimental data by [Janischewskyj *et al.*, 1996; Janischewskyj *et al.*, 2001; Shostak *et al.*, 2002].

Figs. 5.7 and 5.8 present a comparison between sets of simultaneously-measured current (satisfying the condition $t_f < 2h/c$), electric and magnetic field peaks, and the predictions of equations (5-19) and (5-20). In the same figure, we have also included calculations using equations (5-1) and (5-2), disregarding the presence of the elevated strike object.

It can be seen that the values for the peak electromagnetic field predicted by equations (5-1)-(5-2), which assume that the return stroke is initiated at ground level, are underestimated by a factor of about 4. Adjusting the return stroke speed in equations (5-1)-(5-2) to obtain good agreement leads to speeds much higher than the speed of light. It can also be seen that equations (5-19)-(5-20) yield a better estimate of the electromagnetic field peak. However, the field values seem to be still underestimated by the new equations. The differences between theoretical predictions and experimental data can be explained, at least in part, by

- the field enhancement effect of the buildings on which electromagnetic fields were measured. In [Bonyadi Ram *et al.*, 2001], such an enhancement for a 20-m to 30-m building was theoretically estimated, and found to be significant.
- reflections at structural discontinuities of the CN Tower [Janischewskyj *et al.*, 1997];
- the fact that, at 2 km from the channel, where the electric and magnetic fields were measured, not only the radiation term, but also the electrostatic term (for the E-field) and the induction terms (for both E- and H-fields) contribute to the peak value [Rachidi *et al.*, 2001]; and, finally,
- assumptions in the theoretical model and experimental errors.

Figs. 5.9 and 5.10 present similar results to those presented in figs. 5.7 and 5.8, considering two values for the return stroke speed, namely (1) $v = 1.2 \times 10^8$ m/s, a value reported by [Wang *et al.*, 1995], and (2) $v = 1.9 \times 10^8$ m/s, a value corresponding to the average speed for subsequent return strokes along the lower 500 m of the lightning channel, reported by [Mach and Rust, 1989]. It can

be seen that the field peak increases with the return stroke speed, although this increase remains rather insignificant.

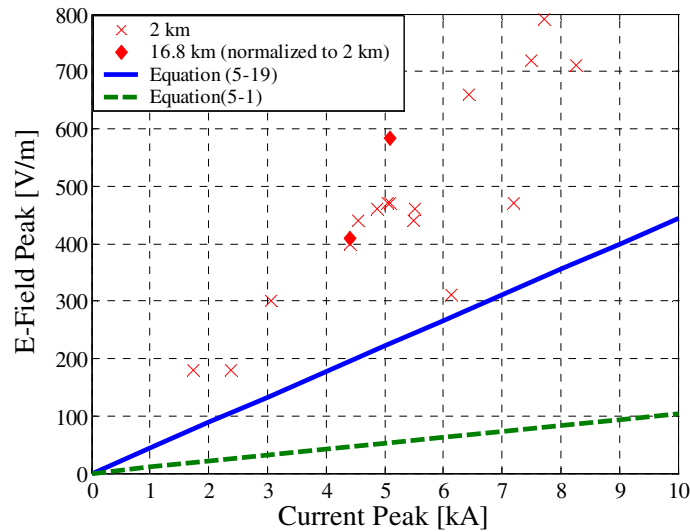


Figure 5.7 - Electric field peak as a function of return stroke current peak. Comparison between experimental data and computed results using the derived Equation (5-19), and Equation (5-1). The values for the field peaks at 16.8 km have been normalized to those at 2 km assuming 1/r dependence (Reported current peaks are those satisfying the condition

$$t_f < h/c).$$

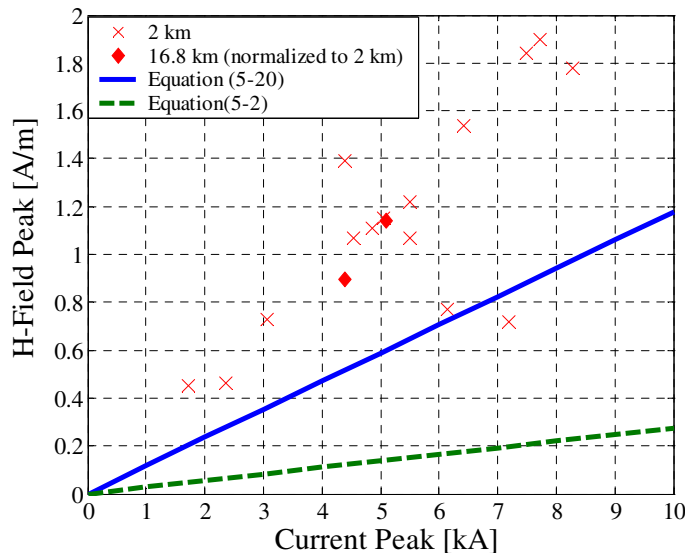


Figure 5.8 - Magnetic field peak as a function of return stroke current peak. Comparison between experimental data and computed results using the derived Equation (5-20), and Equation (5-2). The values for the field peaks at 16.8 km have been normalized to those at 2 km assuming 1/r dependence (Reported current peaks are those satisfying the

$$\text{condition } t_f < h/c).$$

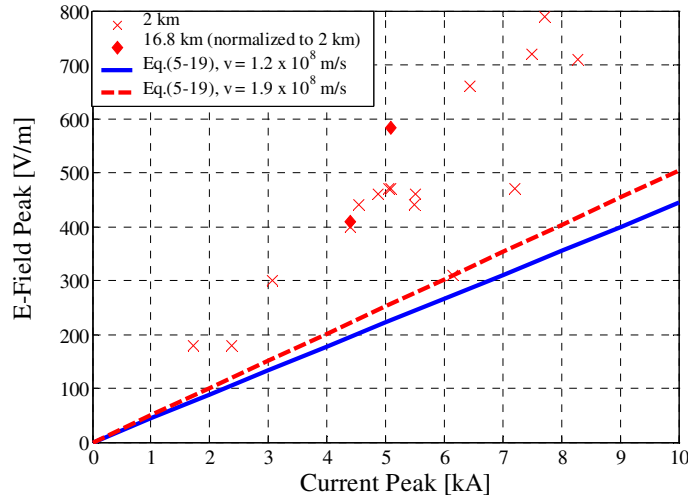


Figure 5.9 - Electric field peaks as a function of return stroke current peak. Comparison between experimental data and computed results using the derived Equation (5-19), considering two different values for the return stroke speed. The values for the field peaks at 16.8 km have been normalized to those at 2 km assuming $1/r$ dependence. (Reported current peaks are those satisfying the condition $t_f < h/c$).

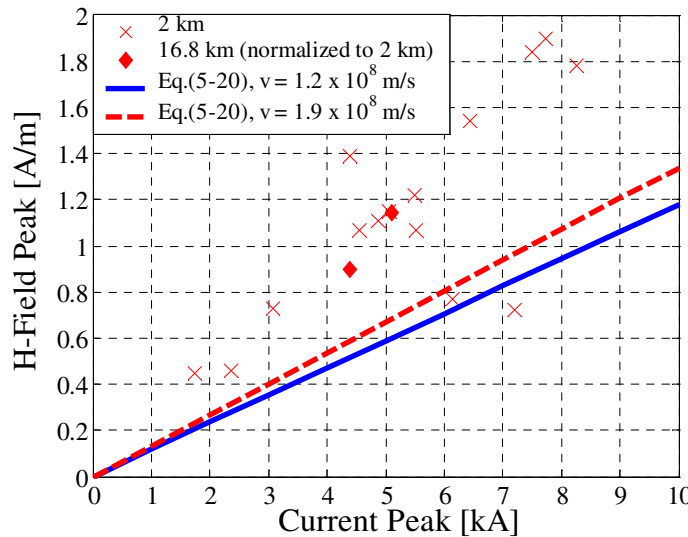


Figure 5.10 - Magnetic field peaks as a function of return stroke current peak. Comparison between experimental data and computed results using the derived Equation (5-20), considering two different values for the return stroke speed. The values for the field peaks at 16.8 km have been normalized to those at 2 km assuming $1/r$ dependence. (Reported current peaks are those satisfying the condition $t_f < h/c$).

5.5 Summary and conclusions

We derived in this chapter new expressions relating lightning return stroke currents and far radiated electric and magnetic fields, taking into account the presence of an elevated strike object, whose presence is included as an extension to the TL model.

The derived expressions show that, for electrically-tall structures satisfying condition (5-13), the field enhancement with respect to a return stroke initiated at ground level is expressed simply

through a factor equal to $(k = \frac{1+(1-2\rho_t)c/v}{1-\rho_t})$, where v and c are the return stroke speed and the speed of light, respectively, and ρ_t is the top reflection coefficient. Since the top reflection coefficient ρ_t is typically negative, electrically-tall towers result in an important enhancement of the radiated electromagnetic field, which could be as large as 4 times the field radiated by a similar return stroke but initiated at ground level.

For very short towers and/or very slow return stroke current wavefronts, when condition (5-22) applies, an expression relating the far electromagnetic field and the return stroke current was also derived. For the case of return strokes initiated at ground level ($h = 0$), this expression represents a generalization of equations (5-1) and (5-2), in which the reflections at ground are taken into account.

We performed the first simultaneous measurements of the electric and magnetic fields at two distances and of the return stroke current associated with lightning strikes to the Toronto CN Tower. The lightning current was measured using a Rogowski coil installed at a height of 474 m above ground level. The vertical component of the electric field and the azimuthal component of the magnetic field were measured simultaneously at distances of 2 km (Rosebrugh building of the University of Toronto) and 16.8 km (Environment Canada Building) from the CN Tower.

The derived expressions for electrically-tall strike objects were tested versus sets of simultaneously-measured currents and fields associated with lightning strikes to the CN Tower in Toronto, and reasonable agreement was found. A major source of disagreement is presumably the enhancement effect of the buildings on which field sensors were located.

Additionally, it was shown that the peak of the electromagnetic field radiated by a lightning strike to a tall structure is relatively insensitive to the value of the return stroke velocity, in contrast with lightning strikes to ground.

The proposed expressions could find a useful application when lightning currents are measured directly on instrumented towers to calibrate the performances of lightning location systems.

5.6 References Chapter 5

- Baba, Y., and M. Ishii, Numerical electromagnetic field analysis on lightning surge response of tower with shield wire, *IEEE Transactions on Power Delivery*, 15 (3), 1010-15, 2000.
- Bermudez, J.L., F. Rachidi, W. Janischewskyj, A.M. Hussein, M. Rubinstein, C.A. Nucci, M. Paolone, V. Shostak, and J.S. Chang, On the Enhancement of Radiated Electric and

Magnetic Fields Associated with Lightning Return Strokes to Tall Structures, in *IEEE International Conference on Electromagnetic Compatibility*, Montreal, Canada, 2001.

Bermudez, J.L., F. Rachidi, W. Janischewskyj, A.M. Hussein, V. Shostak, M. Rubinstein, C.A. Nucci, J.S. Chang, P. Joe, and M. Nyffeler, Simultaneous Measurements of Electromagnetic Fields at Two Distances and of Current Associated with Lightning Return Strokes to the CN Tower, in *26th ICLP (International Conference on Lightning Protection)*, Cracow, Poland, 2002.

Bonyadi Ram, S., R. Moini, S.H.H. Sadeghi, and A. Mahanfar, The effects of tall buildings on the measurement of electromagnetic fields due to lightning return strokes, in *2001 IEEE EMC International Symposium*, pp. 1001-1004, IEEE EMC Society, Montreal, Canada, 2001.

Cummins, K.L., E.P. Krider, and M.D. Malone, The US National Lightning Detection Network (TM) and applications of cloud-to-ground lightning data by electric power utilities, *IEEE Transactions on Electromagnetic Compatibility*, 40 (4) Part 2, 465-480, 1998.

Diendorfer, G., Effect of an elevated strike object on the lightning electromagnetic fields, in *9th International Symposium on Electromagnetic Compatibility*, pp. pp. 235-238, Zurich, Switzerland, 1991.

Guerrieri, S., F. Heidler, C.A. Nucci, F. Rachidi, and M. Rubinstein, Extension of two return stroke models to consider the influence of elevated strike objects on the lightning return stroke current and the radiated electromagnetic field: comparison with experimental results, in *EMC '96 (International Symposium on Electromagnetic Compatibility)*, pp. 701-6, Rome, Italy, 1996.

Herodotou, N., W.A. Chisholm, and W. Janischewskyj, Distribution of lightning peak stroke currents in Ontario using an LLP system, *IEEE Transactions on Power Delivery*, 8 (3), 1331-9, 1993.

- Hussein, A.M., W. Janischewskyj, J.S. Chang, V. Shostak, W.A. Chisholm, P. Dzurevych, and Z.I. Kawasaki, Simultaneous measurement of lightning parameters for strokes to the Toronto Canadian National Tower, *Journal of Geophysical Research*, 100 (D5), 8853-61, 1995.
- Janischewskyj, W., A.M. Hussein, and V. Shostak, Propagation of lightning current within the CN Tower, in *CIGRE Study Committee 33 Colloquium*, Toronto, Canada, 1997.
- Janischewskyj, W., A.M. Hussein, V. Shostak, P. Dzurevych, and W.A. Chisholm, Analysis of Electromagnetic Fields from Lightning Strikes to the Toronto CN Tower and from Lightning in the Surrounding Area, in *CIGRE Symposium on Power System Electromagnetic Compatibility*, pp. 1-6, Lausanne, Switzerland, 1993.
- Janischewskyj, W., V. Shostak, J. Barratt, A.M. Hussein, I. Rusan, and J.S. Chang, Collection and use of lightning return stroke parameters taking into account characteristics of the struck object, in *23rd ICLP (International Conference on Lightning Protection)*, pp. 16-23, Florence, Italy, 1996.
- Janischewskyj, W., V. Shostak, and A.M. Hussein, Comparison of lightning electromagnetic field characteristics of first and subsequent return strokes to a tall tower 1. Magnetic field, in *24th ICLP (international conference on lightning Protection)*, pp. 245-251, Birmingham, U.K., 1998.
- Janischewskyj, W., V. Shostak, and A.M. Hussein, Multi-Section Lightning-Current Model of the CN Tower, in *International Symposium on Lightning Protection, VI SIPDA*, Santos, Brazil, 2001.
- Lin, Y.T., M.A. Uman, J.A. Tiller, R.D. Brantley, W.H. Beasley, E.P. Krider, and C.D. Weidman, Characterization of lightning return stroke electric and magnetic fields from simultaneous two-station measurements, *Journal of Geophysical Research*, 84 (C10), 6307-14, 1979.
- Mach, D.M., and W.D. Rust, A photoelectric technique for measuring lightning-channel propagation velocities from a mobile laboratory, *Journal of Atmospheric and Oceanic Technology*, 6 (3), 439-45, 1989.

- Motoyama, H., W. Janischewskyj, A.M. Hussein, R. Rusan, W.A. Chisholm, and J.S. Chang, Electromagnetic field radiation model for lightning strokes to tall structures, *IEEE Transactions on Power Delivery*, 11 (3), 1624-32, 1996.
- Rachidi, F., M. Ianoz, C.A. Nucci, and C. Mazetti, Modified transmission line model for LEMP calculations. Effect of the return stroke velocity decreasing and elevated strike objects on close fields, in *9th International Conference on Atmospheric Electricity*, pp. 664-667, St. Petersburg, Russia, 1992.
- Rachidi, F., W. Janischewskyj, A.M. Hussein, C.A. Nucci, S. Guerrieri, and J.S. Chang, Electromagnetic fields radiated by lightning return strokes to high towers, in *24th ICLP (International Conference on Lightning Protection)*, Birmingham, UK, 1998.
- Rachidi, F., W. Janischewskyj, A.M. Hussein, C.A. Nucci, S. Guerrieri, B. Kordi, and J.S. Chang, Current and electromagnetic field associated with lightning return strokes to tall towers, *IEEE Transactions on Electromagnetic Compatibility*, 43 (3), 356-366, 2001.
- Rachidi, F., V.A. Rakov, C.A. Nucci, and J.L. Bermudez, The Effect of Vertically-Extended Strike Object on the Distribution of Current Along the Lightning Channel, *Journal of Geophysical Research*, 107 (D23), 4699, 2002.
- Rachidi, F., and R. Thottappillil, Determination of lightning currents from far electromagnetic fields, *Journal of Geophysical Research*, 98 (D10), 18315-20, 1993.
- Rakov, V.A., Transient response of a tall object to lightning, *IEEE Transactions on Electromagnetic Compatibility*, 43 (4), 654-61, 2001.
- Rusan, I., W. Janischewskyj, A.M. Hussein, and J.S. Chang, Comparison of measured and computed electromagnetic fields radiated from lightning strikes to the Toronto CN tower, in *23rd ICLP (International Conference on Lightning Protection)*, pp. 297-303, Florence, Italy, 1996.
- Shostak, V., W. Janischewskyj, A. Hussein, J.S. Chang, F. Rachidi, and J.L. Bermudez, Modeling of the electromagnetic field associated with lightning return strokes to a complex tall tower,

in *26th ICLP (International Conference on Lightning Protection)*, pp. 167-172, Cracow, Poland, 2002.

Shostak, V., W. Janischewskyj, A. Hussein, and B. Kordi, Electromagnetic fields of lightning strikes to a tall tower: a model that accounts for upward-connecting discharges, in *25th ICLP (International Conference on Lightning Protection)*, pp. 60 - 65, Rhodes, Greece, 2000.

Uman, M.A., D.K. McLain, and E.P. Krider, The electromagnetic radiation from a finite antenna, *American Journal of Physics*, 43 (1), 33-8, 1975.

Wang, D., Z.I. Kawasaki, K. Yamamoto, K. Matsuura, C. Jen Shin, and W. Janischewskyi, Luminous propagation of lightning attachment to CN tower, *Journal of Geophysical Research*, 100 (D6), 11661-7, 1995.

Willett, J.C., J.C. Bailey, V.P. Idone, A. Eybert-Berard, and L. Barret, Submicrosecond Intercomparison of Radiation Fields and currents in triggered Lightning Return Strokes Based on the Transmission-Line Model, *Journal of Geophysical Research*, 94 (D11), 13,275 - 13,286, 1989.

Willett, J.C., V.P. Idone, R.E. Orville, C. Leteinturier, A. Eybert Berard, L. Barret, and E.P. Krider, An experimental test of the 'transmission-line model' of electromagnetic radiation from triggered lightning return strokes, *Journal of Geophysical Research*, 93 (D4), 3867-78, 1988.

Chapter 6

Characterization of the elevated strike object and extraction of primary current waveform

6.1 Introduction

In Chapter 4, we introduced the effect of a strike object on the most commonly used engineering return stroke models. This resulted in expressions for the return stroke current both in the channel and in the strike object itself. In Chapter 5, we used those expressions to investigate the influence of the strike object on the associated distant electromagnetic fields. Up to now, we have assumed that the reflection coefficients at the top and at the bottom of the strike object are frequency independent and known. In this chapter, we address the problem of the estimation of those reflection coefficients, taking into account their frequency dependence, based on direct current measurements. That problem was addressed by [Bermudez *et al.*, 2001b] and [Bermudez *et al.*, 2002b], on which this chapter is based.

We will proceed as follows: First, a closed form expression for the infinite summation formula given in Chapter 4 for the current along the lightning channel and along the strike object will be derived. The derivations will be carried out both in the time domain and in the frequency domain. Further, we will show how the reflection coefficient at the ground can be obtained from lightning current measurements at two different heights along the elevated strike object. We will also show that the exact calculation of the reflection coefficient at the top is impossible from any number of lightning current measurements unless the tower is tall enough that the current or its time derivative do not overlap with any of their reflections. We will propose two methods to estimate the top reflection coefficient. One of the methods is based on an extrapolation technique. The second method is based on the fact that the waveshape of the time derivative of the current is much narrower than that of the current itself.

The proposed methods to infer the ground and top reflection coefficients will be tested versus experimental data obtained at the Peissenberg Tower and compared with estimated values found by [Heidler *et al.*, 2001] and [Fuchs, 1998a].

At the end of this chapter, we will show how genetic algorithms can be used to extract, from experimental current data, the tower reflection coefficients and the parameters of the undisturbed

current modeled as a sum of two Heidler functions. These parameters can be used to reproduce the initial part of experimentally measured current waveshapes.

Some workers [Beierl, 1992; Guerrieri et al., 1996; Guerrieri et al., 1998] obtained the ‘primary’ undisturbed current (which they call “decontaminated” current) by assuming constant, frequency independent reflection coefficients at the top and the bottom of the strike object (ρ_t and ρ_g , respectively). In those studies, the authors inferred the value of the reflection coefficients from a reduced experimental set of current waveforms found in the literature [Beierl, 1992; Montandon and Beyeler, 1994; Willett et al., 1988].

To decontaminate the current, [Guerrieri et al., 1998] proposed a formula, corrected by [Rachidi et al., 2002] as explained in Chapter 4, that involves an infinite summation in the time domain, assuming that the reflection coefficients, ρ_t and ρ_g , are constant and known.

[Gavric, 2002] proposed an iterative method based on the Electromagnetic Transient Program (EMTP) to remove superimposed reflections caused by a strike tower from digitally recorded lightning flash currents.

[Rakov, 2001] reviewed experimental data showing the transient behavior of tall objects struck by lightning and concluded that the peak current measured at the bottom of the strike object is more strongly affected by the transient process in the object than the peak current at the top.

[Janischewskyj et al., 1996], derived reflection coefficients at the CN Tower in Toronto and stated that the values depend on the initial rise time of the measured current, although the limited number of points in their plots render the drawing of conclusions difficult. A dependence on the risetime would suggest that at least one of the reflection coefficients is a function of the frequency. They also proposed a method to extract the reflection coefficients from the measured current waveform. However, their method is applicable only assuming a simplified current waveform (double ramp) and neglecting any frequency dependence for the reflection coefficients.

It is interesting to note that the effect of the strike object may have had an influence on the measurements of Berger and co-workers [Berger et al., 1975], on which a considerable fraction of the lightning statistics applied to lightning protection are based today. [Rakov, 2002] estimated that, for subsequent strokes, the difference in the peak current measured (1) at an ideally grounded object of negligible height ($h=0$) and (2) at the top of Berger's tower ($h=70$ m) would be about 10%. The difference in the peak currents of individual strokes depends not only on the height of the tower, but also on the rise time of the current itself. If the return stroke current statistics measured on one tower are to be extrapolated to other strike objects of different heights and electrical characteristics, it is desirable to obtain statistics on the ‘primary’ current, exempt from the disturbances introduced

by the transient processes along the tower. To obtain this ‘primary’ current, it is important to correctly infer the values of the tower’s reflection coefficients.

6.2 Model of a vertically-extended strike object

The geometry of the tower is shown in Fig. 6.1a. We begin with the same assumptions made in chapters 4 and 5, similar to recent studies (e.g. [Guerrieri et al., 1998], [Janischewskyj et al., 1996], [Rachidi et al., 2001], [Rakov, 2001], [Rachidi et al., 2002]).

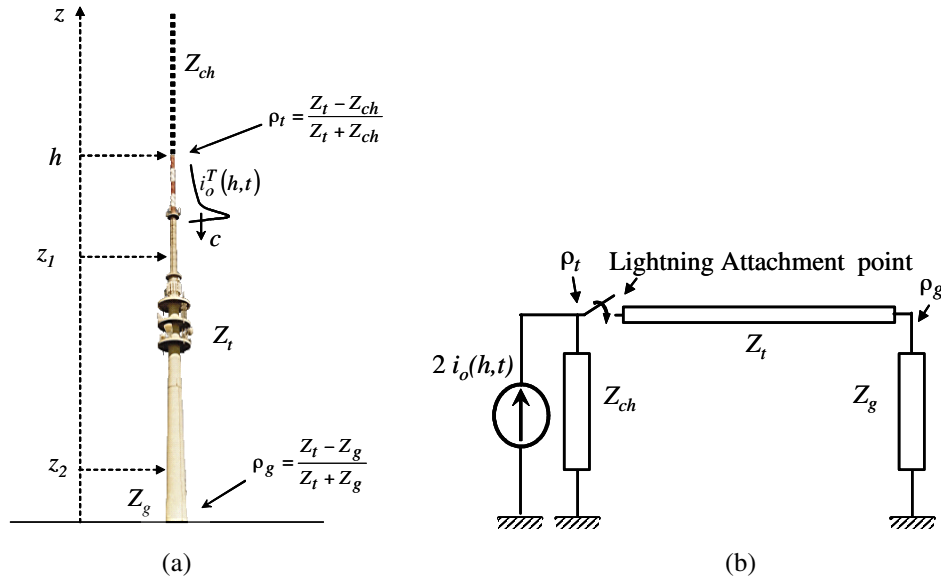


Figure 6.1 - (a) Struck object geometry, and (b) equivalent circuit.

A debate has recently arisen (e.g. [Kordi et al., 2002; Thottappillil et al., 2001; Thottappillil et al., 2002]) concerning the validity of a lossless transmission line assumption for the case of a vertical structure above a ground plane. This controversy is not yet settled. However, based on measurements on reduced-scale models of towers (see Appendix 4), in which it is shown that the errors are small for the first few reflections (e.g. [Bermudez et al., 2001a], [Gutierrez et al., 2002]), we consider in this chapter the strike object as a lossless uniform transmission line of length h with a propagation speed equal to the speed of light c . We further assume that the reflection coefficients, defined for the currents propagating in the tower, are constant (this last assumption will be relaxed later). We also disregard any upward connecting leader and any reflections at the return stroke wavefront. At the onset of the return stroke at the tower top, the return stroke current depends only on the impedances of the lightning channel and of the tower top, until information about the ground gets to the top of the tower in the form of ground reflections. We model the ground plane as lumped impedance at the bottom of the tower.

Fig. 6.1b is a reproduction of Fig. 4.4 introduced in Chapter 4, which presents the generalized equivalent circuit of the lightning channel, the strike object, and the ground. In the figure, lightning channel is represented as the current source with its associated equivalent impedance, Z_{ch} . As explained in Chapter 4, the amplitude of the current source, equal to $2 i_o(h,t)$, was chosen so that the current injected into the top of the tower equals the so-called ‘undisturbed current’ $i_o(h,t)$ when both reflection coefficients ρ_t and ρ_g are equal to zero. The reflection coefficients are zero when the equivalent impedance of the channel, Z_{ch} , is identical to the characteristic impedance of the tower, Z_t , and to the grounding impedance, Z_g . Using that model, we can obtain the expression describing the spatial-temporal distribution of the current along the strike object, Equation (6-1a). This expression is identical to equations (4-25) and (5-5).

$$i(z,t) = (1 - \rho_t) \sum_{n=0}^{\infty} \left[\rho_t^n \rho_g^n i_o \left(h, t - \frac{h-z}{c} - \frac{2nh}{c} \right) u \left(t - \frac{h-z}{c} - \frac{2nh}{c} \right) + \rho_t^n \rho_g^{n+1} i_o \left(h, t - \frac{h+z}{c} - \frac{2nh}{c} \right) u \left(t - \frac{h+z}{c} - \frac{2nh}{c} \right) \right] \quad 0 \leq z \leq h \quad (6-1a)$$

Equation (6-1a) can be rewritten in terms of the transmitted current into the top of the tower as

$$i(z,t) = \sum_{n=0}^{\infty} \left[\rho_t^n \rho_g^n i_o^T \left(h, t - \frac{h-z}{c} - \frac{2nh}{c} \right) u \left(t - \frac{h-z}{c} - \frac{2nh}{c} \right) + \rho_t^n \rho_g^{n+1} i_o^T \left(h, t - \frac{h+z}{c} - \frac{2nh}{c} \right) u \left(t - \frac{h+z}{c} - \frac{2nh}{c} \right) \right] \quad 0 \leq z \leq h \quad (6-1b)$$

where $i_o^T(h,t)$ is the current transmitted into the top of the tower, z is the height of the measurement point along the strike object, h is the total strike object’s height, ρ_t and ρ_g are the reflection coefficients for current at the top and bottom of the object, respectively, and $u(t)$ is the Heaviside unit step function, which, for the sake of simplicity, will be omitted in the following developments. Equation (6-1b) differs from the expression used in [Guerrieri et al., 1998] in that the current $i_o^T(h,t)$ is used instead of the undisturbed current $i_o(h,t)$ to take into account the impedance discontinuity at the top of the tower as explained in [Rachidi et al., 2002], where the current injected into the tower is expressed as $i_o^T(h,t) = (1 - \rho_t) i_o(h,t)$.

Using Equation (6-1b) and assuming that both reflection coefficients, ρ_t and ρ_g , are known, it is possible to write an expression to extract the ‘undisturbed’ current from the current measured at the top of the tower as proposed by [Guerrieri et al., 1998]. This reads

$$\begin{cases} i_o(h,t) = \frac{1}{1 - \rho_t} i(h,t) & \text{for } t < \left(\frac{2h}{c} \right) \\ i_o(h,t) = \frac{1}{1 - \rho_t} i(h,t) - \frac{1}{1 - \rho_t} \sum_{n=0}^k \rho_t^{n-1} \rho_g^n (1 + \rho_t) i_o \left(h, t - \frac{2nh}{c} \right) & \text{for } \frac{2kh}{c} \leq t \leq \frac{2(k+1)h}{c} \text{ with } k = 1, 2, \dots \end{cases} \quad (6-2)$$

where, again, the factor $(1-\rho_t)$ appears in accordance with [Rachidi et al., 2002] (Chapter 4).

Let us now relax the assumption that the reflection coefficients are constant and independent of frequency and let us transform Equation (6-1b) into the frequency domain. The time domain versions of the frequency dependent reflection coefficients in Equation (6-1b) become impulse response functions ($\rho_t(t)$ and $\rho_g(t)$), and the multiplications become convolution products. Making these changes, we obtain

$$i(z,t) = \sum_{n=0}^{\infty} \left[\rho_t^n(t) * \rho_g^n(t) * i_o^T\left(h,t - \frac{h-z}{c} - \frac{2nh}{c}\right) + \rho_t^n(t) * \rho_g^{n+1}(t) * i_o^T\left(h,t - \frac{h+z}{c} - \frac{2nh}{c}\right) \right] \quad (6-3)$$

where the current transmitted into the top of the tower is now $i_o^T(h,t) = (\delta(t) - \rho_t(t)) * i_o(h,t)$.

In Equation (3), “*” represents a convolution product and the powers “ n ” and “ $n+1$ ” in the reflection coefficients $\rho_t(t)$ and $\rho_g(t)$ are implicitly carried out using convolution products.

In terms where the exponential variable n equals zero, the expression $\rho_i^0(t) = \delta(t)$ (where the subindex $i = t$ or g) should be used.

Now, transforming Equation (6-3) into the frequency domain, we obtain

$$I(z,\omega) = \sum_{n=0}^{\infty} \left[\rho_t^n(\omega) \rho_g^n(\omega) I_o^T(h,\omega) e^{-j\omega \frac{h-z+2nh}{c}} + \rho_t^n(\omega) \rho_g^{n+1}(\omega) I_o^T(h,\omega) e^{-j\omega \frac{h+z+2nh}{c}} \right] \quad (6-4)$$

Regrouping terms, Equation (6-4) can be written as,

$$I(z,\omega) = I_o^T(h,\omega) e^{-j\omega \frac{h}{c}} \left(e^{j\omega \frac{z}{c}} + \rho_g(\omega) e^{-j\omega \frac{z}{c}} \right) \sum_{n=0}^{\infty} \left(\rho_t(\omega) \rho_g(\omega) e^{-j\omega \frac{2h}{c}} \right)^n \quad (6-5)$$

The summation on the right-hand side of Equation (6-5) is recognized as a geometrical series (Chapter 4, Section 4.5.1). Using the expression of the sum of its terms and letting n go to infinity, we get

$$I(z,\omega) = \frac{I_o^T(h,\omega) e^{-j\omega \frac{h}{c}} \left(e^{j\omega \frac{z}{c}} + \rho_g(\omega) e^{-j\omega \frac{z}{c}} \right)}{1 - \rho_t(\omega) \rho_g(\omega) e^{-j\omega \frac{2h}{c}}} \quad (6-6a)$$

Transforming Equation (6-6a) into the time domain, we obtain,

$$i(z,t) = \frac{i_o^T(h,t - \frac{h}{c}) * \left(\delta\left(t + \frac{z}{c}\right) + \rho_g\left(t - \frac{z}{c}\right) \right)}{\delta(t) - \rho_t(t) * \rho_g\left(t - \frac{2h}{c}\right)} \quad (6-6b)$$

Equations (6-6a) and (6-6b) are closed form expressions for the current at any point z along the strike object taking into account all the reflections at the bottom and at the top.

If the reflection coefficients $\rho_t(\omega)$ and $\rho_g(\omega)$ are known, the current transmitted into the tower $I_o^T(h,\omega)$ and the ‘undisturbed’ current $I_o(h,\omega) = I_o^T(h,\omega)/(1 - \rho_t(\omega))$, can be directly inferred from the measured current $I(z,\omega)$ using Equation (6-6a) or, in the time domain, using Equation (6-6b).

6.3 Determination of the ground reflection coefficient from two simultaneous current measurements

In this section, we derive an expression to calculate the reflection coefficient $\rho_g(\omega)$ from currents measured simultaneously at two different heights along the strike object, for the general case in which no conditions are imposed on the height of the tower.

Let us assume that $I(z_1,\omega)$ and $I(z_2,\omega)$ are the currents measured simultaneously at heights z_1 and z_2 in the frequency domain. Making use of Equation (6-6a), we can write expressions for each of the currents as follows

$$I(z_1,\omega) = \frac{I_o^T(h,\omega) e^{-j\omega\frac{h}{c}} \left(e^{j\omega\frac{z_1}{c}} + \rho_g(\omega) e^{-j\omega\frac{z_1}{c}} \right)}{1 - \rho_t(\omega) \rho_g(\omega) e^{-j\omega\frac{2h}{c}}} \quad (6-7)$$

$$I(z_2,\omega) = \frac{I_o^T(h,\omega) e^{-j\omega\frac{h}{c}} \left(e^{j\omega\frac{z_2}{c}} + \rho_g(\omega) e^{-j\omega\frac{z_2}{c}} \right)}{1 - \rho_t(\omega) \rho_g(\omega) e^{-j\omega\frac{2h}{c}}} \quad (6-8)$$

Dividing Equation (6-8) by Equation (6-7), we obtain

$$\frac{I(z_2,\omega)}{I(z_1,\omega)} = \frac{e^{j\omega\frac{z_2}{c}} + \rho_g(\omega) e^{-j\omega\frac{z_2}{c}}}{e^{j\omega\frac{z_1}{c}} + \rho_g(\omega) e^{-j\omega\frac{z_1}{c}}} \quad (6-9)$$

Solving for the ground reflection coefficient $\rho_g(\omega)$ in Equation (6-9), we obtain the result sought:

$$\rho_g(\omega) = \frac{I(z_2, \omega) e^{j\omega \frac{z_1}{c}} - I(z_1, \omega) e^{j\omega \frac{z_2}{c}}}{I(z_1, \omega) e^{-j\omega \frac{z_2}{c}} - I(z_2, \omega) e^{-j\omega \frac{z_1}{c}}} \quad (6-10)$$

Interestingly, the ground reflection coefficient can be found without prior knowledge of the reflection coefficient at the top of the strike object. Equation (6-10) allows us to infer the ground reflection coefficient at any frequency from two simultaneously measured currents at two different heights along the strike object. The application of Equation (6-10) is illustrated and numerically validated in the Appendix 3.

Equation (6-10) can be expressed in terms of current derivatives by multiplying the numerator and the denominator of the right-hand side by “ $j\omega$ ”,

$$\rho_g(\omega) = \frac{\dot{I}(z_2, \omega) e^{j\omega \frac{z_1}{c}} - \dot{I}(z_1, \omega) e^{j\omega \frac{z_2}{c}}}{\dot{I}(z_1, \omega) e^{-j\omega \frac{z_2}{c}} - \dot{I}(z_2, \omega) e^{-j\omega \frac{z_1}{c}}} \quad (6-11)$$

in which $\dot{I}(z, \omega) = j\omega I(z, \omega)$ represents the Fourier transform of $\partial i(z, t) / \partial t$.

The new equation is better suited for instrumented towers where the current derivative is measured directly using, for example, magnetic loops or Rogowski coils; this is for example the case of the well known Peissenberg tower, the CN Tower, and the Saint Chrischona tower.

In Section 6.5, we will apply Equation (6-11) to recover the ground reflection coefficient in the frequency domain for current derivatives measured at the Peissenberg Tower, using simultaneous measurement at two different heights.

6.4 Estimation of the top reflection coefficient of the strike object

Either Equation (6-3) or equations (6-6) give the measurable (disturbed) current at any height along the strike object. The variables that appear in Equation (6-6a) are listed in Table 6-1. In the second column of that table, we have identified the variables that are directly known from a current measurement at a given height z .

Three of the variables in Table 6.1, the current transmitted into the tower, $i_o^T(h, \omega)$, the reflection coefficient at the ground, $\rho_g(\omega)$, and the reflection coefficient at the top, $\rho_t(\omega)$, are unknown. As already mentioned in Section 6.2, [Guerrieri et al., 1998] assumed values for two of the three parameters (the reflection coefficients) and used Equation (6-3) to find the only remaining unknown, the current $i_o^T(h, \omega)$. The following question arises: Is it possible to make three

independent measurements to obtain from them all three unknown parameters? We now attempt to answer that question.

Table 6.1 - Variables in Equation (6-6): The second column indicates which variables are known from direct current measurements.

Variable	Known
Strike object length h	✓
Measurement height z	✓
Measured current $i(z, \omega)$	✓
Ground reflection coeff. $\rho_g(\omega)$	x
Top reflection coeff. $\rho_t(\omega)$	x
Injected current $i_o^T(h, \omega)$	x

In Section 6.3, we particularized Equation (6-6a) for two different heights (equations (6-7) and (6-8)) and we were able to solve for the ground reflection coefficient. As we are about to show, once the ground reflection coefficient is known, measurements at other heights do not provide any additional information and, therefore, do not allow us to calculate the top reflection coefficient or the “undisturbed” current.

For convenience, we rewrite Equation (6-6a) here:

$$I(z, \omega) = \frac{I_o^T(h, \omega) e^{-j\omega \frac{h}{c}} \left(e^{j\omega \frac{z}{c}} + \rho_g(\omega) e^{-j\omega \frac{z}{c}} \right)}{1 - \rho_t(\omega) \rho_g(\omega) e^{-j\omega \frac{2h}{c}}} \tag{6-12}$$

Rearranging terms, Equation (6-12) can be rewritten as follows,

$$I(z, \omega) = K(\omega) \left[e^{j\omega \frac{z}{c}} + \rho_g(\omega) e^{-j\omega \frac{z}{c}} \right] \tag{6-13}$$

where

$$K(\omega) = \left(\frac{I_o^T(h, \omega) e^{-j\omega \frac{h}{c}}}{1 - \rho_t(\omega) \rho_g(\omega) e^{-j\omega \frac{2h}{c}}} \right) \tag{6-14}$$

The factor $K(\omega)$ is independent of the height of the measurement system along the tower and it can be determined from two simultaneous measurements of the current at different heights as follows: First, the ground reflection coefficient can be found from Equation (6-10) using the two simultaneous current measurements. Then, to find $K(\omega)$, we rewrite Equation (6-13) as follows,

$$K(\omega) = \left(\frac{I(z, \omega)}{e^{j\omega \frac{z}{c}} + \rho_g(\omega) e^{-j\omega \frac{z}{c}}} \right) \quad (6-15)$$

We can now substitute one of the two measured currents and the ground reflection coefficient into Equation (6-15) to obtain $K(\omega)$.

Now, since $K(\omega)$ and the ground reflection coefficient are known from two current measurements for a given strike, we can use Equation (6-13) to find the current at any other height z along the elevated strike object without prior knowledge of the top reflection coefficient or the injected current. The implication is that a current measurement at a third height does not supply any new information and it is therefore impossible, under the current assumptions, to find exactly the frequency dependent reflection coefficient at the top or the undisturbed current from any number of simultaneous current measurements.

Nevertheless, if the strike-object is long enough that the undisturbed current or its time derivative falls to zero before any reflections arrive, it would be possible to measure the reflection coefficients both at the top and at the bottom using just one current measurement in the time domain. For practical tower heights, only the derivative may be narrow enough.

In the next two sections, we propose two approximate methods to estimate the top reflection coefficient.

6.4.1 Extrapolation technique using measured current waveforms at the top of the tower

The current at any given height along the tower is composed of the original current transmitted into the tower plus multiple reflections coming from mismatched impedances at its top and bottom. In this first method to calculate $\rho_t(t)$, we will employ a current waveform measured at the top of the tower, although the method can be extended to currents measured anywhere along it. Fig. 6-2a reproduces the components of current at the top of the strike object, $z = h$.

The choice of the polarities for the components of the current in Fig. 6-2a, is based on the following observation made by [Rakov, 2001]: “The effective grounding impedance of the tower is much smaller than its characteristic impedance and the latter impedance is appreciably lower than the equivalent impedance of the lightning channel”. The observation implies that the current reflection coefficient at the ground is positive and that the top reflection coefficient is negative. The total current is the addition of all the components.

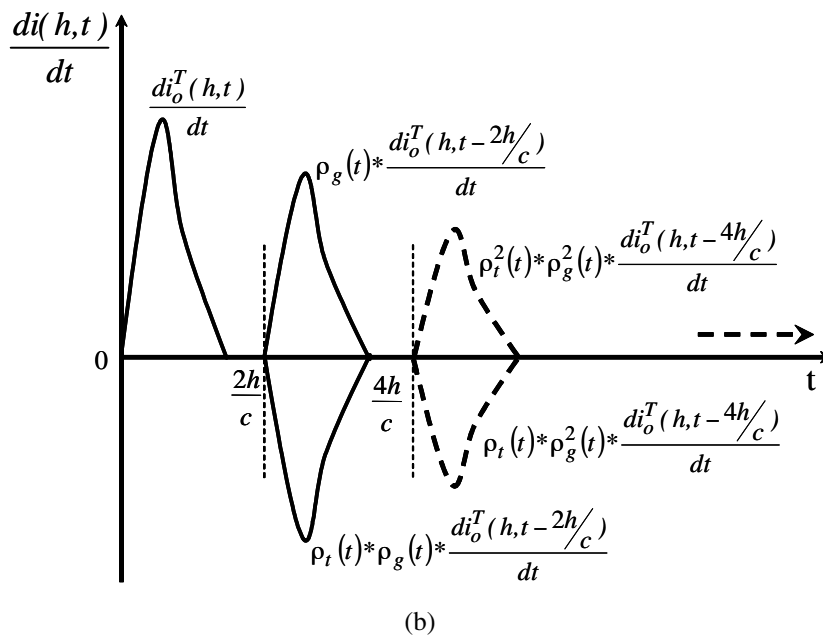
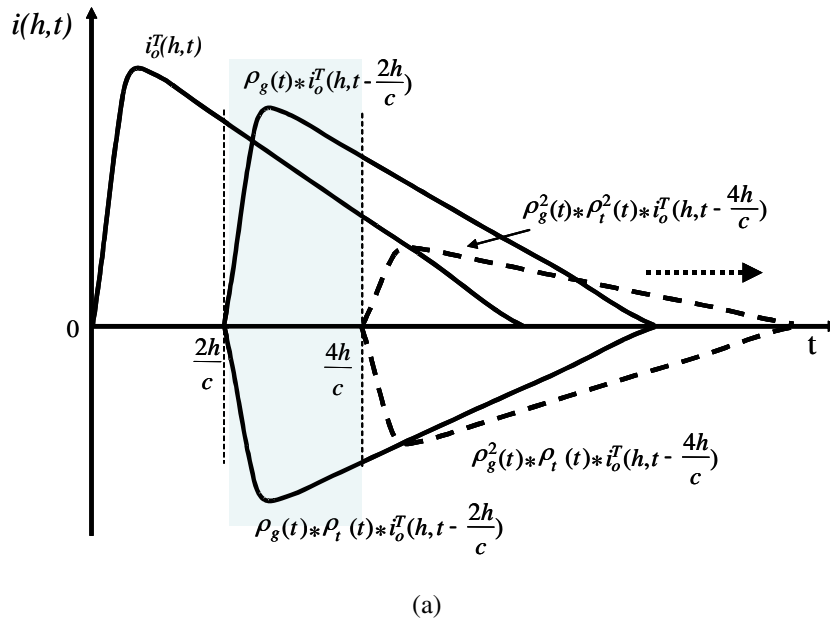


Figure 6.2 - Components of the lightning return stroke at the tower top, $h = z$, (a) current, and (b) current derivative

Let us observe, in Fig. 6-2a, the terms composing the measured current for times ranging from $t = 2h/c$ to $t = 4h/c$. Three terms make up that current:

- a) $i_o^T(h, t)$,
- b) $\rho_g(t) * i_o^T(h, t - 2h/c)$, and
- c) $\rho_t(t) * \rho_g(t) * i_o^T(h, t - 2h/c)$

The total current in that time range is therefore given by

$$i(h, t) = i_o^T(h, t) + \rho_g(t) * i_o^T(h, t - 2h/c) + \rho_t(t) * \rho_g(t) * i_o^T(h, t - 2h/c) \quad \forall \quad \frac{2h}{c} \leq t < \frac{4h}{c} \quad (6-16)$$

Solving for $\rho_t(t)$, we obtain

$$\rho_t(t) = \frac{i(h,t) - i_o^T(h,t) - \rho_g(t) * i_o^T(h,t - 2h/c)}{\rho_g(t) * i_o^T(h,t - 2h/c)}, \quad \forall \quad \frac{2h}{c} < t < \frac{4h}{c} \quad (6-17)$$

where the division operation represents an inverse convolution.

The known and unknown terms in Equation (6-17) are included in Table 6-2.

Table 6.2 - Unknowns in Equation (6-17)

Variable	Known	Comment
$i(h,t)$	✓	Measured quantity
$i_o^T(h,t - 2h/c)$ $2h/c < t < 4/c$	✓	Measured quantity. First $2h/c$ seconds in Fig. 6.7 before any reflection from the bottom
$i_o^T(h,t)$ $2h/c < t < 4h/c$	X	
$\rho_g(t)$	✓	From Equation(6-10) or (6-11)
$\rho_t(t)$	X	

From Table 6-2 we can see that the only unknowns are $\rho_t(t)$ (which we are trying to estimate) and $i_o^T(h,t)$ for $2h/c < t < 4h/c$. The term $i_o^T(h,t - 2h/c)$ for $2h/c < t < 4h/c$ is identical to $i_o^T(h,t)$ for $0 < t < 2h/c$ and it is directly measurable. If we extrapolate it for times into the range $2h/c < t < 4h/c$, we can obtain an estimate for $\rho_t(t)$. In Section 6.5, we will illustrate the application of Equation (6-17) to estimate the top reflection coefficient in the time domain for a current measured at the Peissenberg Tower (Germany), using simultaneously measured currents at two different heights but assuming that both the top and the bottom reflection coefficients are constant.

6.4.2 No-overlap current derivative components method

This second method to estimate $\rho_t(t)$ in the time domain makes use of: (1) the ground reflection coefficient obtained using, for example, the techniques presented in Section 6-3, and (2) a directly measured current derivative. We will employ the current derivative waveform measured at the top of the tower, although the method can be extended to currents measured anywhere along it. We now show that, given a tower height, it is possible to calculate the reflection coefficients at the top of the strike object if the derivative of the current injected at the top of the tower is narrow enough that none of the reflections overlap with it. For convenience we reproduce Equation (6-3) here,

$$i(z,t) = \sum_{n=0}^{\infty} \left[\rho_t^n(t) * \rho_g^n(t) * i_o^T\left(h,t - \frac{h-z}{c} - \frac{2nh}{c}\right) + \rho_t^n(t) * \rho_g^{n+1}(t) * i_o^T\left(h,t - \frac{h+z}{c} - \frac{2nh}{c}\right) \right] \quad \forall 0 \leq z \leq h$$

Let us take the derivative of Equation (6-3) with respect to time:

$$\frac{di(z,t)}{dt} = \sum_{n=0}^{\infty} \left[\rho_t^n(t) * \rho_g^n(t) * \frac{di_o^T(h,t - \frac{h-z}{c} - \frac{2nh}{c})}{dt} + \rho_t^n(t) * \rho_g^{n+1}(t) * \frac{di_o^T(h,t - \frac{h+z}{c} - \frac{2nh}{c})}{dt} \right] \quad \forall 0 \leq z \leq h \quad (6-18)$$

where we have made use the property of convolution products that $d[f(t) * g(t)]/dt = df(t)/dt * g(t)$

In Equation (6-18), we can identify a “transmitted current derivative” into the tower top $di_o^T(h,t)/dt$. This transmitted current derivative propagates down the tower and it is reflected at the bottom, then reflected again at the tower top and so on.

Let us consider the current derivative at the top of the tower, $z = h$. The first reflection from the bottom arrives $2h/c$ after the onset of the injected current derivative, $di_o^T(h,t)/dt$. The arrival of this reflection triggers a reflection from the top. No further reflections arrive until $t = 4h/c$. For $0 < t < 4h/c$, Equation (6-18) reduces therefore to three terms and we can write,

$$\frac{di(h,t)}{dt} = \frac{di_o^T(h,t)}{dt} + \rho_g(t) * \frac{di_o^T(h,t - \frac{2h}{c})}{dt} + \rho_t(t) * \rho_g(t) * \frac{di_o^T(h,t - \frac{2h}{c})}{dt} \quad \forall 0 \leq t \leq \frac{4h}{c} \quad (6-19)$$

As can be seen from Figure 6-2b, the first term on the right-hand side of Equation (6-19), $di_o^T(h,t)/dt$, can be measured directly since it corresponds to the measured current derivative for $0 < t < 2h/c$. Note that, although lightning current derivatives are bipolar, we have used unipolar waveforms in Fig. 6.2b for clarity. Once $di_o^T(h,t)/dt$ is known, and assuming that the ground reflection coefficient has been obtained from two simultaneous measurements at two heights, it is possible to calculate the reflection coefficient at the top as follows:

Observe that the current for the interval $2h/c < t < 4h/c$ in Fig. 6.2b is the sum of the second and third terms on the right-hand side of Equation (6-19). One of those two terms, $\rho_g(t) * di_o^T(h,t - 2h/c)/dt$, can be readily calculated since it equals the convolution of two known quantities. Subtracting that term from the measured current, we are left with $\rho_t(t) * \rho_g(t) * di_o^T(h,t - 2h/c)/dt$, where only $\rho_t(t)$ is unknown. It is now easy to obtain $\rho_t(t)$ by dividing (convolutionally) by the known functions $\rho_g(t)$ and $di_o^T(h,t - 2h/c)/dt$.

In Section 6.5, we will apply the present method to estimate the top reflection coefficient in the time domain for current measurements at the Peissenberg Tower (Germany).

6.5 Application of the proposed methodology to Peissenberg Tower

6.5.1 Peissenberg Tower measurement set-up and experimental data

The 168 m tall Peissenberg telecommunication tower (Fig. 6.3) was used from 1978 until 1999 to study lightning currents and the associated electromagnetic fields. Two current derivative measurement systems were installed, one near the top of the tower, at approximately 167 m, and a second one near the bottom, at 13 m. The systems were able to measure return stroke currents and their derivatives with a time resolution of 10 ns, a vertical resolution of 10 bits and record duration of 50 μ s [Fuchs, 1998b].

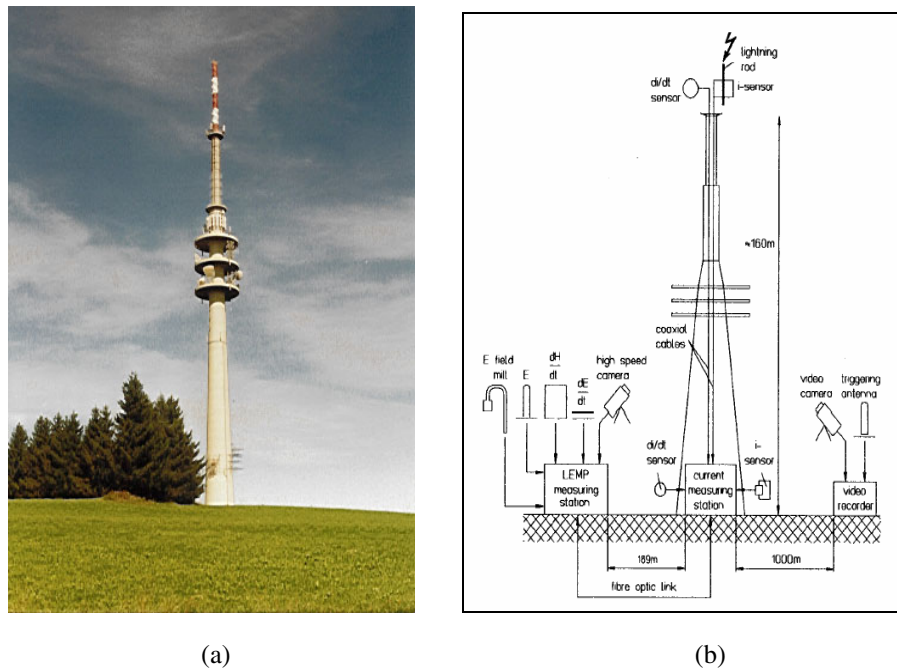


Figure 6.3 - Peissenberg tower: (a) Photograph (courtesy of Prof. F. Heidler, University of the Federal Armed Forces, Germany), (b) Schematic representation of measurement systems (adapted from [Fuchs et al., 1998]).

In this section, current derivatives measured simultaneously at the two heights will be employed to evaluate the expressions found for the ground and top reflection coefficients. These reflection coefficients have been estimated in the past considering that they are constant and frequency independent. [Heidler et al., 2001] analyzed 117 samples and reported average values for the ground and top reflection coefficients of 0.7 and -0.53, respectively. Using 13 samples from strikes to the same tower, [Fuchs, 1998a] estimated average values for the ground and top reflection coefficients of 0.698 and -0.529, respectively. Fuchs estimated additionally maximum and minimum values of 0.805 and 0.638 for the ground reflection coefficient and -0.684 and -0.392 for the top reflection coefficient.

Fig. 6.4a shows the first 10 μ s of current derivatives, near the top and bottom of the tower, for a return stroke recorded by the Peissenberg tower system on January 6, 1998. Fig. 6.4b shows the

associated currents after numerical integration. The presence of multiple reflections is clearly discernible in the current waveforms.

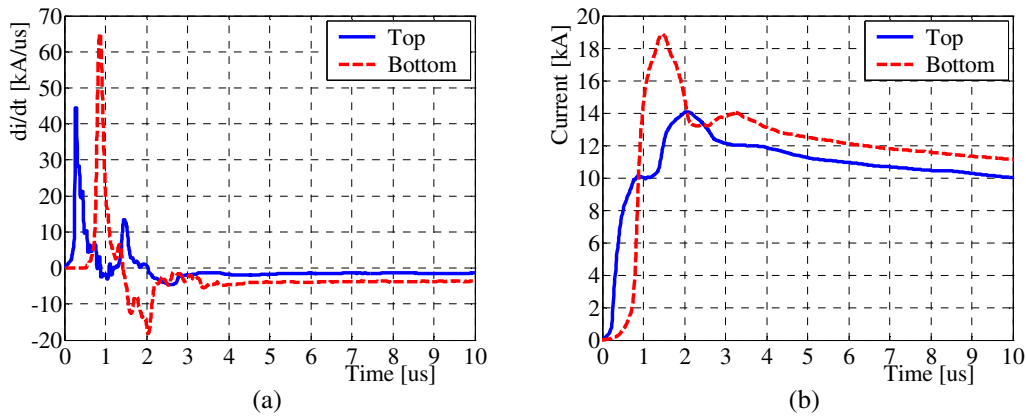


Figure 6.4 - Current derivatives and associated currents (after numerical integration) measured in January 1998 at the Peissenberg tower (168 m height), I_{top} measured at 167 m, I_{bottom} measured at 13 m (courtesy of Prof. F. Heidler, University of the Federal Armed Forces, Germany)

6.5.2 Application of the methodology in the frequency domain to recover the ground reflection coefficient

We will now apply Equation (6-11) to recover the ground reflection coefficient in the frequency domain from two simultaneously measured return stroke current derivatives. To do that, we will consider three sets of experimentally-measured current derivative waveforms presented in Figs. 6.5a, b, and c.

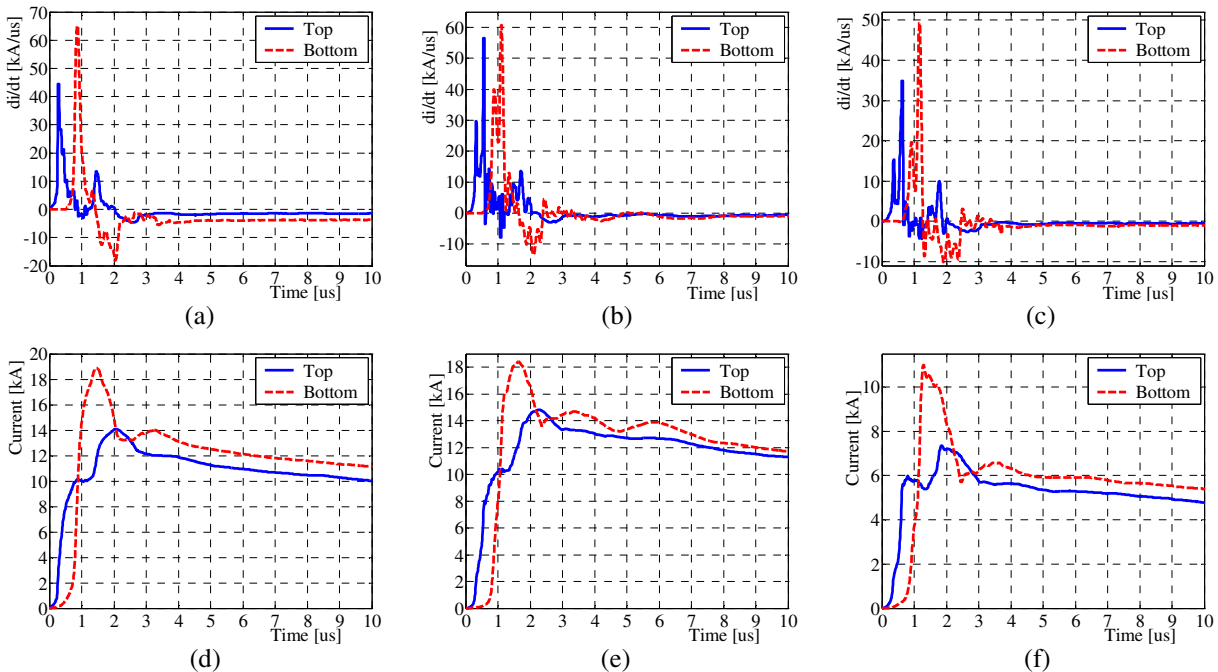


Figure 6.5 - Three sets of experimentally-measured current derivative waveforms and their associated current (after numerical integration) at Peissenberg Tower (168m height), I_{top} measured at 167 m, I_{bottom} measured at 13 m.

Fig. 6.6 presents the ground reflection coefficient determined using Equation (6-11) in the frequency range of 6 kHz up to 940 kHz. These two frequencies correspond approximately to $1/(\pi t_{max})$ and $1/(\pi t_r)$, where $t_{max} = 50 \mu s$ and $t_r = 0.34 \mu s$ are, respectively, the duration and the average risetime of the current samples employed in this analysis.

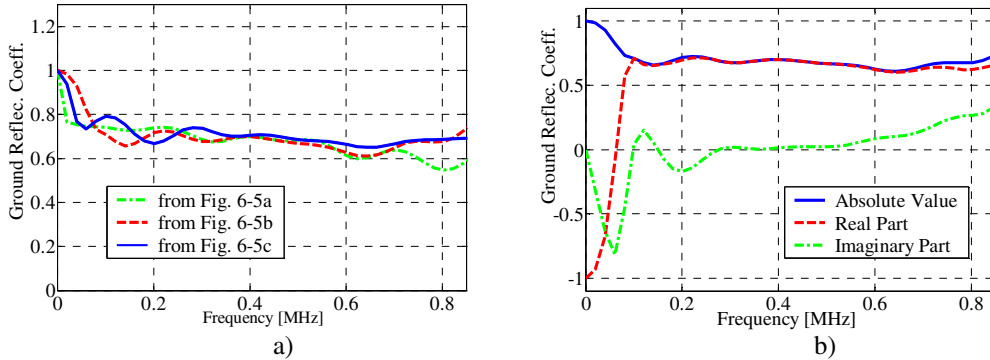


Figure 6.6 - (a) Absolute value of $\rho_g(\omega)$ calculated from Equation (6-11) for three experimental samples showed on Fig. 6.5; (b) Average of the real and imaginary parts of $\rho_g(\omega)$.

In Fig. 6.6a, the fact that the values of the reflection coefficients are comparable to those obtained by [Heidler et al., 2001] and [Fuchs, 1998a], and the similarity in the behavior for the absolute value of $\rho_g(\omega)$ obtained for all three cases examined supports the validity of the methodology. The obtained $\rho_g(\omega)$ decreases slowly with frequency from 0.8 to 0.6 for intermediate frequencies. Note that, in Fig. 6.6b, the real part of ρ_g approaches -1 at DC. This value, however, is to be taken with caution since at very low frequencies, no traveling waves are present and concepts such as reflection coefficients lose their significance. The imaginary part of $\rho_g(\omega)$ is negligible for a large interval of frequencies (Fig. 6.6b), implying an essentially resistive behavior of the grounding impedance.

6.5.3 Application of the methodology to recover the top reflection coefficient in the time domain

In this section, we use the two methods introduced in Section 6.4 to estimate the top reflection coefficient $\rho_t(t)$ by applying them to currents and current derivatives measured at the Peissenberg Tower.

6.5.3.1 Extrapolation technique using measured current waveforms at the top of the tower

Using the technique based on linear extrapolation described in Section 6.4, we will now estimate the top reflection coefficient from the current waveform presented in Fig. 6.4b. Although the measurement was made one meter below the top of the tower, we will assume for our calculations

that it was measured exactly at the top and that the ground reflection coefficient has a constant value of 0.7, independent of frequency. This value is the average of the maximum and minimum obtained in Section 6.5.2. We will disregard for this validation the frequency dependence of the top reflection coefficient and assume it constant.

Let us go back to the time domain expression introduced in Section 6.4 (Equation (6-17)). With constant reflection coefficients, the convolution terms in Equation (6-17) disappear and they are replaced by standard multiplications:

$$\rho_t(t) = \frac{i(h,t) - i_o^T(h,t) - \rho_g(t) i_o^T(h,t - 2h/c)}{\rho_g(t) i_o^T(h,t - 2h/c)}, \quad \forall \quad \frac{2h}{c} < t < \frac{4h}{c} \tag{6-20}$$

Fig. 6.7a shows the three components of the current employed to calculate the top reflection coefficient from Equation (6-20). Fig. 6.7b presents the behavior of the top reflection coefficient as a function of the time instant at which the reflection coefficient is estimated. It is interesting to observe that, under the current assumptions, the average value for the top reflection coefficient tends to a constant value of -0.43 ± 0.02 . This result is in agreement with the values for the top reflection coefficient reported by [Fuchs, 1998a] using 13 samples and mentioned in Section 6.5.1.

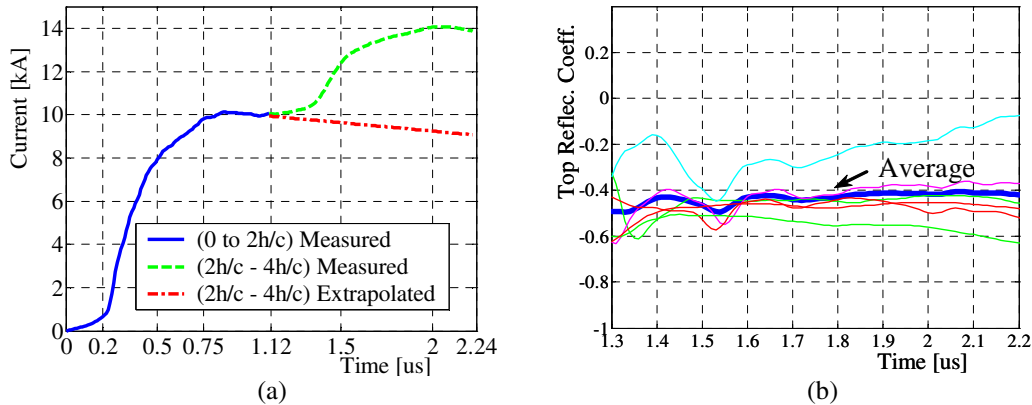


Figure 6.7 - (a) Current sections employed in the calculation of the top reflection coefficient by the extrapolation technique - Section 6.4; (b) Average of the top reflection coefficient from 6 samples

6.5.3.2 Current derivative method

The second method to obtain $\rho_t(t)$, introduced in Section 6.4.2, employs the current derivative waveforms observed at the top of the tower, $z = h$. In Section 6.4.2., we assumed a transmitted current derivative $di_o^T(h,t)/dt$ sharp enough for subsequent reflections produced in the tower not to overlap with it. In practice, however, the reflected terms do overlap with the transmitted current derivative $di_o^T(h,t)/dt$. Since the overlap is small compared with the peak values attained by the current derivatives, it can be disregarded for the evaluation of ρ_t . To minimize the error, we will use only peak values of the current derivative as shown in Fig. 6.8.

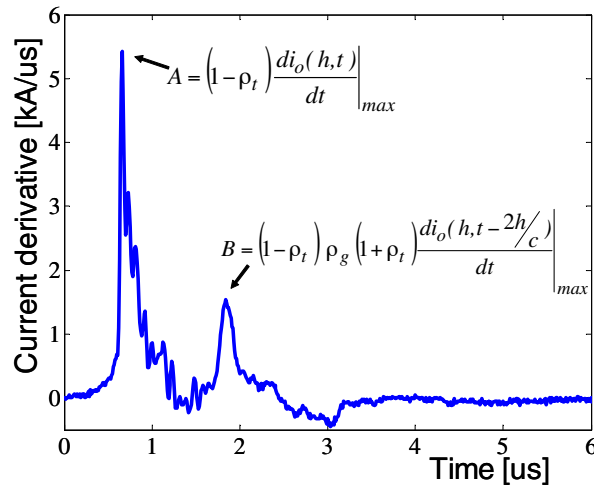


Figure 6.8 - Maximum values for the first two components in a current derivative waveform

The values obtained for the top reflection coefficient ρ_t are equal to -0.59 ± 0.05 . This result is somewhat higher than that obtained using the first technique but it is in excellent agreement with the estimates of -0.53 and -0.529 given by [Heidler et al., 2001] and [Fuchs, 1998a], respectively. Moreover, estimated values for the top reflection coefficient are in agreement with estimates of return stroke channel impedance given by [Rakov, 1998] (a value of about 570Ω for frequencies ranging from 10 kHz to 10 MHz), and assuming a reasonable value of about $100\text{-}300 \Omega$ for the tower impedance (e.g. [Gavric, 2002; Rakov, 2001]).

The difference between the results obtained from the two methods can be explained, at least in part, by errors in the first method due to the approximation involved in the extrapolation process.

Another possible explanation for the discrepancy between the values obtained using the two methods is the fact that the first method uses an extrapolation of the low frequency tail of $i_o^T(h,t)$ whereas, for the current derivative method, we have used the peak value of the $di_o^T(h,t)/dt$, which is associated with high frequencies, suggesting a dependence of the top reflection coefficient on frequency, in agreement with the observations of [Janischewskyj et al., 1996].

For practical tower heights and typical currents, the current derivative rarely (if ever) decays to zero by the time its reflection off the bottom of the tower arrives at the top. As done in this section, the current derivative method can still be applied if the current derivative has decayed to negligible amplitudes by the time the reflection from the bottom arrives. To minimize the error due to the overlap, the peak amplitudes of the current derivative and of its first reflection were used. The use of peak values greatly simplifies the calculations but it presents the disadvantage of disregarding the frequency dependence information of the top reflection coefficient.

The importance of the extrapolation method lies in the fact that, although it is inherently less reliable than the current derivative method, it is applicable even if the overlap between the derivative and its reflection is not negligible.

6.6 Use of genetic algorithms to extract primary lightning current parameters

We now introduce a method to estimate the reflection coefficients of the strike object that is based on an adaptation of genetic algorithms. This section is based on the work presented in [Bermudez et al., 2002a].

The new technique allows for the extraction, from experimental current data consisting of the current measured simultaneously at a two different heights, of the tower reflection coefficients and the parameters of the undisturbed current, $i_o(h,t)$, modeled as a sum of two Heidler functions, Equation (3-10). These parameters can then be used in Equation (6-1a) to reproduce the initial part of experimentally measured current waveshapes. The tower reflection coefficients are assumed, in this section, to be constant.

The idea of applying the biological principle of natural evolution to artificial systems, introduced more than three decades ago, has seen impressive growth in the past few years. We find the domains of genetic algorithms, evolution strategies, evolutionary programming, and genetic programming usually grouped under the terms “evolutionary algorithms” or “evolutionary computation” (e.g. [Fogel, 1995; Koza, 1992; Michalewicz, 1996]). Such algorithms are common nowadays, having been successfully applied to numerous problems across different domains, including optimization, automatic programming, machine learning, economics, medicine, ecology, population genetics, and social systems.

6.6.1 Genetic algorithms

Evolutionary computation makes use of a metaphor of natural evolution. According to this metaphor, a problem plays the role of an environment wherein a population of individuals, each representing a possible solution to the problem, lives. The degree of adaptation of each individual (i.e., candidate solution) to its environment is expressed by an adequate measure known as the “fitness function”. The candidate solution is generally encoded in some manner into its “genome”. Like evolution in nature, evolutionary algorithms potentially produce progressively better solutions to the problem. This is possible thanks to the introduction of new genetic material into the population, by applying so-called genetic operators that are the computational equivalents of natural evolutionary mechanisms [Peña-Reyes, 2002].

Proposed by John Holland in the 1960s, genetic algorithms are the best known class of evolutionary algorithms. A genetic algorithm is an iterative procedure that consists of a constant-size population of individuals, each one represented by a finite string of symbols, known as the “genome”, encoding a possible solution in a given problem space. This space, referred to as the search space, comprises

all possible solutions to the problem at hand. Generally speaking, the genetic algorithm is applied to spaces which are too large to be exhaustively searched [Michalewicz, 1996].

A genetic algorithm or, in general, an evolutionary algorithm, can be described as follow: first an initial population of individuals, $P(0)$, is generated at random or heuristically. At every generation step t , the individuals in the generation are decoded and evaluated according to some predefined quality criterion, referred to as fitness function. A subset of individuals, $P'(t)$, is selected from $P(t)$ to reproduce the winners. Then, high-fitness (“good”) individuals stand a better chance of “reproducing”, while low-fitness ones are more likely to disappear. The selected population $P'(t)$ is then modified via crossover and mutation to generate new individuals into the population, $P''(t)$. Finally, the new individuals $P''(t)$ are introduced into the next-generation population $P(t+1)$; although a part of $P(t)$ can be preserved. The termination condition can be specified as some fixed maximal number of generations or as the attainment of an acceptable fitness level. Fig. 6.9 shows the structure of a genetic evolutionary algorithm in pseudo-code format [Peña-Reyes, 2002].

```

Begin Evolutionary Algorithm (EA)
t = 0 - Initialization of Generation steps
P(t = 0) - Creation of population
While not done do
  Evaluation of P(t) – in the fitness function
  P'(t) = Select[P(t)] – for reproduction
  P''(t) = Genetic Operators [P'(t)]
  P(t+1) = Merge [P''(t), P(t)]
end while
end of EA

```

Figure 6.9 - Pseudo-code of an evolutionary algorithm.

6.6.2 Application of genetic algorithms to extract lightning current and reflection coefficients

The concept of genetic or evolutionary algorithms will now be adapted to the case of lightning return stroke currents measured on instrumented towers. The aim is to find, from two simultaneously measured lightning return stroke currents at different heights along the tower, $i(z_1, t)$ and $i(z_2, t)$ (Fig 6.1a), an individual with a ‘genome’ composed of a set of unknown parameters capable of reproducing the measured currents using Equation (6-1a). The unknown primary current $i_o(h, t)$ is represented by a sum of two Heidler’s functions, Equation (3-10) [Heidler, 1985]. Equation (3-10) is reproduced here for the case of the sum of two Heidler’s functions,

$$i_o(t) = \frac{I_{o1}}{\eta_1} \frac{(t/\tau_{11})^{N_1}}{1 + (t/\tau_{11})^{N_1}} \exp(-t/\tau_{12}) + \frac{I_{o2}}{\eta_2} \frac{(t/\tau_{21})^{N_2}}{1 + (t/\tau_{21})^{N_2}} \exp(-t/\tau_{22}); \quad (6-21)$$

$$\eta_i = \exp \left[- \left(\frac{\tau_{i1}}{\tau_{i2}} \right) \left(N \frac{\tau_{i2}}{\tau_{i1}} \right)^{1/N_i} \right] \quad i = 1, 2$$

Now, the aim is to extract, from equations (6-1a) and (6-21), the unknown parameters and construct with them a ‘genome’, which will be evolved by the genetic algorithm. Table 6-3, shows the composition of the ‘genome’ with 10 unknown parameters, the allowed maximum and minimum values in the algorithm for each parameter, as well as their size expressed in bits. The limits for each parameter have been defined to cover a wide range of possible cases. The size for each parameter is defined according to the required precision for the results.

Table 6.3 - Variables in the genome and their associated limits.

Variable	ρ_g	ρ_t	I_{o1}	τ_{11}	τ_{21}	N_1	I_{o2}	τ_{12}	τ_{22}	N_2
Lower bound	-1	-1	1e3	1e-8	1.5e-6	2	1e3	1e-6	50e-6	2
Higher bound	+1	+1	30e3	1e-6	10e-6	9	20e3	10e-6	500e-6	9
Number of bits	4	4	6	6	6	3	6	6	6	3

6.6.3 Application of the algorithm to a theoretical case

Let us first start by applying the algorithm to a purely theoretical case. The unknown variables into the genome will be found from two lightning return stroke currents represented by Equation (6-1a), with the aim of optimizing the fitness function, the population size, the probability of mutation and the number of generations needed.

Fig. 6.10 shows the first 10 μ s of the theoretical currents generated at heights $z_1=167$ m and $z_2=13$ m, for a tower of height $h = 168$ m. The parameters used to reproduce the primary current waveform are shown in Table 6.4.

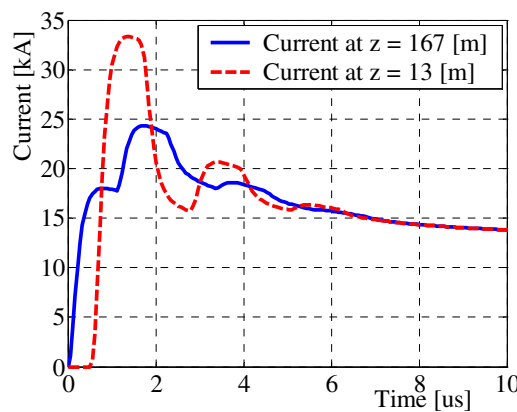


Figure 6.10 - Theoretical currents generated for a tower height of 168 m.

Table 6.4 - Parameters of two Heidler functions that reproduce the “undisturbed” current wave shapes $i_o(h, t)$ at the top of the elevated object.

I_{o1} [kA]	τ_{11} [μ s]	τ_{21} [μ s]	I_{o2} [kA]	τ_{12} [μ s]	τ_{22} [μ s]
10.7	0.25	2.5	6.5	2.1	230

The evolutionary parameters required to start the genetic algorithm simulation are given in Table 6-5. The parameters encoded into an individual's genome are applied in equations (6-1a) and (6-21) to obtain the current waveforms $i(z_1,t)$ and $i(z_2,t)$, which will serve to compute the fitness of the individual. The fitness function, measured for each current, is composed of two conditions: first, the general “mse” (minimum square error) between the calculated and the reference currents; and second, the mse, for the most significant part of the waveforms (the first 200 points). For each condition, a factor of preponderance ($\alpha=0.2$ and $\beta=1.0$) is introduced giving more weight to the second error term (see Equation 6-22).

$$f = \frac{\alpha}{e_{mse}^{z_1} - e_{mse}^{z_2}} + \frac{\beta}{e_{mse}^{z_1}(1:200) - e_{mse}^{z_2}(1:200)} \tag{6-22}$$

where

$$e_{mse}^{z_i} = \frac{mse[i(z_i,t) - i_{ref}(z_i,t)]}{mse[i_{ref}(z_i,t)]} \tag{6-23}$$

Table 6.5 - Additional parameter settings for the genetic algorithm simulation.

Parameter	Value
Population size	50
Mutation probability	0.02
Number of generations	400
Fitness function	Equation (6-22)

Fig. 6.11 shows a comparison between the reference waveform (Fig. 6.10) and the predicted one, for the two currents. It can be seen that the genetic algorithm allows us to obtain a good approximation of the original (reference) waveform.

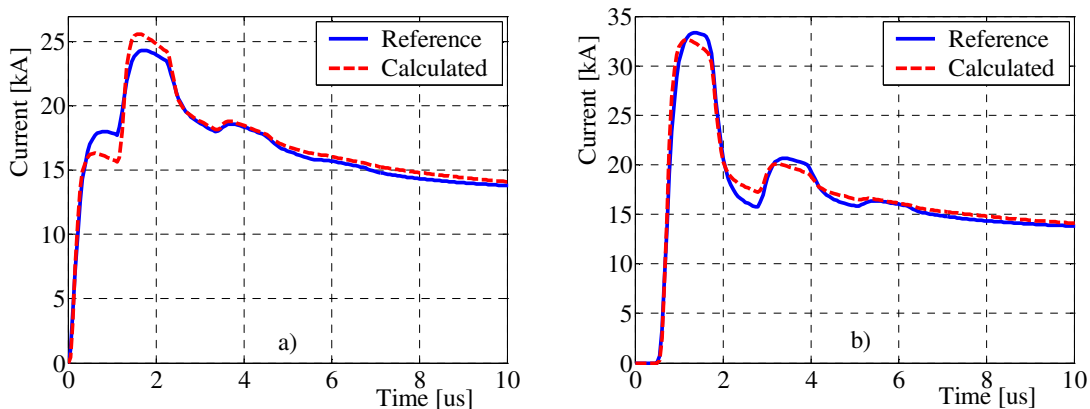


Figure 6.11 - Comparison between reference and calculated waveforms, (a) at 167 m, (b) at 13 m.

Table 6-6 contains both, the values employed to generate the theoretical reference waveform, and those predicted by the genetic algorithm with the fitness function given by Equation (6-22). It can

be seen that, although the two waveforms are very close to each other, the predicted values for some of the parameters are considerably different from the original ones.

Table 6.6 - Comparison between reference and predicted parameters (genome).

Parameter	Reference value	Predicted value
ρ_g	0.85	1.0
ρ_t	-0.5	-0.33
I_{o1} [kA]	10.7	12.05
τ_{11} [μ s]	0.25	0.18
τ_{21} [μ s]	2.5	7.30
N_1	2	3
I_{o2} [kA]	6.5	5.52
τ_{12} [μ s]	2.1	10.00
τ_{22} [μ s]	230	221.43
N_2	2	2

The universe of variations to improve the results is, in theory, infinitely large. However, in practice, the main objective is to reproduce as close as possible experimental waveforms based on the theoretical model expressed by equations (6-1a) and (6-21), with special emphasis on the part of the waveform which has the most important information content. The next section will show an example of the validation of the methodology using real experimental data.

6.6.4 Application of the GA to experimental data obtained on Peissenberg tower

Fig. 6-12 shows the first 10 μ s of a return stroke current, obtained by numerical integration of the current derivatives, recorded by the Peissenberg tower system at two heights on January 6, 1998 (solid lines).

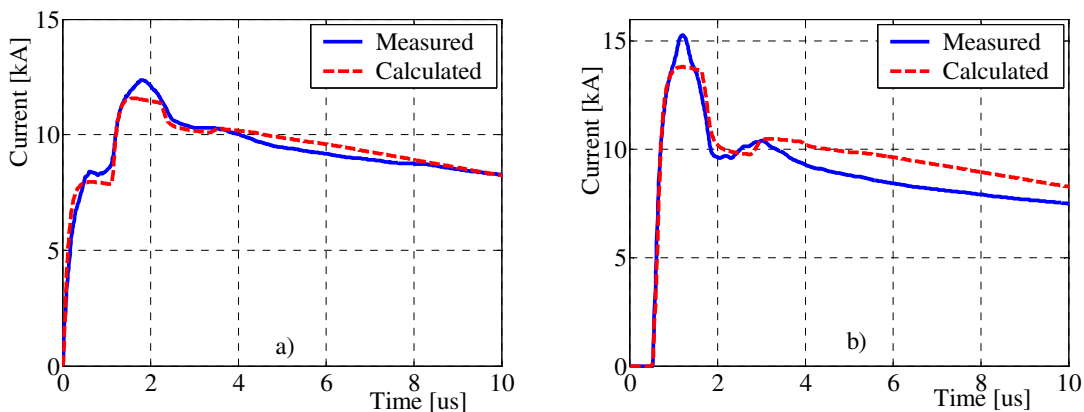


Figure 6.12 - Lightning return stroke currents measured at the Peissenberg tower in 1998: a) at 167 m, b) at 13 m

These measured current waveforms will be defined as the reference waveforms and they will be introduced into the genetic algorithm. All but two of the parameters for the genetic algorithm (reported in Table 6-5) as well as the fitness function given by Equation (6-22) remain unchanged;

only the number of generations was increased to 1000 and the factor α was modified to 0.1. Fig. 6-12 shows, in dashed lines, the first 10 μs of the waveforms calculated using equations (6-1a) and (6-21), with the parameters encoded by the best individual of the population after 1000 generations. Table 6-7 summarizes the values of the specific parameters.

It can be seen that, despite the simplifying assumptions of the study, the computed waveforms are reasonable approximations to the measured currents. This methodology based on genetic algorithms can be extended to more complex representations of the ‘undisturbed’ and ‘contaminated’ return stroke currents including more details of the strike object.

Table 6.7 - Values obtained for the best evolved individuals in the population.

Parameter	Individual values
ρ_g	0.73
ρ_t	-0.33
I_{o1} [kA]	5.60
τ_{11} [μs]	0.10
τ_{21} [μs]	9.73
N_1	2
I_{o2} [kA]	2.21
τ_{12} [μs]	4.43
τ_{22} [μs]	457.14
N_2	2

The values obtained by the genetic algorithm (reported in Table 6.7) for the mentioned parameters are in reasonable agreement with the estimations obtained in sections 6.5.2 and 6.5.3, as well as with the estimations of [Heidler et al., 2001] and they are within the limits reported by [Fuchs, 1998a].

6.7 Comments and conclusions

In this chapter, we have developed a closed form expression in the frequency domain to calculate the lightning current at any height along a strike object taking into account frequency-dependent reflection coefficients at the top and at the bottom.

We have derived an expression to calculate the reflection coefficient as a function of frequency at the bottom of the lightning strike object from two currents measured simultaneously at different heights along the strike object. We found that the ground reflection coefficient can be found without prior knowledge of the reflection coefficient at the top of the strike object.

We showed that, unless the tower is tall enough that the current injected at the top of the object or its derivative drops to zero before the arrival of reflections, it is impossible, at least under our assumptions, to derive either the reflection coefficient $\rho_t(\omega)$ at the top of the strike object or the

“undisturbed” current from any number of simultaneous current measurements. We proposed two methods to estimate the top reflection coefficient.

The proposed methods were applied to experimental data obtained on Peissenberg Tower, where lightning currents were measured simultaneously at two heights. It was found that the reflection coefficient at ground level can be considered as practically constant over a relatively wide range of frequencies from 100 kHz up to 800 kHz.

The estimated top reflection coefficients are in good agreement with values found in the literature. Nevertheless, we found that the estimated values for the top reflection coefficient from the extrapolation method are lower than those found employing the current derivative method. The difference might be due to possible experimental errors and also to the fact that the extrapolation method provides values for the top reflection coefficient calculated from the low-frequency tail of the current waveforms, while the current derivative method uses values associated with the faster parts of the waveform. This observation suggests that the top reflection coefficient is dependent of frequency.

Additionally, we applied a standard genetic algorithm to extract automatically primary lightning parameters from experimental records obtained on instrumented towers. The algorithm was tested first using theoretical waveforms which included the presence of ground and tower-top reflection coefficients and approximating the ‘undisturbed’ current by two Heidler’s functions. The algorithm was then applied to real lightning return stroke measurements obtained at the Peissenberg tower in Germany. The best individuals satisfying the fitness function conditions proposed by the genetic algorithms were compared with the measured waveforms and a good agreement was found. The derived reflection coefficients at ground and at the top of the tower were also compared with values estimated by other authors, and a good agreement was found. The genetic algorithm method can be extended to more complex ‘undisturbed’ current models as well as to more complete representation of the lightning return stroke attachment process.

6.8 References Chapter 6

- Beierl, O., Front Shape Parameters of Negative Subsequent Strokes Measured at the Peissenberg Tower, in *21st ICLP (International Conference on Lightning Protection)*, pp. 19-24, Berlin, Germany, 1992.
- Berger, K., R.B. Anderson, and H. Kroninger, Parameters of Lightning Flashes, *Electra*, 41, 23-37, 1975.

- Bermudez, J.L., J.A. Gutierrez, W.A. Chisholm, F. Rachidi, M. Paolone, and P. Moreno, A Reduced-Scale Model to Evaluate the Response of Tall Towers Hit by Lightning, in *International Symposium on Power Quality: SICEL'2001*, Bogotá, Colombia, 2001a.
- Bermudez, J.L., C.A. Peña-Reyes, F. Rachidi, and F. Heidler, Use of Genetic Algorithms to Extract Primary Lightning Current Parameters, in *International Symposium on EMC*, pp. 241-246, Sorrento, Italy, 2002a.
- Bermudez, J.L., M. Rubinstein, F. Rachidi, F. Heidler, and M. Paolone, Determination of Reflection Coefficients at the Top and Bottom of Elevated Strike Objects Struck by Lightning, *Journal of Geophysical Research*, to be published, 2002b.
- Bermudez, J.L., M. Rubinstein, F. Rachidi, and M. Paolone, A Method to Find the Reflection Coefficients at the Top and Bottom of Elevated Strike Objects from Measured Lightning Currents, in *14th International Zurich Symposium on Electromagnetic Compatibility*, pp. 6, Zurich, Switzerland, 2001b.
- Fogel, D.B., *Evolutionary Computation: Toward a New Philosophy of Machine Intelligence*, in *IEEE Press*, Piscataway - NJ, 1995.
- Fuchs, F., On the transient behaviour of the telecommunication tower at the mountain Hoher Peissenberg, in *24th ICLP (International Conference on Lightning Protection)*, pp. 36-41, Birmingham, U.K., 1998a.
- Fuchs, F., Overall experimental setup for the lightning current and LEMP research at the mountain Hoher Peissenberg, in *24th ICLP (International Conference on Lightning Protection)*, pp. 95-100, Birmingham, U.K., 1998b.
- Fuchs, F., L.E. U., R. Schmid, and J. Wiesinger, Lightning current and magnetic field parameters caused by lightning strikes to tall structures relating to interference of electronic systems, *IEEE Transactions on Electromagnetic Compatibility*, 40 (4), 444-451, 1998.
- Gavric, M.R., Iterative method for waveshape restoration of directly measured lightning flash currents, *IEE Proceedings Generation, Transmission and Distribution*, 149 (1), 66-70, 2002.

- Guerrieri, S., F. Heidler, C.A. Nucci, F. Rachidi, and M. Rubinstein, Extension of two return stroke models to consider the influence of elevated strike objects on the lightning return stroke current and the radiated electromagnetic field: comparison with experimental results, in *EMC '96 (International Symposium on Electromagnetic Compatibility)*, pp. 701-6, Rome, Italy, 1996.
- Guerrieri, S., C.A. Nucci, F. Rachidi, and M. Rubinstein, On the influence of elevated strike objects on directly measured and indirectly estimated lightning currents, *IEEE Transactions on Power Delivery*, 13 (4), 1543-55, 1998.
- Gutierrez, J.A., J.L. Bermudez, F. Rachidi, M. Paolone, C.A. Nucci, W.A. Chisholm, P. Moreno, and J.L. Naredo, A Reduced-Scale Model to Evaluate the Response of Nonuniform Towers to a Lightning Strike, in *26th ICLP (International Conference on Lightning Protection)*, pp. 487-490, Cracow, Poland, 2002.
- Heidler, F., J. Wiesinger, and W. Zischank, Lightning Currents Measured at a Telecommunication Tower from 1992 to 1998, in *14th International Zurich Symposium on Electromagnetic Compatibility*, pp. 6, Zurich, Switzerland, 2001.
- Heidler, H., Analytische Blitzstromfunktion zur LEMP- Berechnung, in *18th ICLP (International Conference on Lightning Protection)*, pp. 63-66, Munich, Germany, 1985.
- Janischewskyj, W., V. Shostak, J. Barratt, A.M. Hussein, I. Rusan, and J.S. Chang, Collection and use of lightning return stroke parameters taking into account characteristics of the struck object, in *23rd ICLP (International Conference on Lightning Protection)*, pp. 16-23, Florence, Italy, 1996.
- Kordi, B., R. Moini, and V.A. Rakov, Comment on 'Return stroke transmission line model for stroke speed near and equal that of light by R. Thottappillil, J. Schoene, and M.A. Uman', *Geophysical Research Letters* (29), 2002.
- Koza, J.R., *Genetic Programming*, Cambridge, Massachusetts, 1992.
- Michalewicz, Z., *Genetic Algorithms + Data Structures = Evolution Programs*, 1996.

- Montandon, E., and B. Beyeler, The Lightning Measuring Equipment on the Swiss PTT Telecommunications Tower at St. Chrischona, Switzerland, in *22nd ICLP (International Conference on Lightning Protection)*, pp. 6, Budapest, Hungary, 1994.
- Peña-Reyes, C.A., Coevolutionary Fuzzy Modeling, Scientific thesis, EPFL, Lausanne, 2002.
- Rachidi, F., W. Janischewskyj, A.M. Hussein, C.A. Nucci, S. Guerrieri, B. Kordi, and J.S. Chang, Current and electromagnetic field associated with lightning return strokes to tall towers, *IEEE Transactions on Electromagnetic Compatibility*, 43 (3), 356-366, 2001.
- Rachidi, F., V.A. Rakov, C.A. Nucci, and J.L. Bermudez, The Effect of Vertically-Extended Strike Object on the Distribution of Current Along the Lightning Channel, *Journal of Geophysical Research*, 107 (D23), 4699, 2002.
- Rakov, V.A., Some inferences on the propagation mechanisms of dart leaders and return strokes, *Journal of Geophysical Research*, 103 (D2), 1879-86, 1998.
- Rakov, V.A., Transient response of a tall object to lightning, *IEEE Transactions on Electromagnetic Compatibility*, 43 (4), 654-61, 2001.
- Rakov, V.A., Lightning Return Stroke Modeling: Recent Developments, in *International Conference on Grounding and Earthing - GROUND 2002*, Rio de Janeiro, Brazil, 2002.
- Thottappillil, R., J. Schoene, and M.A. Uman, Return stroke transmission line model for stroke speed near and equal that of light, *Geophysical Research Letters*, 28 (18), 3593-6, 2001.
- Thottappillil, R., J. Schoene, and M.A. Uman, Reply to the 'Comment on "Return stroke transmission line model for stroke speed near and equal that of light by R. Thottappillil, J. Schoene, and M.A. Uman' " by G. Kordi, R. Moini, and V.A. Rakov, *Geophysical Research Letters* (29), 2002.
- Willett, J.C., V.P. Idone, R.E. Orville, C. Leteinturier, A. Eybert Berard, L. Barret, and E.P. Krider, An experimental test of the 'transmission-line model' of electromagnetic radiation from triggered lightning return strokes, *Journal of Geophysical Research*, 93 (D4), 3867-78, 1988.

Chapter 7

Conclusions and Perspectives

During the past three years, I have gained a great deal of experience and insight into the fields of lightning return stroke current modeling and electromagnetic field calculations. I had also the opportunity to participate in lightning measurement campaigns and to present part of the results developed in this work before international experts through my participation in conferences and symposia.

The focus of the present thesis was the analysis and modeling of lightning return strokes to elevated strike objects. After the introductory Chapters 1 and 2, we presented in Chapter 3 a brief review of models for lightning return strokes initiated at ground level. We generalized, in Chapter 4, the so-called engineering models to include the presence of an elevated strike object. The generalization is based on a distributed-source representation of the return stroke channel which allowed more general and straightforward formulations of these models, including a self-consistent treatment of the impedance discontinuity at the top of the tower, as opposed to previous representations that use a lumped current source at the bottom of the channel. In the models presented, the object was represented by a vertically-extended lossless uniform transmission line, characterized by reflection coefficients at its extremities. This representation was validated through experimental data obtained on a reduced scale model designed and constructed as part of the work of this thesis (Appendix 4). Special expressions were also derived for the case of electrically-short structures which can be used to quantify the effect of grounding conditions on the current distribution along the strike object and along the channel.

New equations were derived in Chapter 5 for the electric and magnetic fields at far distances using the general expressions for the spatial and temporal distribution of the current in the channel and in the elevated strike object. The expressions were evaluated for the cases of electrically-tall and electrically-short structures.

For electrically-tall structures, it was found that the presence of the strike object enhances the radiated electric and magnetic field peaks in comparison to return strokes initiated at ground level. The enhancement was quantified through a simple factor that depends on the return stroke speed and on the top reflection coefficient associated with the strike object.

During the summers of 2000 and 2001, we performed simultaneous measurements of the electric and magnetic fields at two distances, and of the return stroke current associated with lightning strikes to the Toronto CN Tower. The lightning current was measured using a Rogowski coil installed at a height of 474 m above ground level. The vertical component of the electric field and the azimuthal component of the magnetic field were measured simultaneously at distances of 2 km (Rosebrugh building of the University of Toronto) and 16.8 km (Environment Canada Building) from the CN Tower.

The obtained sets of simultaneously-measured currents and fields associated with lightning strikes to the CN Tower were used to test the theoretical expressions and reasonable agreement was found. The main source of disagreement is attributed to the enhancement effect of the buildings on which field sensors were installed.

The derived expressions could find a useful application when lightning currents are measured directly on instrumented towers to calibrate the performances of lightning location systems.

In Chapter 6, we analyzed the current into the elevated strike object in the frequency domain, and we derived a closed form expression to evaluate this current taking into account frequency-dependent reflection coefficients at the top and at the bottom of the elevated strike object.

We derived an expression to calculate the reflection coefficient as a function of frequency at the bottom of the lightning strike object from two currents measured simultaneously at different heights along the strike object. We found that the ground reflection coefficient can be found without prior knowledge of the reflection coefficient at the top of the strike object.

We showed that, unless the tower is tall enough that the current injected at the top of the object or its derivative drop to zero before the arrival of reflections, it is impossible, at least under our assumptions, to derive either the reflection coefficient at the top of the strike object or the “undisturbed” current from any number of simultaneous current measurements. We proposed two methods to estimate the top reflection coefficient.

The proposed methods were applied to experimental data obtained on Peissenberg Tower where lightning currents were measured simultaneously at two heights. It was found that, for our experimental data set, the reflection coefficient at ground level can be considered as practically constant over a relatively wide range of frequencies from 100 kHz up to 800 kHz.

The estimated top reflection coefficients were found to be in good agreement with values found in the literature. Nevertheless, we found that the estimated values for the top reflection coefficient from one of the estimation methods, the extrapolation method, were lower than those found employing the current derivative method. The difference might be due to possible experimental

errors and also to the fact that the extrapolation method provides values for the top reflection coefficient calculated from the low-frequency tail of the current waveforms, while the current derivative method uses values associated with the faster parts of the waveform. This observation suggests that the top reflection coefficient is dependent on frequency.

In the same Chapter, we applied a standard genetic algorithm to extract automatically primary lightning parameters from experimental records obtained on instrumented towers. The algorithm was first tested using theoretical waveforms, which included the presence of ground and tower-top reflection coefficients and approximating the ‘undisturbed’ current by two Heidler’s functions. The algorithm was then applied to real lightning return stroke measurements obtained at the Peissenberg tower in Germany. The best individuals satisfying the fitness function conditions proposed by the genetic algorithms were compared with the measured waveforms and a good agreement was found.

Outlook and Future work:

A number of new ideas appeared during the development of theoretical parts of this work and during the experimental campaigns. Although some of these ideas were considered and resolved within the present work, we could not address them all for lack of time and resources. As a natural closure of this thesis, we would like to briefly discuss these ideas in the hope that they may inspire future research.

The general development for lightning return strokes to elevated strike objects presented in Chapter 4 disregarded the possible reflections produced at the return stroke channel wavefront. These reflections could, in principle, be included in the model and in the general equations derived in Chapter 4 describing the spatial and temporal behavior of the current along the channel and along the strike object.

Prior to the return stroke phase of the lightning discharge, the formation of upward connecting leaders has been observed for downward negative lightning. To the extent that such connecting leaders can be represented as transmission lines, the developments presented in this thesis allow the analysis of their influence on the initial waveshape of the lightning current as well as the electric and magnetic fields.

The elevated strike object was represented in this study by a lossless transmission line. Experimental results obtained using reduced scale models have shown the validity of such an approximation for the first few reflections and dwindling accuracy for longer times. A more complete characterization of the strike object could be performed in future works, using (a) more sophisticated models based on antenna theory, and, (b) more thorough experimental analyses using reduced scale models.

Regarding the electromagnetic field analysis performed in Chapter 5, our experimental efforts revealed the importance of a possible enhancement effect of the building on the measured waveforms. This enhancement needs to be quantified through thorough numerical calculations and careful experimental measurements. Another factor disregarded in our analysis was the finite conductivity of the ground. That factor affects the field magnitudes and waveshapes, especially at distant ranges and it is an essential improvement to our computations.

The electromagnetic fields were studied assuming the far-field approximation, while experimental data for fields at 2 km were used for comparison. Although, such an assumption can be acceptable to describe the early-time response of the fields at distances as close as 1 or 2 km, other field components (static and induction for E-field and induction for H-field) would certainly affect the later-time response of the field. It would be interesting to include other field components in the calculations.

Regarding the experimental aspects of the present study, it is worth mentioning that lightning measurement systems need to operate for long periods of time under very rough environmental conditions and at different distances from the lightning channel. No commercial system is designed specially for lightning and the ones that could be used are very expensive. It is therefore desirable to clearly define the specifications for performance, endurance, reliability and test procedures of electric, magnetic and current measurement systems adapted to the measurement of lightning.

In general, more data needs to be accumulated in order to adequately validate the models and to improve them in order to reproduce as closely as possible the experimental measurements. The author highly encourages continuing the participation in international measurement campaigns of lightning parameters around the world.

We would like to conclude with the hope that this work can represent a helpful contribution to the interesting domain of electromagnetic lightning characterization. With the present pace in lightning research, however, there is not doubt that the contributions presented in this thesis will be overtaken sooner rather than later by alternative, improved methods, proposed by the research groups active in this field. I look forward to watching and participating in this exciting “game” of lightning return stroke modeling.

APPENDICES

Appendices

Appendix 1 - Derivation of equations (5-11) and (5-12)

Two equivalent approaches can be adopted to derive equations (5-11) and (5-12): (a) using a brute-force method by inserting the expressions for the spatial-temporal distribution of the current (5-5)-(5-6) into (5-9)-(5-10) and solving for the integrals, or (b) by making use of the superposition principle and using the equations corresponding to a return stroke initiated at ground level (5-1) and (5-2). In what follows, we will use both approaches which will result in identical equations.

A1.1 Approach based on the superposition principle

Consider an infinitely long lightning channel initiated at ground level, with a similar geometry as in Fig. 5.2a (Chapter 5), where $i_o(t)$ represents the injected current at the channel base. In this case, the far (radiated) electric and magnetic field according to the TL model are given by the well-known equations (5-1) and (5-2).

Let us focus first on the magnetic field. For a channel of finite length H , the magnetic field can be obtained using the superposition principle from two current pulses flowing into infinitely-long paths but with opposite sign and delayed in time, as illustrated in Fig. A1.

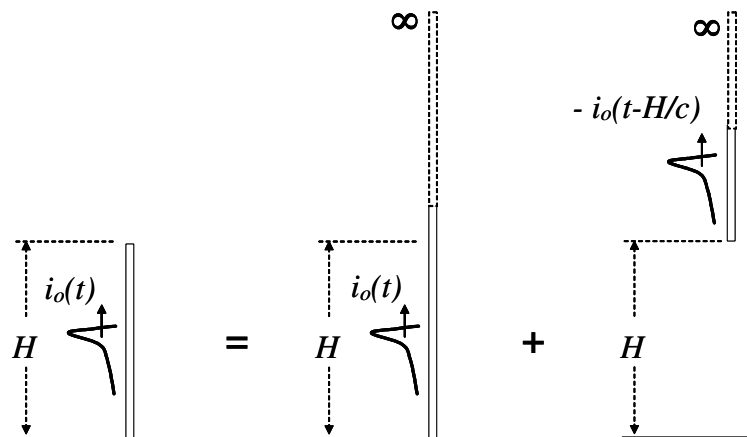


Figure A1 - Radiated field from a finite-length antenna: calculation using fields radiated by two infinitely-long antennas.

The first equivalent antenna extends from the ground level to infinity; while the second one extends from a height H to infinity. The current carried by the second equivalent antenna has an opposite sign with respect to the first one. In this case and under the current far-field assumptions, the magnetic field can be simply expressed as

$$H_{\varphi}(r, t + r/c) = \frac{v}{2\pi cr} i_o(t) - \frac{v}{2\pi cr} i_o(t - H/c) \tag{A-1}$$

The above procedure will now be applied to a lightning return stroke initiated at the top of an elevated strike object (tower) of height h . For this case, according to equations (5-5) and (5-6), two current pulses initiate at the strike object top at time $t=0$, one traveling downward in the tower at the speed of light c , and the other traveling upward in the channel and composed by two terms one of them traveling at the return stroke speed v and the second at the speed of light c ¹.

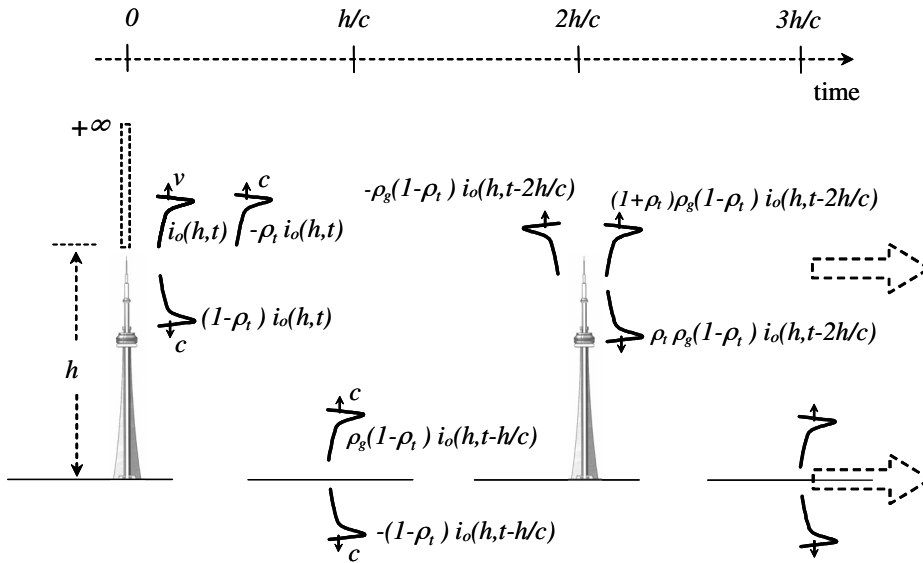


Figure A2 - Illustration of various current pulses to be taken into account in the calculation of radiated field produced by a lightning return stroke to a tall structure.

Considering the multiple reflections occurring at the tower top and bottom as being due to pulses traveling along infinitely-long antennas with appropriate delay times, as indicated in Fig. A2, we can write expressions for the radiated far magnetic field as,

$$H_{\varphi}^{far}(r, t + r/c) = \frac{1}{2\pi cr} \left[\begin{aligned} &v i_o(h, t) - c \rho_t i_o(h, t) + c(1 - \rho_t) i_o(h, t) - c(1 - \rho_t) i_o(h, t - h/c) \\ &+ c(1 - \rho_t) \rho_g i_o(h, t - h/c) - c(1 - \rho_t) \rho_g i_o(h, t - 2h/c) \\ &+ c(1 - \rho_t) \rho_g (1 + \rho_t) i_o(h, t - 2h/c) + c(1 - \rho_t) \rho_g \rho_t i_o(h, t - 2h/c) \\ &- c(1 - \rho_t) \rho_g \rho_t i_o(h, t - 3h/c) + \dots \end{aligned} \right] \tag{A-2}$$

The above expression can be re-written in the following compact form

$$H_{\varphi}^{far}(r, t + r/c) = \frac{v}{2\pi cr} \left[1 + \frac{c}{v} (1 - 2\rho_t) \right] i_o(h, t) + \frac{(1 - \rho_t)}{2\pi r} \sum_{n=0}^{\infty} \left\{ \begin{aligned} &(\rho_g - 1) \rho_g^n \rho_t^n i_o \left(h, t - \frac{(2n + 1)h}{c} \right) \\ &+ 2 \rho_g^{n+1} \rho_t^{n+1} i_o \left(h, t - \frac{2(n + 1)h}{c} \right) \end{aligned} \right\} \tag{A-3}$$

¹ Note that this second term of current, traveling at speed c , is supposed to be absorbed when it reaches the return stroke wavefront ('matched termination').

which is the final equation for the magnetic field. Note that in the above derivation, we have neglected terms associated with the abrupt vanishing of the current pulses at the return stroke wavefront.

In a similar way, the expression for the radiated far electric field is given by

$$E_z^{far}(r, t + r/c) = -\frac{v}{2\pi\epsilon_0 c^2 r} \left[1 + \frac{c}{v} (1 - 2\rho_t) \right] i_o(h, t) - \frac{(1 - \rho_t)}{2\pi\epsilon_0 c r} \sum_{n=0}^{\infty} \left\{ \begin{array}{l} (\rho_g - 1) \rho_g^n \rho_t^n i_o \left(h, t - \frac{(2n+1)h}{c} \right) \\ + 2\rho_g^{n+1} \rho_t^{n+1} i_o \left(h, t - \frac{2(n+1)h}{c} \right) \end{array} \right\} \quad (\text{A-4})$$

A1.2 Direct approach

Let us re-write, for convenience, equations (5-9) and (5-10) describing far electric and magnetic fields at ground level from a vertical antenna,

$$E_z(r, t) \cong -\frac{1}{2\pi\epsilon_0 c^2 r} \int_0^H \frac{\partial i(z, t - r/c)}{\partial t} dz \quad (\text{A-5})$$

$$H_\phi(r, t) \cong \frac{1}{2\pi c r} \int_0^H \frac{\partial i(z, t - r/c)}{\partial t} dz \quad (\text{A-6})$$

Equations (A-5) and (A-6) involve the spatial-temporal distribution of the current derivative along the antenna (strike object and lightning channel) $i(z, t)$.

Let us consider first the magnetic field expression. Introducing the current spatial-temporal distribution (5-5) and (5-6) into (A-6), we obtain

$$H_\phi(r, t + \frac{r}{c}) \cong \frac{(1 - \rho_t)h}{2\pi c r} \int_0^{\frac{\partial}{\partial t}} \left\{ \sum_{n=0}^{\infty} \left[\rho_g^n \rho_t^n i_o \left(h, t - \frac{h-z}{c} - \frac{2nh}{c} \right) + \rho_g^{n+1} \rho_t^n i_o \left(h, t - \frac{h+z}{c} - \frac{2nh}{c} \right) \right] \right\} dz + \frac{1}{2\pi c r} \int_h^H \frac{\partial}{\partial t} \left\{ \begin{array}{l} i_o \left(h, t - \frac{z-h}{v} \right) - \rho_t i_o \left(h, t - \frac{z-h}{c} \right) \\ + (1 - \rho_t)(1 + \rho_t) \sum_{n=0}^{\infty} \rho_g^{n+1} \rho_t^n i_o \left(h, t - \frac{h+z}{c} - \frac{2nh}{c} \right) \end{array} \right\} dz \quad (\text{A-7})$$

We will proceed term by term in Equation (A-7). The first term of Equation (A-7) can be written as

$$\frac{(1 - \rho_t)h}{2\pi c r} \int_0^{\frac{\partial}{\partial t}} \left[\sum_{n=0}^{\infty} \rho_g^n \rho_t^n i_o \left(h, t - \frac{h-z}{c} - \frac{2nh}{c} \right) \right] dz = \frac{(1 - \rho_t)}{2\pi c r} \sum_{n=0}^{\infty} \rho_g^n \rho_t^n \int_0^h \frac{\partial i_o \left(h, t - \frac{h-z}{c} - \frac{2nh}{c} \right)}{\partial t} dz \quad (\text{A-8})$$

The current time derivative can be transformed into a space derivative using the following relation

$$\frac{\partial i_o \left(h, t - \frac{h-z}{c} - \frac{2nh}{c} \right)}{\partial t} = c \frac{\partial i_o \left(h, t - \frac{h-z}{c} - \frac{2nh}{c} \right)}{\partial z} \quad (\text{A-9})$$

Introducing (A-9) in (A-8), and solving the integral we obtain,

$$\frac{(1-\rho_t)c}{2\pi cr} \sum_{n=0}^{\infty} \rho_g^n \rho_t^n \int_0^h \frac{\partial i_o \left(h, t - \frac{h-z}{c} - \frac{2nh}{c} \right)}{\partial z} dz = \frac{(1-\rho_t)c}{2\pi cr} \sum_{n=0}^{\infty} \rho_g^n \rho_t^n \left[i_o \left(h, t - \frac{2nh}{c} \right) - i_o \left(h, t - \frac{h}{c} - \frac{2nh}{c} \right) \right] \quad (\text{A-10})$$

The second term of Equation (A-7) can be written as

$$\frac{(1-\rho_t)^h}{2\pi cr} \int_0^h \frac{\partial}{\partial t} \left[\sum_{n=0}^{\infty} \rho_g^{n+1} \rho_t^n i_o \left(h, t - \frac{h+z}{c} - \frac{2nh}{c} \right) \right] dz = \frac{(1-\rho_t)}{2\pi cr} \sum_{n=0}^{\infty} \rho_g^{n+1} \rho_t^n \int_0^h \frac{\partial i_o \left(h, t - \frac{h+z}{c} - \frac{2nh}{c} \right)}{\partial t} dz \quad (\text{A-11})$$

Transforming the current derivative similar than in (A-9), we can get,

$$\frac{\partial i_o \left(h, t - \frac{h+z}{c} - \frac{2nh}{c} \right)}{\partial t} = -c \frac{\partial i_o \left(h, t - \frac{h+z}{c} - \frac{2nh}{c} \right)}{\partial z} \quad (\text{A-12})$$

Introducing (A-12) in (A-11), and solving the integral we obtain,

$$\begin{aligned} \frac{(1-\rho_t)(-c)}{2\pi cr} \sum_{n=0}^{\infty} \rho_g^{n+1} \rho_t^n \int_0^h \frac{\partial i_o \left(h, t - \frac{h+z}{c} - \frac{2nh}{c} \right)}{\partial z} dz \\ = \frac{(1-\rho_t)(-c)}{2\pi cr} \sum_{n=0}^{\infty} \rho_g^{n+1} \rho_t^n \left[i_o \left(h, t - \frac{2h}{c} - \frac{2nh}{c} \right) - i_o \left(h, t - \frac{h}{c} - \frac{2nh}{c} \right) \right] \end{aligned} \quad (\text{A-13})$$

The third and four terms of Equation (A-7) can be written as

$$\frac{1}{2\pi cr} \int_h^H \frac{\partial}{\partial t} \left[i_o \left(h, t - \frac{z-h}{v} \right) - \rho_t i_o \left(h, t - \frac{z-h}{c} \right) \right] dz = \frac{1}{2\pi cr} \int_h^H \left[\frac{\partial i_o \left(h, t - \frac{z-h}{v} \right)}{\partial t} - \rho_t \frac{\partial i_o \left(h, t - \frac{z-h}{c} \right)}{\partial t} \right] dz \quad (\text{A-14})$$

Transforming the current derivatives similar as in (A-9), we can get,

$$\frac{\partial i_o \left(h, t - \frac{z-h}{v} \right)}{\partial t} = -v \frac{\partial i_o \left(h, t - \frac{z-h}{v} \right)}{\partial z} \quad \text{and} \quad \frac{\partial i_o \left(h, t - \frac{z-h}{c} \right)}{\partial t} = -c \frac{\partial i_o \left(h, t - \frac{z-h}{c} \right)}{\partial z} \quad (\text{A-15})$$

Introducing (A-15) in (A-14), and solving the integral we obtain,

$$\begin{aligned}
& \frac{1}{2\pi cr} \int_h^H \frac{\partial}{\partial z} \left[(-v) i_o \left(h, t - \frac{z-h}{v} \right) + c \rho_t i_o \left(h, t - \frac{z-h}{c} \right) \right] dz \\
&= \frac{1}{2\pi cr} \left\{ (-v) \left[i_o \left(h, t - \frac{H-h}{v} \right) - i_o(h, t) \right] + (c \rho_t) \left[i_o \left(h, t - \frac{H-h}{c} \right) - i_o(h, t) \right] \right\}
\end{aligned} \tag{A-16}$$

Finally, the last term of Equation (A-7) can be written as

$$\begin{aligned}
& \frac{1}{2\pi cr} \int_h^H \frac{\partial}{\partial t} \left[(1-\rho_t)(1+\rho_t) \sum_{n=0}^{\infty} \rho_g^{n+1} \rho_t^n i_o \left(h, t - \frac{h+z}{c} - \frac{2nh}{c} \right) \right] dz \\
&= \frac{1}{2\pi cr} (1-\rho_t)(1+\rho_t) \sum_{n=0}^{\infty} \rho_g^{n+1} \rho_t^n \int_h^H \frac{\partial}{\partial t} \left[i_o \left(h, t - \frac{h+z}{c} - \frac{2nh}{c} \right) \right] dz
\end{aligned} \tag{A-17}$$

again, transforming the current derivatives similar than in (A-9), we can get,

$$\frac{\partial i_o \left(h, t - \frac{h+z}{c} - \frac{2nh}{c} \right)}{\partial t} = -c \frac{\partial i_o \left(h, t - \frac{h+z}{c} - \frac{2nh}{c} \right)}{\partial z} \tag{A-18}$$

Introducing (A-18) in (A-17), and solving the integral we obtain,

$$\begin{aligned}
& \frac{1}{2\pi cr} \int_h^H \frac{\partial}{\partial z} \left[(1-\rho_t)(1+\rho_t) \sum_{n=0}^{\infty} \rho_g^{n+1} \rho_t^n (-c) i_o \left(h, t - \frac{h+z}{c} - \frac{2nh}{c} \right) \right] dz \\
&= \frac{1}{2\pi cr} (1-\rho_t)(1+\rho_t) \sum_{n=0}^{\infty} \rho_g^{n+1} \rho_t^n (-c) \left[i_o \left(h, t - \frac{h+H}{c} - \frac{2nh}{c} \right) - i_o \left(h, t - \frac{2h}{c} - \frac{2nh}{c} \right) \right]
\end{aligned} \tag{A-19}$$

The magnetic field at far distances, Equation (A-7), can be then obtained by the summation of equations (A-10), (A-13), (A-16) and (A-19).

Applying straightforward mathematical manipulations, and disregarding terms associated with the abrupt vanishing of the current pulses at the return stroke wavefront, we obtain the final expression for the far magnetic field,

$$H_{\varphi}(r, t + r/c) = \frac{v}{2\pi cr} \left[1 + \frac{c}{v} (1 - 2\rho_t) \right] i_o(h, t) + \frac{(1-\rho_t)}{2\pi r} \sum_{n=0}^{\infty} \left\{ \begin{aligned} & (\rho_g - 1) \rho_g^n \rho_t^n i_o \left(h, t - \frac{(2n+1)h}{c} \right) \\ & + 2\rho_g^{n+1} \rho_t^{n+1} i_o \left(h, t - \frac{(2n+1)h}{c} \right) \end{aligned} \right\} \tag{A-20}$$

Following a similar development, the final expression for the electric field is given by

$$E_z(r, t + r/c) = -\frac{v}{2\pi \epsilon_o c^2 r} \left[1 + \frac{c}{v} (1 - 2\rho_t) \right] i_o(h, t) - \frac{(1-\rho_t)}{2\pi \epsilon_o c r} \sum_{n=0}^{\infty} \left\{ \begin{aligned} & (\rho_g - 1) \rho_g^n \rho_t^n i_o \left(h, t - \frac{(2n+1)h}{c} \right) \\ & + 2\rho_g^{n+1} \rho_t^{n+1} i_o \left(h, t - \frac{(2n+1)h}{c} \right) \end{aligned} \right\} \tag{A-21}$$

Equations (A-20) and (A-21) are identical to equations (A-3) and (A-4) derived using the superposition principle.

Appendix 2 - Derivation of equations (5-25) and (5-26)

Let us re-write for convenience equations (5-23) and (5-24) describing the spatial-temporal distribution of current for an electrically-short strike object

$$i(z, t) = (1 + \rho_{ch-g}) i_o(h, t) \quad 0 \leq z < h \quad (\text{A-22})$$

$$i(z, t) = i_o\left(h, t - \frac{z-h}{v}\right) + \rho_{ch-g} i_o\left(h, t - \frac{z-h}{c}\right) \quad h < z < H_{\text{tot}} \quad (\text{A-23})$$

The far electric and magnetic fields are given by

$$E_z^{\text{far}}(r, t) \cong -\frac{1}{2\pi\epsilon_0 c^2 r} \int_0^H \frac{\partial i(z, t - r/c)}{\partial t} dz \quad (\text{A-24})$$

$$H_\varphi^{\text{far}}(r, t) \cong \frac{1}{2\pi cr} \int_0^H \frac{\partial i(z, t - r/c)}{\partial t} dz \quad (\text{A-25})$$

Let us consider first the magnetic field expression. Introducing the current spatial-temporal distribution (A-22) and (A-23) into (A-25), and taken into account assumptions made in Section 5.2, we obtain

$$H_\varphi^{\text{far}}\left(r, t + \frac{r}{c}\right) \cong \frac{(1 + \rho_{ch-g})h}{2\pi cr} \int_0^h \frac{\partial i_o(h, t)}{\partial t} dz + \frac{1}{2\pi cr} \int_h^H \frac{\partial}{\partial t} \left[i_o\left(h, t - \frac{z-h}{v}\right) + \rho_{ch-g} i_o\left(h, t - \frac{z-h}{c}\right) \right] dz \quad (\text{A-26})$$

The first term in Equation (A-26), representing the contribution of the strike object to the total field, is independent of z ; therefore, it can be extracted from the integral which can be directly evaluated. The second and third terms, representing the contribution of the channel, are similar to those evaluated by the first two terms in Equation (A-2) or in Equation (A-16). Applying a similar development, the resulting far magnetic field for electrically-short structures becomes,

$$H_\varphi^{\text{far}}\left(r, t + \frac{r}{c}\right) \cong \frac{(1 + \rho_{ch-g})h}{2\pi cr} \left(\frac{\partial i_o(h, t)}{\partial t} \right) + \frac{1}{2\pi cr} \left(v i_o(h, t) + c \rho_{ch-g} i_o(h, t) \right) \quad (\text{A-27})$$

The expression above can be re-written in the following form

$$H_\varphi^{\text{far}}\left(r, t + \frac{r}{c}\right) \cong \frac{v}{2\pi cr} \left(1 + \frac{c}{v} \rho_{ch-g} \right) i_o(h, t) + \frac{(1 + \rho_{ch-g})h}{2\pi cr} \frac{\partial i_o(h, t)}{\partial t} \quad (\text{A-28})$$

In a similar way, the expression for the radiated far electric field for electrically-short structures is given by

$$E_z^{far} \left(r, t + \frac{r}{c} \right) \cong -\frac{v}{2\pi\epsilon_0 c^2 r} \left(1 + \frac{c}{v} \rho_{ch-g} \right) i_o(h, t) - \frac{(1 + \rho_{ch-g})h}{2\pi\epsilon_0 c^2 r} \frac{\partial i_o(h, t)}{\partial t} \quad (\text{A-29})$$

Appendix 3 - Numerical validation of equations (6-6a) and (6-10)

The numerical validation presented below evaluates possible numerical errors committed when the methods developed in Chapter 6, involving transformation from time domain to frequency domain, and vice versa, are used. First an evaluation of the close form current expression in the frequency domain, Equation (6-6a) is performed, compared with the time domain expression from [Guerrieri et al., 1998] using the new expression defined by [Rachidi et al., 2002]. Then the frequency domain expression to calculate the ground reflection coefficients from two simultaneously measured return-stroke currents is tested in two situations: with constant ground reflection coefficient in function of frequency and with variable ground reflection coefficient in function of frequency.

A3.1 The closed form current equation

Equations (6-1b) and (6-6a) have been programmed into the Matlab environment to reproduce the results obtained by [Guerrieri et al., 1998] using the new expression defined by [Rachidi et al., 2002]. We used the same lightning current waveforms chosen by [Guerrieri et al., 1998] to represent the undisturbed current $i_o(h,t)$, namely the sum of two Heidler's functions (Section 3.3, Chapter 3). A Heidler function is of the form [Heidler, 1985]:

$$i_o(h,t) = \frac{I_o}{\eta} \frac{(t/\tau_1)^N}{1+(t/\tau_1)^N} \exp(-t/\tau_2); \quad (A-30)$$

$$\eta = \exp \left[- \left(\frac{\tau_1}{\tau_2} \right) \left(N \frac{\tau_2}{\tau_1} \right)^{1/N} \right]$$

where, I_o is the amplitude of the channel-base current, τ_1 is the front-time constant, τ_2 is the decay-time constant, η is the amplitude correction factor and N is an exponent (ranging from 2 to 10). The Heidler current parameters used are given in Table A.1. These parameters can be obtained manually (try and error) or using an automatic implementation developed on Section 6.6, based on genetic algorithms, in which, additionally, the values for the top and bottom reflection coefficients are inferred to fit as perfect as possible experimental observed current waveshapes of lightning return strokes.

Table A.1 - Parameters of two Heidler functions that reproduce the “undisturbed” current wave shapes $i_o(h,t)$ at the top of the elevated object.

I_{o1} [kA]	τ_{11} [μs]	τ_{21} [μs]	I_{o2} [kA]	τ_{12} [μs]	τ_{22} [μs]
10.7	0.25	2.5	6.5	2.1	230

In Fig. A.3, we compare, for the first 20 μs , the disturbed current expression defined by [Guerrieri et al., 1998] and the new expression introduced by [Rachidi et al., 2002] which includes the additional term $(1-\rho_t)$ to take into account the impedance discontinuity at the tower top.

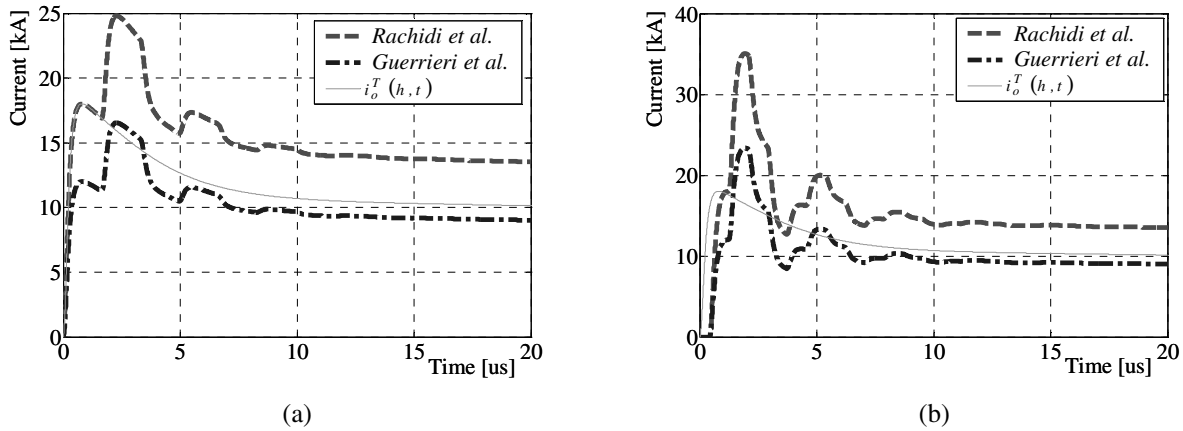


Figure A3 - Evaluation of the disturbed current along the strike object ($h = 248 \text{ m}$, $\rho_t = -0.5$, $\rho_g = 1$); (a) Current calculated at the tower top, $z = h$; (b) Current calculated at the middle of the tower, $z = 0.5 h$.

The factor $(1-\rho_t)$ introduced by [Rachidi et al., 2002] increases the amplitude of the current waveform flowing down into the tower for all the cases where the top reflection coefficient ρ_t has negative values (ρ_t has been found to have negative values from experimental measurements in instrumented towers available today - [Rakov, 2001]).

Indeed, [Guerrieri et al., 1998] did not take into account the treatment of the impedance discontinuity at the tower top in the attachment process, the Guerrieri et al. Equation disregards the mentioned factor considering, implicitly, ρ_t equal to 0 for the first contact to the tower ($Z_{ch} = Z_t$).

A comparison of two cases of currents using Equation (6-1b) [Rachidi et al., 2002] in the time domain and Equation (6-6a) in the frequency domain is presented in figs. A4 and A5, for currents at $z_1 = 160 \text{ m}$ and $z_2 = 5 \text{ m}$. The tower height ($h = 168 \text{ m}$) and the observation points correspond to those of the Peissenberg tower, and the undisturbed current was obtained using the parameters given in Table A.1. The frequency domain formula is transformed back into the time domain to the effect of comparisons. The reflection coefficients were assumed to be constant and independent of frequency.

As can be seen from figs. A4 and A5, our results obtained in the frequency domain using Equation (6-6a) are indistinguishable from those obtained in the time domain by Equation (6-1b). Inaccuracies due to the numerical Fourier Transforms are negligible.

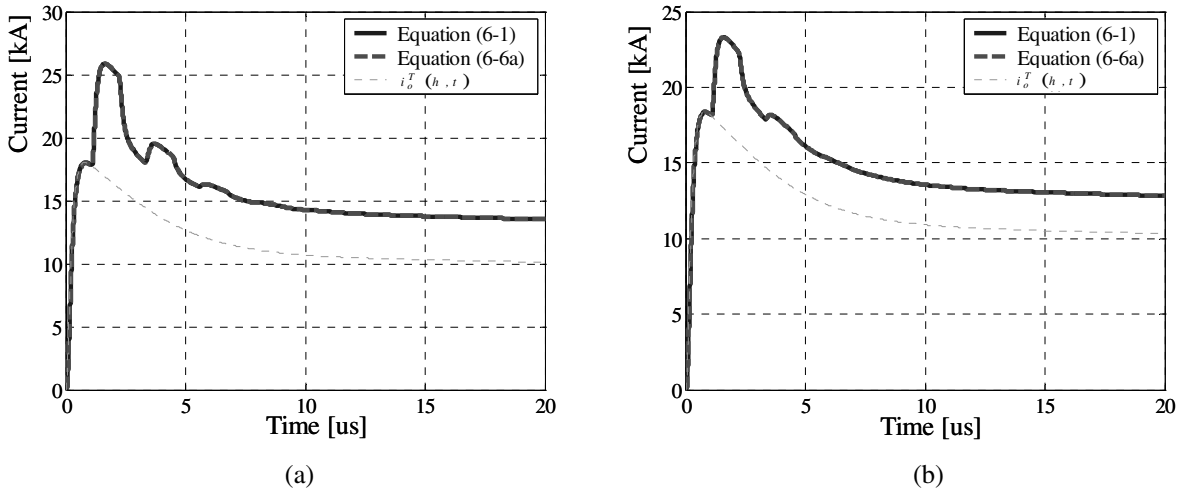


Figure A4 - Comparison between Equation (6-1b) in the time domain and Equation (6-6a) in the frequency domain (transformed to the time domain for comparison), for a tower height $h = 168$ m, and current calculated at $z = 160$ m. Two cases are presented: (a) $\rho_t = -0.5$ and $\rho_g = 1$, and (b) $\rho_t = -0.53$ and $\rho_g = 0.7$. Note that the results obtained in the frequency domain using Equation (6-6a) are indistinguishable from those obtained in the time domain by Equation (6-1b).

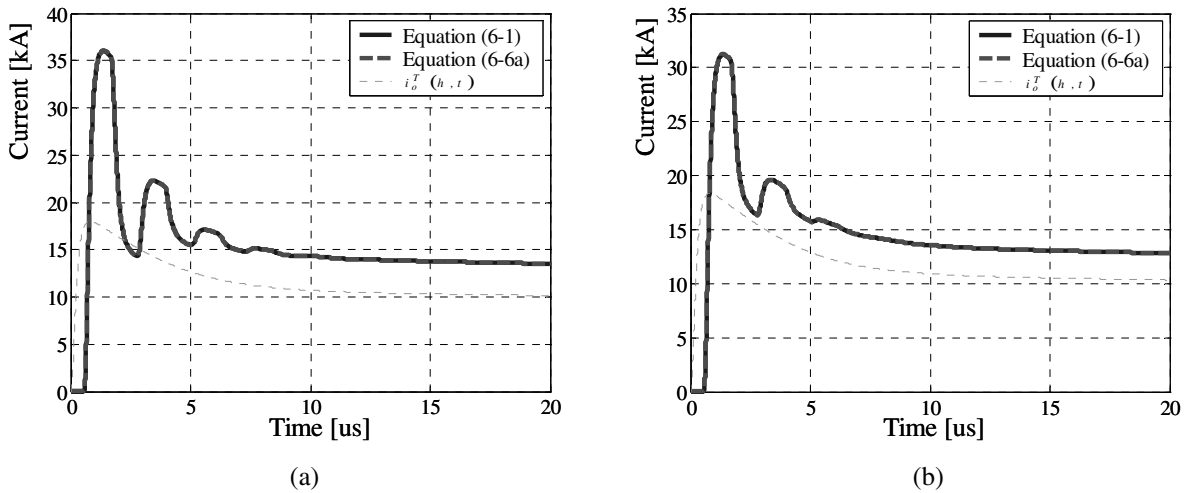


Figure A5 - Same comparison as Figure A4 but in this case the current is evaluated at $z = 5$ m. (a) $\rho_t = -0.5$ and $\rho_g = 1$, and (b) $\rho_t = -0.53$ and $\rho_g = 0.7$. Note that the results obtained in the frequency domain using Equation (6-6a) are indistinguishable from those obtained in the time domain by Equation (6-1).

A3.2 The ground reflection coefficient formula

In this section, we use Equation (6-10) to recalculate the constant reflection coefficients that were used to generate the currents in the last section, for $h = 168$ m, $z_1=160$ m and $z_2=5$ m (shown in figs. A4 and A5). The results are presented in Fig. A6. Both curves in that figure are in agreement with the original values of the ground reflection coefficients at the ground.

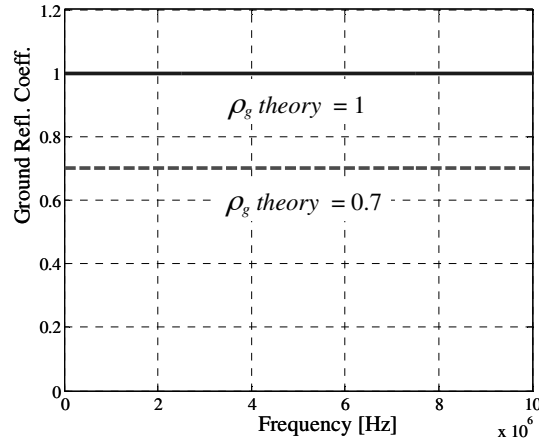


Figure A6 - Ground reflection coefficient, calculated by way of Equation (6-10), with $h=168$ m, $z_1 = 160$ m and $z_2 = 5$ m. Top $\rho_t = -0.5$ and $\rho_g = 1$; bottom $\rho_t = -0.53$ and $\rho_g = 0.7$.

We will now use Equation (6-10) to recover a frequency-dependent ground reflection coefficient. The objective here is to apply Equation (6-10) numerically and not to investigate the actual frequency behavior of the reflection coefficient at the ground. We will proceed in a manner similar to that used for the constant reflection coefficients above: We will first generate the currents and we will then use Equation (6-10) to re-extract the ground reflection coefficient.

Let us first define a frequency dependent function for ρ_g using, as sole criterion, the existence of an analytical form of its Fourier transform:

$$\rho_g(\omega) = \frac{10.5 \times 10^3}{j\omega + 10^4} - \frac{5 \times 10^3}{j\omega + 10^5} \quad (\text{A-31})$$

which, in the time domain, can be expressed as

$$\rho_g(t) = 10.5 \times 10^3 e^{-10^4 t} - 5 \times 10^3 e^{-10^5 t} \quad (\text{A-32})$$

To find the currents, we can proceed two different ways: (1) We can substitute Equation (A-31) into Equation (6-6a) and then apply the inverse Fourier transform, or (2) we can substitute Equation (A-32) into Equation (6-3) or Equation (6-6b), which involves convolution operations. We have chosen the first method. The currents at $z_1 = 160$ m and $z_2 = 5$ m, are plotted in Fig. A7 for the case where $\rho_t = -0.5$.

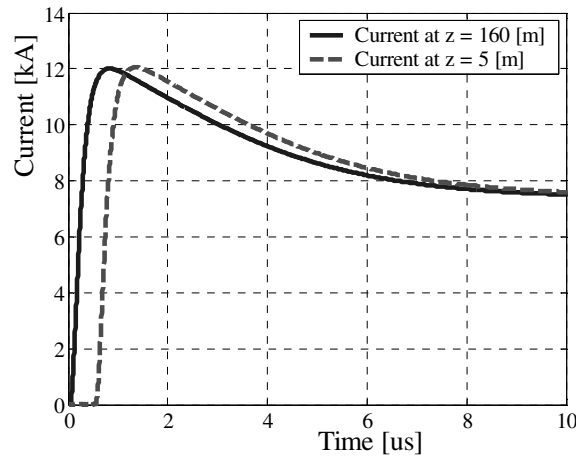


Figure A7 - Currents calculated at the top of the tower (solid lines) and at the middle (dashed line) using

$$\rho_g(\omega) = 10.5 \times 10^3 / (j\omega + 10^4) - 5 \times 10^3 / (j\omega + 10^5), \quad \rho_t = -0.3. \quad \text{Tower height, } h = 168 \text{ m.}$$

Note that, as reported by Guerrieri et al., the reflections are not readily discernible from the wave shapes. We have extracted the ground reflection coefficient as a function of frequency using these currents in Equation (6-10), and we have plotted it in Fig. A8. The original reflection coefficient $\rho_g(\omega)$, Equation (A-31), is also plotted for comparison. Clearly, the original reflection coefficient has been accurately recovered.

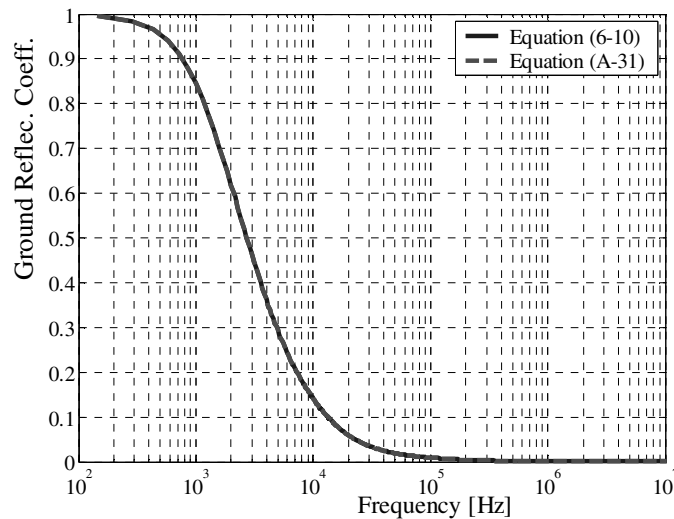


Figure A8 - Reflection coefficient, $\rho_g(\omega)$. The solid lines are our result, Equation (6-10), and the dashed line that of theoretical solution, Equation (A-31). Note that the two results are practically superimposed.

Appendix 4 - Reduced-scale model to evaluate the response of nonuniform vertically-extended object struck by lightning

The lightning return stroke models, originally developed for return strokes initiated at ground level, have been extended in Chapter 4 to include an elevated strike object. The elevated strike object is modeled as an ideal (lossless) transmission line. In order to include structural nonuniformities of the elevated strike object, several transmission line sections in cascade have also been considered (e.g. [Rusan et al., 1996; Shostak et al., 2002]). The transmission line representation of the elevated strike object has been shown to yield reasonable results in comparison with experimental data. However, the validity of the TL approach has never been investigated to the best of our knowledge. This is essentially due to the fact that experimental data associated with lightning to tall structures are ‘affected’ by other less-controlled factors such as the variability of lightning channel impedance and possible reflections at the return stroke wavefront (e.g. [Shostak et al., 2000]). In the frame of this thesis, a reduced scale model to study the behavior of transient current flowing through a complex geometry has been designed, constructed and tested ([Bermudez et al., 2001; Gutierrez et al., 2002]). A series of elementary geometries, as well as a model for the CN Tower in Canada have been studied.

A4.1 Experimental Set-up

The reduced scale model was developed based on the studies carried out by Chisholm et al. [Chisholm and Chow, 1983; Chisholm and Janischewskyj, 1989].

Fig. A9 presents the experimental set up consisting of two parallel plates of 1 m radius each separated by a distance that can be varied from 40 cm to 1 m. The lower circular plate (made of copper) represents the ground plane.

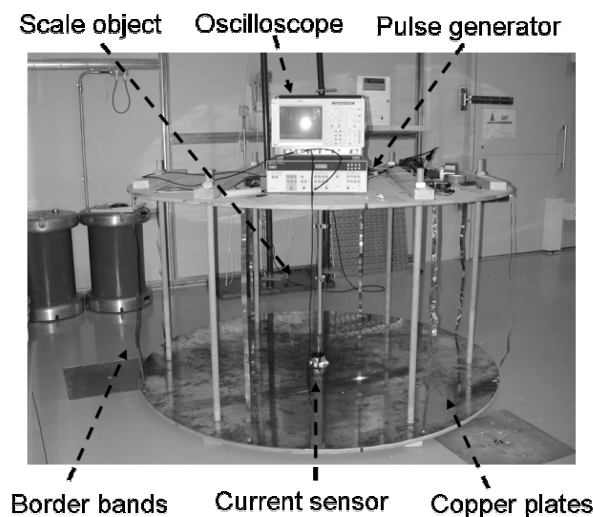


Figure A9 - Experimental set up.

Lightning currents and electromagnetic fields associated with return strokes to elevated strike objects

A very fast pulse is injected into the reduced scale model for the elevated strike object (ESO) through a hole at the center of the upper plate. The two plates can be connected using copper ribbons representing the displacement current path. The injection of the fast pulse is made through a 50 Ω coaxial cable connecting the pulse generator and the top of ESO under study.

An equivalent diagram of the system is presented in Fig. A10. The pulse generator is a HP 8131A (500 MHz, 0.05 A Norton equivalent, 2.5 Volt Thevenin equivalent). The injected voltage and currents along the ESO were digitized using a Lecroy LC574AL oscilloscope (1 GHz, 1 to 10 GS/s, 8Mpt of memory). The currents were measured using EMCO sensors having a bandwidth of 1 MHz to 1 GHz.

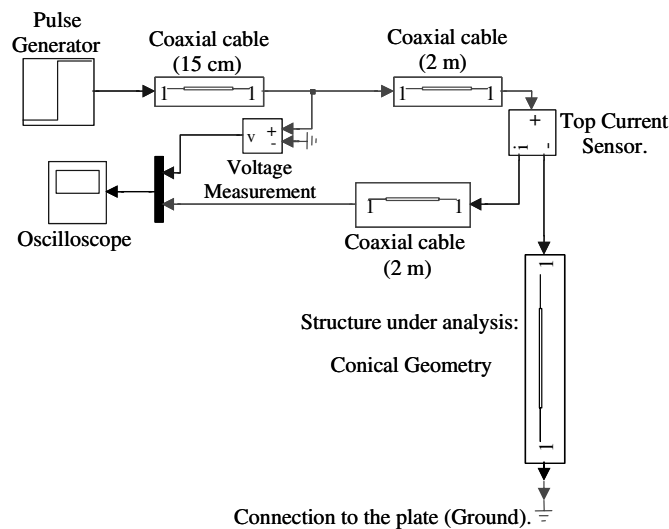


Figure A10 - Equivalent diagram of the reduced-scale model.

Fig. A11a shows the reduced scale structure of the CN Tower in Canada (Fig. A11b). Lightning current measurements made at the CN Tower have clearly shown that the measured waveforms are 'disturbed' by multiple reflections produced at the elevated strike object discontinuities (see Chapter 2, and also [Janischewskyj et al., 1996; Rusan et al., 1996]). The removal of this disturbance on the measured waveforms and the extraction of primary data is possible only if the strike object is accurately characterized [Guerrieri et al., 1998; Rachidi et al., 2002].

The reduced scale representation of the tower has a total height of 95 cm (Fig. A11a). It consists of three sections: upper conical, middle cylindrical, and lower conical. Fig. A12 shows the three-section model of the CN tower into the reduced scale system.

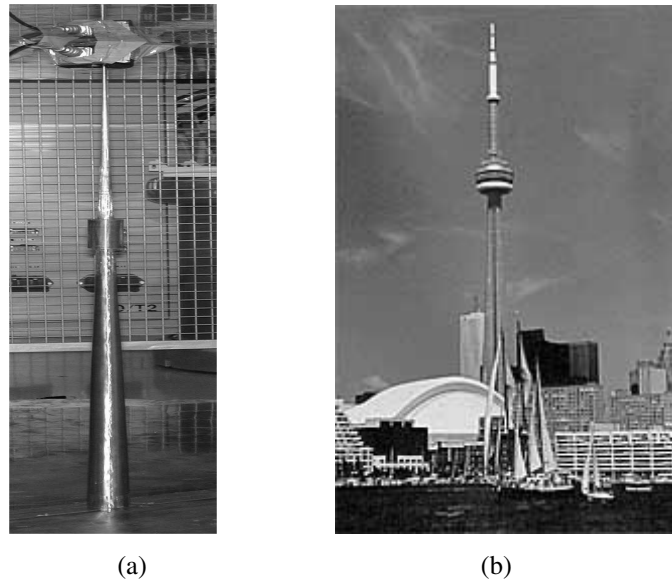


Figure A11 - Reduced-scale model of the CN Tower (a), and CN Tower (b).

A4.2 Simulations and comparison with experimental data

The characteristic impedance of the three transmission line sections composing the CN Tower reduced scale model have been calculated using well-known equations ([Jordan and Balmain, 1968; Sargent and Darveniza, 1969]). Fig. A13 presents a comparison between measured and calculated waveforms of the voltage measured at the input of the structure ([Bermudez et al., 2003]). It can be seen that the computed results are in excellent agreement with experimental data.



Figure A12 - Three-section CN Tower model into the reduced-scale system

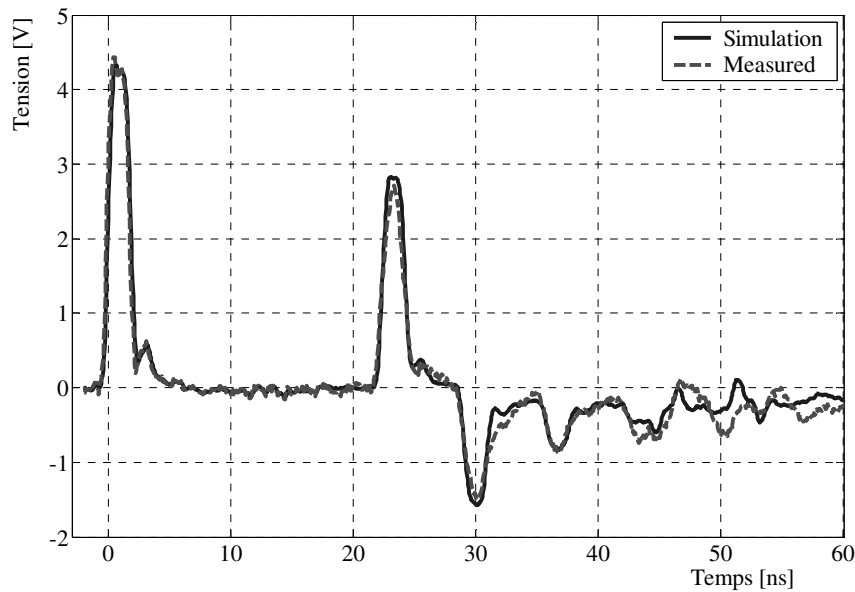


Figure A13 - Experimental and calculated transient signals in a reduced-scale model of the CN Tower

References Appendix

- Bermudez, J.L., J.A. Gutierrez, W.A. Chisholm, F. Rachidi, M. Paolone, and P. Moreno, A Reduced-Scale Model to Evaluate the Response of Tall Towers Hit by Lightning, in *International Symposium on Power Quality: SICEL'2001*, Bogotá, Colombia, 2001.
- Bermudez, J.L., F. Rachidi, W.A. Chisholm, M. Rubinstein, W. Janischewskyj, A.M. Hussein, V. Shostak, and J.S. Chang, On the use of transmission line theory to represent a nonuniform vertically-extended object struck by lightning, in *Submitted to the 2003 IEEE Symposium on Electromagnetic Compatibility (EMC)*, Boston, USA, 2003.
- Chisholm, W.A., and Y.L. Chow, Lightning surge response of transmission towers, *IEEE Transactions on Power Apparatus and Systems*, vol.PAS-102 (9), 3232-42, 1983.
- Chisholm, W.A., and W. Janischewskyj, Lightning surge response of ground electrodes, *IEEE Transactions on Power Delivery*, 4 (2), 1329-37, 1989.
- Guerrieri, S., C.A. Nucci, F. Rachidi, and M. Rubinstein, On the influence of elevated strike objects on directly measured and indirectly estimated lightning currents, *IEEE Transactions on Power Delivery*, 13 (4), 1543-55, 1998.

- Gutierrez, J.A., J.L. Bermudez, F. Rachidi, M. Paolone, C.A. Nucci, W.A. Chisholm, P. Moreno, and J.L. Naredo, A Reduced-Scale Model to Evaluate the Response of Nonuniform Towers to a Lightning Strike, in *26th ICLP (International Conference on Lightning Protection)*, pp. 487-490, Cracow, Poland, 2002.
- Heidler, H., Analytische Blitzstromfunktion zur LEMP- Berechnung, in *18th ICLP (International Conference on Lightning Protection)*, pp. 63-66, Munich, Germany, 1985.
- Janischewskyj, W., V. Shostak, J. Barratt, A.M. Hussein, I. Rusan, and J.S. Chang, Collection and use of lightning return stroke parameters taking into account characteristics of the struck object, in *23rd ICLP (International Conference on Lightning Protection)*, pp. 16-23, Florence, Italy, 1996.
- Jordan, E.C., and K.G. Balmain, *Electromagnetic Waves and Radiating Systems*, pp. 380-388 pp., Englewood Cliffs, N. J, 1968.
- Rachidi, F., V.A. Rakov, C.A. Nucci, and J.L. Bermudez, The Effect of Vertically-Extended Strike Object on the Distribution of Current Along the Lightning Channel, *Journal of Geophysical Research*, 107 (D23), 4699, 2002.
- Rakov, V.A., Transient response of a tall object to lightning, *IEEE Transactions on Electromagnetic Compatibility*, 43 (4), 654-61, 2001.
- Rusan, I., W. Janischewskyj, A.M. Hussein, and J.S. Chang, Comparison of measured and computed electromagnetic fields radiated from lightning strikes to the Toronto CN tower, in *23rd ICLP (International Conference on Lightning Protection)*, pp. 297-303, Florence, Italy, 1996.
- Sargent, M.A., and M. Darveniza, Tower surge impedance, *IEEE Transactions on Power Apparatus and Systems*, vol.PAS-88 (5), 680-7, 1969.
- Shostak, V., W. Janischewskyj, A. Hussein, J.S. Chang, F. Rachidi, and J.L. Bermudez, Modeling of the electromagnetic field associated with lightning return strokes to a complex tall tower,

in *26th ICLP (International Conference on Lightning Protection)*, pp. 167-172, Cracow, Poland, 2002.

Shostak, V., W. Janischewskyj, and A.M. Hussein, Expanding the modified transmission line model to account for reflections within the continuously growing lightning return stroke channel, in *IEEE Power Engineering Society Summer Meeting*, Cat. IEEE, Piscataway, USA, 2000.

Curriculum vitae

José Luis BERMUDEZ ARBOLEDA, IEEE member
 born February 8, 1970 in Zarzal
 Colombian
 Married
 Rue de Verdeaux 17
 CH-1020 Renens (VD)
 Tel: 41 21 635 5010
 E-Mail: Jose-Luis.Bermudez@epfl.ch

EDUCATION

- Graduate course in Computer Science and Biology (1997)
 - From the “Ecole Polytechnique Fédérale de Lausanne”
 - Master’s degree in Electrical Energy Generation (1992–1996)
 - From the “Universidad del Valle”, Cali (Colombia)
 - Electrical Engineering Diploma (1986–1992)
 - From the “Universidad del Valle”, Cali (Colombia)
-

PROFESSIONAL EXPERIENCE

- Research Assistant at the Electrical Power Systems Laboratory of the EPFL (2000-2003)
 - Research in lightning electromagnetics, return stroke modeling, elevated strike objects
 - EMC Engineer for the development of EMC standards: Services to the industry
 - Participation in laboratories and courses on EMC, High Voltage and Electric Circuits
 - Supervisor of student projects
 - Research Assistant at the Robotic Systems Institute of the EPFL (1999-2000)
 - Research in the area of passive magnetic bearings: design, construction and testing
 - Research Assistant at the Electrical Power Systems Laboratory of the EPFL (6 months, 1998)
 - Research in artificial neural networks applied to electrical power system representations
 - R&D Engineer at Montena Components SA - Fribourg (3 months, 1998)
 - Research, construction and testing of a prototype of super-capacitor
 - Consultant Engineer at Montena EMC SA - Fribourg (6 months, 1997-1998)
 - Calibration of anechoic chambers at three locations in Europe
 - Researcher in a project concerning “Tempest” (EMC security in communications)
-

DISTINCTIONS

- Recipient of the “IEEE 2001 best student paper award” at the IEEE International Conference on Electromagnetic Compatibility, Montreal-Canada, August 2001.
- Recipient of the “honorable mention (graduated student category)” for his contribution to the 2001 CAGE CLUB STUDENT CONFERENCE on High Voltage Engineering and Electrostatics, August 23rd, 2001, University of Toronto, Canada.

Publications

Parts of the present work have been published in the following papers:

Journal Papers

Rachidi, F., J.L. Bermudez, M. Rubinstein, and V.A. Rakov, On the estimation of lightning peak currents from measured fields using lightning location systems, *submitted to the Journal of Electrostatics*, 2003.

Bermudez, J.L., M. Rubinstein, F. Rachidi, F. Heidler, and M. Paolone, Determination of Reflection Coefficients at the Top and Bottom of Elevated Strike Objects Struck by Lightning, *Journal of Geophysical Research*, to be published, 2002.

Rachidi, F., V.A. Rakov, C.A. Nucci, and J.L. Bermudez, The Effect of Vertically-Extended Strike Object on the Distribution of Current Along the Lightning Channel, *Journal of Geophysical Research*, 107 (D23), 4699, 2002.

Bermudez, J.L., F. Rachidi, W. Janischewskyj, A.M. Hussein, M. Rubinstein, C.A. Nucci, M. Paolone, V. Shostak, and J.S. Chang, Electromagnetic Fields Radiated by Lightning Return Strokes to Tall Structures, to be submitted to the *Journal of Geophysical Research*, 2002.

Bermudez, J.L., "Medida de corriente de descargas atmosféricas mediante torres instrumentadas", *Energía y Computación*, iX (2), 53-61, 2000.

Conferences Proceedings

Bermudez, J.L., F. Rachidi, W. Janischewskyj, A.M. Hussein, V. Shostak, M. Rubinstein, C.A. Nucci, J.S. Chang, P. Joe, and M. Nyffeler, Simultaneous Measurements of Electromagnetic Fields at Two Distances and of Current Associated with Lightning Return Strokes to the CN Tower, in *26th ICLP (International Conference on Lightning Protection)*, Cracow, Poland, 2002.

Gutierrez, J.A., J.L. Bermudez, F. Rachidi, M. Paolone, C.A. Nucci, W.A. Chisholm, P. Moreno, and J.L. Naredo, A Reduced-Scale Model to Evaluate the Response of Nonuniform Towers to a Lightning Strike, in *26th ICLP (International Conference on Lightning Protection)*, pp. 487-490, Cracow, Poland, 2002.

Rachidi, F., J.L. Bermudez, and M. Rubinstein, Statistical evaluation of lightning current parameters from remote electromagnetic field measurements, in *26th ICLP (International Conference on Lightning Protection)*, Cracow, Poland, 2002.

Shostak, V., W. Janischewskyj, A. Hussein, J.S. Chang, F. Rachidi, and J.L. Bermudez, Modeling of the electromagnetic field associated with lightning return strokes to a complex tall tower, in *26th ICLP (International Conference on Lightning Protection)*, pp. 167-172, Cracow, Poland, 2002.

Bermudez, J.L., C.A. Peña-Reyes, F. Rachidi, and F. Heidler, "Use of Genetic Algorithms to Extract Primary Lightning Current Parameters", in *International Symposium on EMC*, pp. 241-246, Sorrento, Italy, 2002.

Bermudez, J.L., F. Rachidi, W. Janischewskyj, A.M. Hussein, M. Rubinstein, C.A. Nucci, M. Paolone, V. Shostak, and J.S. Chang, On the Enhancement of Radiated Electric and Magnetic Fields Associated

with Lightning Return Strokes to Tall Structures, in *IEEE International Conference on Electromagnetic Compatibility*, Montreal, Canada, 2001.

Bermudez, J.L., M. Rubinstein, F. Rachidi, and M. Paolone, A Method to Find the Reflection Coefficients at the Top and Bottom of Elevated Strike Objects from Measured Lightning Currents, in *14th International Zurich Symposium on Electromagnetic Compatibility*, pp. 6, Zurich, Switzerland, 2001.

Bermudez, J.L., J.A. Gutierrez, W.A. Chisholm, F. Rachidi, M. Paolone, and P. Moreno, A Reduced-Scale Model to Evaluate the Response of Tall Towers Hit by Lightning, in *International Symposium on Power Quality: SICEL'2001*, Bogotá, Colombia, 2001.

Reports

Bermudez, J.L., and F. Rachidi, "Determination of far radiated field from a lightning return stroke to a tall tower", in *Internal Rapport EPFL-DE-LRE-2001/A*, Swiss Federal Institute of Technology, Lausanne, Switzerland, 2001.

Bermudez, J.L., and F. Rachidi, "Summary of the experimental data - summer 2001", report of measurements performed in Canada during the summer 2001, Switzerland, 2002.

Bermudez, J.L., and F. Rachidi, "Report on the summer 2000 experimental data", report of measurements performed in Canada during the summer 2000, Switzerland, 2001.

Supervised graduate and undergraduate projects

Garavini, E., "Strutture verticali colpite da scariche atmosferiche: analisi teorica e sperimentale della distribuzione spazio-temporale della corrente di fulmine", Master's Thesis, University of Bologna, 2002.

Ngampradit, V., "EMC Demonstration: Surge Devices (SPDs) in Low-Voltage System", final project for course Postgrade in Electrical Power Engineering, EPFL, 2001-2002.

Perron, E. and Klauser, M., "Lightning Currents", Mini-project at the Logic Systems Laboratory (LSL), EPFL, 2002.

Laloli, F., « Etude de contamination de la mesure du courant de foudre effectué sur une tour de télécommunication », projet C, EPFL, 2001.

Duron, J., « Détermination indirecte des courants de foudre par la mesure du champ électromagnétique rayonné », projet de diplôme, EPFL, 2001.

Nef, T., « Etude de la "contamination" du courant de foudre sur des tours instrumentées en utilisant un modèle à échelle réduite », projet de semestre de 3^{ème} année, EPFL, 2001.

Porto, D. et Chabloz, G., "Interface Java pour l'analyse interactive des paramètres associés aux modèles théoriques des réflexions du courant de foudre sur une tour instrumentée", projet informatique du 5^{ème} semestre, EPFL, 2001.

Chabloz, J. and Kriebel, G., « Interface java pour l'analyse et visualisation des réflexions de courant produites dans une tour instrumentée au moment de l'impact d'un coup de foudre », projet informatique du 5^{ème} semestre, EPFL, 2001.

